CHARACTERIZING THE BEHAVIOR OF SMART OIL WELL CEMENT FOR ENAHNCING THE MONITORING OF CEMENT SHEATH INTEGRITY

A Thesis

Presented to

the Faculty of the Department of Civil and Environmental Engineering

Cullen College of Engineering

University of Houston

In Partial Fulfillment

of the Requirements for the Degree of

Master of Science

in Civil Engineering

by

Mehrzad Heidari

August 2014

CHARACTERIZING THE BEHAVIOR OF SMART OIL WELL CEMENT FOR ENAHNCING THE MONITORING OF CEMENT SHEATH INTEGRITY

Mehrzad Heidari

Approved:

Chair of the Committee
Cumaraswamy Vipulanandan, Professor,
Civil and Environmental Engineering

Committee Members:

Kalyana Babu Nakshatrala, Assistant Professor,
Civil and Environmental Engineering

Robello Samuel, Adjunct Professor,
Petroleum Engineering

Suresh K. Khator,
Associate Dean,
Cullen College of Engineering

Kaspar J. Willam,
Professor and Chairman,
Civil and Environmental Engineering

AKNOWLEDEGMENTS

I would like to express my sincere gratitude to my research advisor Dr. Cumaraswamy Vipulanandan for his valuable guidance and encouragement throughout my study period at University of Houston. His consistent support reinforced my confidence and helped me grow both academically and personally. I would also like to extend my appreciations to Dr. Robello Samuel from Halliburton and Dr. Kalyana Babu Nakshatrala from Civil and Environmental Engineering Department for serving on my thesis committee and exchanging valuable ideas and suggestions.

I owe my deepest appreciation to the members of the GEM group for their assistance, companionship, and friendship. Special thanks to the faculty and the staff of the Engineering Department at the University of Houston for their valued assistance. In particular, I would like to thank Cherish Wallace, Stephanie Woods, and Michael Smith who contributed to accomplishment of this work.

This study was supported by the Center for Innovative Grouting Materials and Technology (CIGMAT) at University of Houston. Funding of the project provided through the RPSEA and Department of Energy (DOE) is gratefully acknowledged. I would like to recognize my family, whose unconditional love and support played a key role in the successful completion of my research work. Special thanks are due to my friends and relatives for their support and endless patience which kept me encouraged and determined throughout my master's program.

CHARACTERIZING THE BEHAVIOR OF SMART OIL WELL CEMENT FOR ENAHNCING THE MONITORING OF CEMENT SHEATH INTEGRITY

An Abstract

Of a

Thesis

Presented to

the Faculty of the Department of Civil and Environmental Engineering

Cullen College of Engineering

University of Houston

In Partial Fulfillment

of the Requirements for the Degree of

Master of Science

in Civil Engineering

by

Mehrzad Heidari

August 2014

ABSTRACT

Oil well cementing is one of the most important and yet complex steps of a drilling project. One of the challenges in maintaining the well integrity is in monitoring the performance of oil well cement (OWC) used in the construction of the well. Recent oil well failures have clearly identified the importance of well cement on economic and environmental aspects of well drilling and completions. Currently, there is no technology available to monitor cementing operations in real time from the placement of cement through the service life of the wells.

In this study, oil well cement was modified with carbon fibers to have better sensing properties, smart cement, so that its behavior can be monitored at various stages. A series of experiments evaluated the cement behavior with and without modifications in order to identify the most reliable sensing properties that can also be easily monitored. Tests were performed on the cement from the time of mixing the slurry to hardened state. The results indicated that the initial electrical resistivity varied based on the type and amount of additives used in the cement. Electrical resistivity responses during curing of cement all exhibited the same trend with time. Resistivity dropped initially by about 10% to 12% to reach a minimum, and then gradually increased as the hydration progressed. The change in resistivity within the first 24 hours of curing varied from 50% to more than 300% depending on the composition. A new quantification concept has been developed to characterize the compressive strength development of cement based on electrical resistivity changes in the first 24 hours of curing. Modifying the cement with 0.1% of carbon fibers, improved the piezoresistive behavior of the hardened smart cement without

affecting the rheological and setting properties. The resistivity change at peak stress was about 400 times higher than the change in the strain at failure.

Effect of water-to-cement (w/c) ratio and curing temperature were investigated on the performance of smart cement. It was observed that resistivity of cement with different w/c ratios followed the same pattern but the characteristic parameters were significantly varied. Experiments revealed that the water-to-cement ratio, temperature and additives affect the rheological properties of OWC slurries, and a new hyperbolic model was proposed to predict the shear stress-strain rate relationship of cement slurries.

TABLE OF CONTENTS

AKNOWLEDEGMENTS iv

ABSTRACT vi

LIST OF FIGURES xiii

LIST OF TABLES xviii

Chapter 1 INTRODUCTION 1

1.1 General 1

1.2 Problem Description 2

1.3 Objective and Scope of the Study 3

1.4 Organization 4

Chapter 2 BACKGROUND AND LITERATURE REVIEW 6

2.1 History 6

2.2 Oil Well Cement 7

2.3 Properties of Cement Slurries and Set Cement 8

2.3.1 Density 8

2.3.2 Water-to-cement Ratio 9

2.3.3 Rheological Properties 10

2.3.4 Rheological Models 10

2.3.5 Fluid Loss 11

2.3.6 Thickening Time 12

2.3.7 Setting Time 12

2.3.8 Compressive Strength 12

2.4 Oil Well Cement Additives 13

2.4.1 Silica fume 14

2.4.2 Carbon Fibers 16

2.5 Hydration of Oil Well Cement 16

2.5.1 Chemical Reactions during Hydration 16

2.5.2 Kinetics of Hydration 17

2.6 Contamination of Well Cement with Oil Based Drilling Mud 18

2.7 Durability of Hardened OWC Slurries 18

2.8 Continuous Monitoring of Cement 19

2.9 Oil well Cement by Electrical Resistivity 20

2.9.1 Factors Effecting Resistivity of Cement 20

2.9.2 Factors Effecting Resistivity Measurements 21

2.10 Piezoresistive Behavior 21

2.11 Summary 22

Chapter 3 MATERIALS AND METHODS 24

3.1 Materials 24

3.2 Smart Cement 24

3.3 Sample Mixture 25

3.4 Specimen Preparation 26

3.5 Curing Conditions 27

3.6 Density 27

3.7 Rheological Properties 27

3.8 Electrical Resistivity 28

3.8.1 Initial Resistivity of Slurry 29

a) Conductivity Probe 29

b) Digital Resistivity Meter 29

3.8.2 Resistivity during Curing of Cement 30

3.9 Compression Test (ASTM C39) 31

3.10 Piezoresistivity Test 32

Chapter 4 SMART CEMENT CHARACTERIZATION 34

4.1 Density 34

4.2 Rheological Properties 35

4.3 Rheological Models 36

4.4 Rheology of Smart Cement Slurry 39

4.4.1 Effect of Carbon Fibers 39

4.4.2 Rheology Behavior of OWC 41

4.4.3 Model Development 42

4.4.4 Comparison with Existing Models 43

4.5 Electrical Properties 46

4.5.1 Impendence Characterization of Cement 46

4.5.2 Monitoring the Resistivity of Smart Cement during Curing 56

4.5.3 Effect of Admixtures (DC) 57

4.6 Piezoresistivity 59

4.6.1 Theory 59

4.6.2 Piezoresistivite Behavior of Smart Cement 60

4.6 Effect of W/C and Temperature on Properties of Smart Cement 63

4.6.1. Rheological Properties 63

4.6.2 Electrical Resistivity 68

4.6.3 Compressive Strength 73

4.6.4 Relationship between Resistivity and Compressive Strength 74

4.6.5 Piezoresistive Behavior 76

4.7 Effect of Silica fume on Properties of Smart Cement 78

4.7.1 Electrical Resistivity 78

4.7.1 Rheological Properties 79

4.8 Using External Power to Accelerate the Cement Hydration 82

4.10 Summary 85

C h a p t e r 5 SMART CEMENT CONTAMINATED WITH OIL BASED MUD . 87

5.1 Density 87

5.2 Rheological Properties 88

5.2.1 Effect of Contamination 88

5.2.2 Modeling 89

5.3 Electrical Resistivity 92

5.3.1 Initial Resistivity 92

5.3.2 Resistivity during Curing Process 93

5.4 Compressive Strength 95

5.4.1 Effect of Contamination 95

5.4.2. Relationship between Resistivity and Compressive Strength 96

5.5 Piezoresistivity 97

5.6 Summary 103

Chapter 6 CONCLUSIONS AND RECOMMENDATIONS 104

6.1 Conclusions 104

6.2 Recommendations 106

REFERENCES 108

LIST OF FIGURES

Figure 3-1. Typical X-ray-Diffraction (XRD) Pattern for Class H Oil Well Cement 25

Figure 3-2. Schematic diagram of cement specimens 26

Figure 3-3. Digital high speed viscometer 28

Figure 3-4. Schematic illustration of electrical resistivity measurements 30

Figure 3-5. Typical variations of parameter K with AC and DC measurements..... 31

Figure 4-1. Typical shear stress-shear rate relationship for a Bingham-Plastic fluid..... 36

Figure 4-2. Shear stress- strain rate relationship for power law fluid with n<1 37

Figure 4-3. Typical shear thinning behaviour: (a) shear stress vs. shear strain rate, and (b) Viscosity vs. shear strain rate..... 38

Figure 4-4. Variation of shear stress- strain rate Bingham relationships for cement with and without carbon fibers..... 40

Figure 4-5. Relationship between shear stress and shear strain rate for class H oil well cement 41

Figure 4-6. Hyperbolic prediction of shear stress vs. shear strain rate in class H oil well cement 43

Figure 4-7. Prediction of rheology behaviour of cement with Hyperbolic model and the Herschel Bulkley model..... 45

Figure 4-8. Equivalent circuit for case 1, (Vipulanandan & Prashanth et al., 2013)..... 48

Figure 4-9. Equivalent circuit for case 2, (Vipulanandan & Prashanth, 2013)..... 48

Figure 4-10. Comparison of typical responses of equivalent circuits for case 1 and case 2 (Vipulanandan & Prashanth, 2013)..... 49

Figure 4-11. Impedance versus frequency for a) Cement slurry after mixing b) Hardened Cement after 28 days of curing..... 51

Figure 4-12. Initial resistivity of OWC with w/c of 0.38..... 52

Figure 4-13. Effect of various admixtures on initial resistivity of OWC 53

Figure 4-14. Typical bulk resistivity development with curing time..... 55

Figure 4-15. The schematic presentation of conduction paths for a cement paste 55

Figure 4-16. Bulk electrical resistivity development of OWC up to 24 hours of curing.. 57

Figure 4-17. Piezoresistive behavior of cement after 1 day a) Compressive stress vs. change in resistivity b) Change in resistivity normalized by change in stress vs. compressive stress..... 61

Figure 4-18. Piezoresistive behavior of cement after 3 days a)Compressive stress vs. change in resistivity b) Change in resistivity normalized by change in stress vs. compressive stress..... 62

Figure 4-19. Apparent viscosity of cement a) with variable w/c ratios b) at different temperatures..... 64

Figure 4-20. Shear stress- strain relationship for OWC with various w/c at 23℃ and 85℃ 65

Figure 4-21. Experimental data and Hyperbolic model prediction for oil well cement with various w/c ratios 66

Figure 4-22. Variation of yield stress of oil well cement slurry with a) w/c ratio..... 67

Figure 4-23. Effect of w/c ratio and temperature on initial electrical resistivity of OWCs 69

Figure 4-24. Change in resistivity vs. change in Density for cement with various w/c ratios at room temperature (23 °C) 69

Figure 4-25. Bulk electrical resistivity development of OWC with various water-to-cement ratios up to 24 hours of curing..... 70

Figure 4-26. The hyperbolic prediction of the resistivity curves for various w/c ratios... 71

Figure 4-27. Relationship between w/c and A and B paramters of Eq. 4-7 72

Figure 4-28. Compressive strength of cement with different w/cs after 3 days of curing 74

Figure 4-29. Schematic presentation of determination of relationship between the change in resistivity and the compressive strength 75

Figure 4-30. Relationship between bulk resistivity change (RI_{24}) and compressive strength of cement..... 76

Figure 4-31. Piezoresistive behavior of cement with different w/cs and temperature variations..... 77

Figure 4-32. Effect of silica fume on initial resistivity of cement 78

Figure 4-33. Relationship between initial resistivity and percentage of silica fume 79

Figure 4-34. Shear stress- strain relationship and hyperbolic model prediction of cement with a)5% b)10% c)15% d)20% Silica fume. 80

Figure 4-35. Effect of silica fume on yield stress of OWC slurries..... 81

Figure 4-36. Calorimetry of cement with and without the presence of external power ... 82

Figure 4-37. Resistivity response for a) Control sample b) Cement with applied power. 84

Figure 5-1. Experimental data, hyperbolic model and Herschel-Bulkley model prediction of shear stress vs. shear strain rate for a) Uncontaminated b) 0.1% OBM Contaminated c) 1% OBM Contaminated d) 3% OBM Contaminated slurries. 91

Figure 5-2. Initial density and resistivity of the cement slurries with OBM contamination. 92

Figure 5-3. Electrical resistivity response of uncontaminated cement with w/c of 0.38 .. 93

Figure 5-4. Compressive strength development of OBM contaminated cement at 1,7 and 28 days of curing..... 95

Figure 5-5. Linear relationship between 1-day electrical resistivity change and 1-day, 7-day and 28-day compressive strength for uncontaminated and OBM contaminated cement 96

Figure 5-6. Piezoresistive behavior of cement with various OBM contaminations after 1 day of curing 98

Figure 5-7. Piezoresistive behavior of cement without contamination after 1 day of curing a) Compressive stress vs. change in resistivity b) Change in resistivity normalized by change in stress vs. compressive stress..... 99

Figure 5-8. Piezoresistive behavior of cement with 3% OBM contamination after 1 day of curing a) Compressive stress vs. change in resistivity b) Change in resistivity normalized by change in stress vs. compressive stress..... 100

Figure 5-9. Piezoresistive behavior of cement without contamination after 28 days of curing a) Compressive stress vs. change in resistivity b) Change in resistivity normalized by change in stress vs. compressive stress 101

Figure 5-10. Piezoresistive behavior of cement with 3% OBM contamination after 28 day of curing a) Compressive stress vs. change in resistivity b) Change in resistivity normalized by change in stress vs. compressive stress 102

LIST OF TABLES

Table 2-1. Density ranges of various types of cement slurries 9

Table 2-2. Classifications of Oil Well Cement Additives (World Oil Issues, 1995, 1997, 1998, 1999) 13

Table 2-3. Literature review on use of silica as a cement admixture. 15

Table 4-1. Densities of class H oil well cement with different w/c ratios and additives (ppg) 35

Table 4-2. Various rheological models of cement slurries. 39

Table 4-3. Effect of Carbon Fiber Addition on the Rheological Properties of Cement .. 40

Table 4-4. Bingham Plastic, Herschel Bulkley and Hyperbolic model parameters for smart OWC 46

Table 4-5. Summary of electrical resistivity development for cement with water-to-cement ratio of 0.38 in 1 day..... 56

Table 4-6. Resistivity change during curing time for oil well cement with different additives 59

Table 4-7. Herschel Bulkley and Hyperbolic model parameters for various w/c..... 67

Table 4-8. Effect of w/c ratio on density of cement slurries..... 68

Table 4-9. Summary of bulk resistivity parameters for cement with various w/c ratios.. 71

Table 4-10. Hyperbolic model parameters and ultimate resistivity for cement with various w/c ratios 72

Table 4-11. Hyperbolic model parameters for cement with various amount of silica fume replacement 81

Table 4-12. Summary of the calorimetric test for the cement with and without applied current 83

Table 5-1. Effect of OBM contamination on density of cement samples 88

Table 5-2. Summary of rheological model parameters 89

Table 5-3. Electrical resistivity response of uncontaminated and OBM contaminated cement 94

Chapter 1

INTRODUCTION

1.1 General

Petroleum production and exploration has a principal influence on the global economic structure. The world's oil consumption has been growing day by day. It has increased by 171% during the period from 1965 to 2008 (Yahaba et al., 2010). Over the last two decades more than several thousand of wells were drilled and completed throughout the world. Oil and gas wells are drilled to varying depths in many locations and in many harsh environments around the world. A common feature in all of these wells is the well cement. Oil well cement is used to form a sealing layer between the well casing and the geological formation in order to provide zonal isolation. The goal of zonal isolation is to fasten the casing to the borehole wall and to seal off the rock formations. Therefore, this seal must be free of channels and impermeable to gases if the well is to reach its maximum production capability. Improper oil and gas well design and well cementing might jeopardize the oil production.

Oil spills such as the recent Gulf of Mexico deep-water horizon oil spill in 2012 are the dominating reason for oil and gas losses from the existing reservoirs. Moreover, oil spills in marine habitants lead to significant environmental and health disasters. The oil and gas industry has been spending billions of dollars to invent more technologically advanced materials and equipment to improve the extraction of oil and gas. With some of the reported failures and growing interest of environmental and economic concerns in the

industry, integrity of the cement sheath is of major importance. Productive capacity and life of the well is dependent upon the efficiency of the cementing job and cement sheath integrity. Therefore, it is critical to determine the rheology of cement slurry between the casing and surrounding strata, contaminations, setting performance and strength development of the cement during and after hardening. Therefore, there is increasing interest in improving not only the performance, but also the ability to monitor the well cement throughout installation and the operational life of the well and maintaining the oil and gas infrastructures.

1.2 Problem Description

Based on a report by United States Geological Survey (USGS) in 2007, more than 1 million metric tons of cement is being used in oil well drilling, annually. The widespread usage of cement in drilling applications demands further enhancement in the physical, mechanical and sensing properties of the cement from the time of mixing through the service life of well cement. For successful cementing operations two different stages have to be considered. First stage is the placement or dynamic stage and the second is waiting-on-cement or static stage (Smith, 1987). The placement of the cement in the well is associated with numerous uncertainties. The cement slurry is pumped through the casing to fill the space between the formation and the pipe and isolate oil-gas bearing zones. However, due to the complexity of the well path and the formation nature, the actual efficiency of cement placement in the well is unknown to drilling companies. For instance, sometimes there is a crack in the deep rock formation that allows the slurry to escape. Also once the cement has been placed in the well, the drilling may continue after certain cement strength is achieved. Since the company constructing the well cannot

monitor this behavior, it may take a long time to realize the problems. These factors will affect the integrity of the cement sheath. In case of cement failures, fluid formations can flow through the annular space between the casing and the formation. If these fluids reach the surface, it may lead to disastrous blowouts.

The GoM oil spill (also referred to as the BP oil spill) was the largest accidental marine oil spill in history. The oil rig was operated by British Petroleum (BP). It claimed 11 lives following the explosion of the oil rig. A sea-floor oil gusher flowed unabated for 87 days. The estimated total discharge was 4.9 million barrels. One of the biggest questions to come out of the Macondo blowout investigations dealt with the effectiveness of the cement job. The wells are basically inaccessible and the inspection of the cementing job is almost impossible; meaning monitoring their overall health is another major challenge.

1.3 Objective and Scope of the Study

The overall objective of this research study was to develop and characterize “smart” cement with high sensing properties that can be integrated with real-time monitoring of the operations for improving the well integrity through zonal isolation enhancement. By turning the cement slurry to smart piezomaterials, their electrical properties will change when they encounter mechanical stresses, temperature changes and chemical reactions. Hence, the self-sensing ability of oil well cement is achieved. One of the unique aspects of this project was that it was designed to provide information from the cement throughout the life of the well as conditions in the well change over its lifetime. In this report utilization of smart piezoresistive cement and testing methods are broadly discussed. The specific objectives are provided below:

1. The study identified the sensing property that can be used to monitor the setting of the cement and the behavior of cement hardening during the service life.
2. Effect of various curing conditions, temperatures and water-to-cement ratios on rheological, physical and sensing properties of cement was investigated.
3. Effect of oil based mud contamination on sensing properties of smart cement was determined based on up to 3% mud contaminations.
4. Piezoresistive property of cement was studied based on various conditions, and correlations were found to quantify the piezoresistive sensitivity at failure.
5. Quantifications were developed to correlate the electrical resistivity with the other important properties of cement that can help with determination of cement behavior by monitoring its electrical resistivity.
6. Rheological properties of smart cement were determined and a new model was proposed to characterize the flow behavior of cement slurries.

1.4 Organization

This thesis is organized into six chapters. Chapter 2 summarizes the background and literature review related to characterization of oil well cement properties and existing methods to sense the cement-based materials based on their electrical properties. Particularly, studies related to tracking the behavior of the cement by electrical resistivity are reviewed. In chapter 3, materials, admixtures and compositions used for preparing the cement samples are broadly discussed. The experimental procedure and curing conditions for testing of cement is also presented in chapter 3. Chapter 4 discusses about the characterization of smart oil well cement, effect of admixtures and various water-to-cement ratios with respect to the resistivity measurement during and after setting.

Behavior of smart cement contaminated with oil based drilling mud is described in chapter 5. Finally, the conclusions and recommendations of this research work have been summarized in Chapter 6.

Chapter 2

BACKGROUND AND LITERATURE REVIEW

Oil well cementing is the process of placing cement slurry in the annulus space between the well casing and the surrounding geological formations. While drilling fluids can be used to drill a well to a certain depth, the long term stability of the well cannot be achieved by the drilling fluids. Therefore, oil well cement (OWC) was introduced in the late 1920s (Joshi and Lohita, 1997) with the following of objectives: (1) to protect the production zones from the flow of formation fluids, (2) to stabilize the wellbore (3) to protect the casings from collapsing and corrosion, (4) to reduce the risk of ground water contamination by hydrocarbons or salt water, (5) To keep the casing in place, and most importantly (6) to provide a barrier to avoid exchange of fluids among various geological formations. In addition to their exposure to severe temperature and pressure, oil well cements (OWCs) are often designed to comply with weak or permeable formations, corrosive substances, and over-pressured formations.

This chapter provides a review of the literature related to properties of oil well cement. Studies on application of electrical resistivity for characterizing oil well cement slurries and hardened cement are broadly discussed.

2.1 History

Portland cement is a hydraulic product made from limestone and either clay or shale by roasting at 2600 to 3000°F. The high temperature roasts the mixture into material called clinker cement (Smith, 1990). Then, the clinker is ground to a specific size based on the grade of the cement. The size of the cement particles has a direct relationship with

the amount of water that is required to make the slurry without producing free water at the top of cement column (Smith, 1990). Originally Portland cement was used in all oil well drilling applications. It was allowed to set from 10 to 20 days. The demand for rapid hardening led to the use of chemical admixtures in cement to shorten setting time and the early hardening. Hence, special cements that possessed the desirable qualities were developed (Smith, 1990). These were the first oil well cements. These early OWCs appeared to meet the general need of the industry until the drilling of deep wells. Longer placing time and higher bottom-hole temperatures in the deeper sections in some of the wells began to result in the failure of cement to set properly in the well. Because there were many types and brands of Portland cement for various well conditions, the purchasers were often confused about which ones possess the properties needed. Following this, in 1952 the American Petroleum Institute (API) adopted standards for six type of cements used in oil and gas well cementing operations (Smith, 1990).

2.2 Oil Well Cement

Oil well Cementing is an important operation of oil and gas well operations as the productivity of an oil well is significantly affected by the quality of cementing (Becke et al., 1997). The standards of API suggest the chemical requirements determined by ASTM procedures and physical requirements determined in accordance with procedures outlined in API RP 10B and ASTM. There are several types of cements that are being used for oil well cementing based on the oil well conditions. The API specification (API RP 13B-1, 1995) has defined nine different classes of cement, however only Classes A, B, C, G, and H are available from manufacturers and distributed in the U.S. In general, each class is

applicable for a certain range of well depth, temperature, pressure, and sulphate environments. Classes G and H currently are the most widely used cements (Smith et al., 1987). About 80% of the cement used in wells falls into these two categories. Roughly 65% of the well cement made in the U.S. is class H, 15% is Class G, and the rest is either Class A (10%) or C (10%). In international operations, (Smith, 1987) most of the oil well cement used is class G (Canada, Europe, Middle East, South America, and Far East). The grades of OWCs are classified based on the content of Tricalcium Aluminate (C_3A). Compared to the Portland cement, the content of C_3A is less in oil well cement and OWCs are coarsely ground with friction-reducing additives and special retarders in addition to or in place of gypsum (Popovics et al., 1992).

2.3 Properties of Cement Slurries and Set Cement

The quality of oil well cement is important as it will directly impact on various operations during drilling and cementing (Backe et al., 1997). If the quality of cement is bad, it will add unnecessary cost to the drilling operation. But the high quality of cement will provide a high quality supported casing which in turn will have the long-term durability of the wellbore (Pourafshary et al., 2009). In cementing operations and applications, several properties are needed for proper use, which are summarized briefly in the following sections.

2.3.1 Density

Controlling the cement slurry density is critical for placing a column of cement. Heavy cement may fracture the formation and low density cement would allow the flow of formation fluids if the cement is lighter than the pore pressure (Smith, 1990). Barite

and other weighting agents are used to densify the cement slurries (Nelson et al., 2006). The normal density of neat cement slurry is 15 to 17 lb/gal. To achieve lighter cement slurry, bentonite clay may be added to absorb more water to yield a lower cement density (Harms et al., 1981). Ten to 12 lb/gal cement density can be achieved in this manner. Reducing the particle size of the cement by grinding it to a very small size can also lighten the slurry to be in the range of 10 to 12 lb/gal (Davies et al., 1981). Ultra-light-weight cements, using hollow ceramic or glass beads can reduce the overall weight of the cement slurry to less than 9 lb/gal (Harms et al., 1981). Even lower densities are achieved by foaming the cement using a compressed nitrogen gas (Harms et al., 1981). Typical cement densities reported in the literature are summarized in Table 2-1.

Table 2-1. Density ranges of various types of cement slurries

Cement slurry type	**Density (lb/gal)**
Densified and weighted	16 - 22
Neat Slurry	14 -18
High water ratio slurries	11 - 15
Ceramic bead extended slurry	9.5 -12
Glass bubble extended slurry	7.5 -12
Foam cement	6 -12

2.3.2 Water-to-cement Ratio

The specific weight of certain dry cement regulates the minimum or maximum amount of water that can be added. The minimum amount of water, from the aspect of

density, is greater than the stoichiometric quantity necessary for proper setting (Fink et al., 2012). If more than the maximum amount of water is used, pockets of free water will be formed in the set cement column. Hence, typical amounts of water used in oil well cement range from 38 to 46% in the final mixture (Fink et al., 2012).

2.3.3 Rheological Properties

The viscosity of cement affects its pumping properties. The viscosity must be kept low enough to ensure pumpability of the slurry during the entire operation period. In deeper wells, because of the increased temperature, the viscosity decreases due to thermal thinning. This leads to an unwanted flow characteristics (Reddy et al., 2004). Knowledge of the rheological properties of oil well cement are important to optimize cement slurry viscosity to maximize the displacement and safe circulating pressures (Olowolagba & Brenneis, 2010). Viscosifying additives are often used in well cement compositions to prevent the settling of solids in the cement compositions after they are placed in a subterranean zone (Fink et al., 2012) . Undesirable cement rheological properties results in the settling of solids in cement compositions, which results in defective cementing and failure of the set cement to provide zonal isolation (Reddy et al., 2004).

2.3.4 Rheological Models

Existing empirical and time-independent rheological models (Power law, Bingham, Herschel- Buckley, Modified Bingham and Casson model) allow representing shear stress, shear strain rate and viscosity. The estimated rheological properties can vary significantly when calculated using various models (Nehdi and Rahman, 2004). The Bingham plastic model and the Power law model are widely used in the petroleum

industry to describe the flow properties of cement slurries (Guillot, 2006). The Bingham plastic model includes both yield stress and a limiting viscosity at finite shear rates, which the Power law model fails to consider. Herschel-Bulkley model does not have such limitation and can predict the nonlinear shear-thinning/shear-thickening behavior of OWCs, by

$$\tau = \tau_o + k\dot{\gamma}^n, \tag{2-1}$$

If the exponent n is less than one the fluid exhibit shear thinning behavior and when n is greater than 1 fluid becomes shear thickening. Shear thinning is when the apparent viscosity of the fluid decreases with the increase in shear rate. Shear thickening is when viscosity of the cement slurry increases with the shear rate (Shahriar, 2011).

2.3.5 Fluid Loss

Fluid loss refers to the unwanted migration of the liquid part of the drilling mud or cement slurry into a formation. Losses may occur when the fluid comes in contact with a porous formation. This is relevant for drilling and completion fluids, fracturing fluids, and cement slurries. The suspended particles in the fluids move from the borehole into the formation. The particles will gradually accumulate and form a filter cake. The hydrodynamic forces acting on the suspended colloids determine the rate of cake buildup and therefore the fluid loss rate (Fink et al., 2012). Fluid loss tests are performed using the procedures recommended by API (API Recommended Practices 10B-1) at high pressure, high temperature (HPHT) conditions.

2.3.6 Thickening Time

The thickening time covers the time over which the cement can be effectively pumped and placed after mixing with water. It is similar to polymerization of thermosetting resins. Viscosity increases with time after this point, because of the setting reaction. When the viscosity becomes too high, the slurry is no longer pumpable. The cement must remain fluid long enough to be pumped to its desired location in the borehole (Sabins et al., 1986). It is therefore necessary to place the cement within a certain time after mixing; otherwise, serious damage to the well could occur (Fink et al., 2012).

2.3.7 Setting Time

Setting time of oil well cement is very important for management and of control the cementing operations (Zhang et al., 2010). The viscosity of the cement slurry will increase after setting and it will be difficult to pump. Hence it is important that the cement does not reach its setting before the cement slurry is properly placed in the annulus (Smith et al., 1990). Water to cement ratio (w/c), fineness and composition of cement, admixture incorporation, temperature and pressure will affect the setting time of cement (Taylor et al., 1997).

2.3.8 Compressive Strength

The casing and cement sheath are submitted to various types of loading during the drilling, completion, and production. Compressive strength of cement determines the ability of cement to stabilize casing in the wellbore (Thiercelin et al., 1998) and it

depends on the hydration process (Harder et al., 1993). Increase in the compressive stresses and can lead to cement damage.

2.4 Oil Well Cement Additives

A wide variety of cement admixtures are currently available to enhance the OWC slurry properties and achieve successful placement between the casing and the geological formation, rapid compressive strength development, and adequate zonal isolation during the lifetime of the well. In the world oil issues publications comprehensive listings of cementing products and additives available from major suppliers can be found, grouped into functional categories as shown in Table 2-2.

Table 2-2. Classifications of Oil Well Cement Additives (World Oil Issues, 1995, 1997, 1998, 1999)

Additives for Cementing
Accelerators and salts
Extenders and density-reducing additives
Silica to reduce high temperature strength retrogression
Dispersants
Bond improving and expanding agents
Retarders
Fluid loss agents
Anti-gas migration agents
Free water control and solid suspending agents
Antifoam and defoaming agents
Additives and mixtures to reduce or prevent lost circulation
Density-increasing or weighting agents
Free water control and solid suspending agents

For example Roshan (2010) found that addition of carboxymethylcellulose (CMC) polymer along with some other additives with the oil well cement improved early compressive strength and rheological properties as well as enhancing the permeability of cement. Choolaei (2012) studied the effect of silica nano-particles on cement mortars. His work indicated that SiO_2 nanoparticles improved the flow characteristics of cement slurries. It was also reported that addition of nano-silica to cement led to an increase in the compressive and flexural strengths of the cement mortars. Nano-silica helped to reduce the free water in the designed cement slurries. Addition of nano-silica to cement accelerated the hydration by reducing the setting time and the length of the dormant period.

2.4.1 Silica fume

Silica powder has been studied as a stabilizer for oil well cement at high temperatures (Zhang, 1993). Muller and Dillenbeck (1991) experimental results indicated that silica fume improved the stability and pressure resistance strength of cement. The positive effect on the strength regression at increased temperatures is due to a greater rate of carbonation of the set cement (Milestone et al., 1986). The high amount of silica used in oil well cement will reduce the effect of cement strength retrogression in temperature above 110°C (230°F) where cement is degraded very quickly (Gibson et al., 2011). The use of silica fume was found to decrease the permeability only slightly (Banthia et al., 1989). The summarized information on silica fume in the literature is presented in Table 2-3. Silica fume up to 40% has been used as additive to OWC. No rheological and sensing properties of cement have been quantified with the addition of silica fume.

Table 2-3. Literature review on use of silica as a cement admixture

Reference	Cement type	Type of silica	Amount (by the weight of cement)	Remarks
Banthia and Mindess (1989)	Portland Cement	Silica Fume	5-15%	Slight decrease in permeability Tensile strength was improved
Squyres and Lopez (1990)	Oil well cement class H	Silica Fume	10-20%	Substitute by natural pozzolan Acceleration in strength development
Muller and Dillenbeck (1991)	Oil well cement class G	Silica Fume	20- 35%	Dramatically reducing the permeability
Chung (2003)	Portland cement type I	Silica Fume	15%	Increasing the tensile and compressive strength Improving the fiber dispersion
Santra (2012)	Oil well cement class H	Silica Fume	10%	Accelerated the early hydration, Dispersion is a challenge in lower percentages
Gibson (2011)	Oil well cement class G	Liquid Silica	35-40%	Prevented strength retrogression
Remarks	Silica is widely as an admixture in oil well cement.	Silica fume is a common cement additive	Typically 10-20% of silica is used for strength improvement, and 30-40% of silica is used for high-temperature cement applications.	**Silica is highly used in oil well cement to increase the strength and reduce the permeability. Rheological and sensing properties has not been addressed**

2.4.2 Carbon Fibers

Carbon fibers have remarkable electrical properties and other unique characteristics. As a result of these properties coupled with high aspect ratio, small diameter, lightness, and excellent chemical and thermal stability. Carbon fibers can be used as reinforcement to produce multifunctional cement-based composites. The carbon fiber-cement composites present superior mechanical properties (e.g., high compressive, tensile and flexural strengths, and fracture toughness) electrical and thermal conductivity. The electrical behavior of carbon fiber-cement composites is relevant to the use of these composites for developing intrinsically self-sensing composites, which means composites themselves are also sensors. The self-sensing property of the cement composites modified with carbon fibers can be used in developing smart structures for health monitoring of structures, highway traffic monitoring and border security management (Han et al., 2012).

2.5 Hydration of Oil Well Cement

The chemical reaction of cement with water that results in setting and hardening of cement is called hydration. Cement hydration begins as soon as cement comes in contact with water (Smith et al., 1990). This reaction forms a stone like mass which is referred to as hardened cement.

2.5.1 Chemical Reactions during Hydration

When cement is mixed with water, the binding phases in Portland cement (Ca_3SiO_5, Ca_2SiO_4, $Ca_3Al_2O_4$, and $Ca_4AlnFe_{2-n}O_7$) react in different ways. During hydration of Portland cement, due to the chemical reactions between the clinker components, calcium

sulfate and water, cement slurry begins thickening and hardening continuously. More than 80% of the total composition of the Portland cement consists of the silicate phase. Calcium silicate hydrate and calcium hydroxide are the products of hydration of both tricalcium silicate (Ca_3SiO_5) and dicalcium silicate (Ca_2SiO_4) which is shown by (Natarajan et al., 2005),

$$2\ Ca_3SiO_5 + 7\ H_2O \rightarrow 3\ CaO \cdot 2\ SiO_2 \cdot 4\ H_2O + 3\ Ca(OH)_2, \text{ and} \quad (2\text{-}2)$$

$$2\ Ca_2SiO_4 + 4\ H_2O \rightarrow 3\ CaO \cdot 2\ SiO_2 \cdot 4\ H_2O + Ca(OH)_2. \quad (2\text{-}3)$$

The main product of the hydration reactions is the calcium Silicate hydrate (C-S-H) gel. CSH gel is the principal binder of hardened cement. CSH gels cover 70% of fully hydrated Portland cement. At short hydration times, $Ca_3Al_2O_4$ (aluminate phases) are the most reactive phase of the cement. Aluminate phases have a significant influence upon the rheology of the cement slurry and early strength development of the set cement. But their presence is relatively small compared to the silicates. Chemical reactions of Tricalcium aluminates ($Ca_3Al_2O_4$) during hydration are given by (Natarajan, 2005),

$$2Ca_3Al_2O_4 + 27\ H_2O \rightarrow Ca_2{\cdot}Al_2O_3{\cdot}8H_2O + Ca_4{\cdot}Al_2O_3{\cdot}19H_2O. \quad (2\text{-}4)$$

The calcium aluminate hydrates (C_2AH_8 and C_4AH_{19}) will be converted into more stable form ($Ca_3{\cdot}Al_2O_3{\cdot}6H_2O$) from its metastable form by the reaction as (Natarajan, 2005),

$$Ca_2{\cdot}Al_2O_3{\cdot}8H_2O + Ca_4{\cdot}Al_2O_3{\cdot}19H_2O \rightarrow 2\ Ca_3{\cdot}Al_2O_3{\cdot}6H_2O + 15H_2O. \quad (2\text{-}5)$$

2.5.2 Kinetics of Hydration

Cementitous materials have a complex hydration process and microstructure, varying in time and depending on the composition, admixture incorporation and temperature. The

hydration of cement is described by the growth of each cement particle on its own surface which is referred to as the nucleation growth (Xiao & Li, 2008). Upon the hydration of cement, each cement particle forms a type of growth on its surface that gradually spreads until it links up with the growth from the other cement particles or adheres to adjacent substances (Smith, 1990).

The degree of hydration describes the process of hydration, and directly relates to the fraction of the hydration products or porosity in a hydration system that governs the properties of cement-based materials (Ye at al., 2003). The hydration of cement-based materials leads to a continuous decrease in the amount of porosity due to the increase in hydration products. The degree of hydration, porosity and strength development in a hydration system are directly related (Xiao et al., 2008).

2.6 Contamination of Well Cement with Oil Based Drilling Mud

Oil based drilling mud (OBM) is one of the commonly used muds in well drilling. OBM contamination can have a severe impact on cement performance in wellbores. Contamination of cement with OBM will affect the quality of cementing job. Harder and Carpenter (1993) studied the effect of oil based mud contamination on cement. Their laboratory tests indicate that OBMs, even at very low concentrations are extremely detrimental to cement performance. Limited studies have been done to characterize the effect of mud contamination on cement; however monitoring the cement to detect the contamination and other properties during hydration has not been addressed.

2.7 Durability of Hardened OWC Slurries

Cement-based materials are subjected to deterioration under aggressive environments. The extreme temperature cycling of the well bore results in severe mechanical damage

and ultimate failure of the cement sheath, potentially leading to channeling and deboning of cement from the casing (Saidin et al., 2008). The rate of deterioration is generally aggravated at high temperature and pressure such as in the case of oil and gas bores. A strict control of cement reactivity and mechanical properties during the life cycle of the well is thus very important. The oil well cemented system should meet a wide range of short-term criteria such as free water, thickening time, filtrate loss, development of strength and shrinkage. In addition to various long-term requirements including resistance to chemical attack, thermal stability and mechanical integrity of the cement sheath (Ravi et al., 2002).

2.8 Continuous Monitoring of Cement

Several methods have been used by researches to characterize the behavior of cementitous materials, such as calorimetry, ultrasonic methods, X-ray diffraction and image analysis. However, different methods give different results for the degree of hydration due to the different criteria (Ye et al., 2003).

The traditional API tests' include procedures for finding density, free water, fluid loss, compressive strength, thickening time, rheology, and gel strength. All these tests are important for composing a successful cement composition, but most of them consider only one or a few points of time during the setting process, or only the time period before the start of the hardening process. Thus, no continuous description of the entire setting process of cement is obtained (Backe & Lyomov, 2001). The only procedure for tracking the entire setting process that has won some acceptance is the ultrasonic cement analyzer (UCA) which estimates the cement compressive strength from the sound velocity through a cement sample (Rao et al., 1982). Although UCA can be used throughout the entire

setting process over several days or weeks, but has several limitations (Backe & Lyomov, 2001).

2.9 Oil well Cement by Electrical Resistivity

Electrical resistivity measurement has been applied by many researches on concrete and cement applications (Taylor 1974, McCarter et al., 1994, McCarter et al., 2000, Baoguo et al., 2008, Xiao et al., 2008, Banthia, 2012, Liao et al., 2014). However, there are no reports in the literature of electrical resistivity measurements for characterizing oil well cement. Electrical response characteristics measurement has appropriate sensitivity in monitoring the characteristics of cementitious materials (Mc Carter et al., 2000). Wei (2008) and Han (2012) have applied electrical measurement methods to study the microstructural evolution in hydrating cement-based material systems. The advantages in using this technique include its accuracy, easy test procedure, and nondestructive characteristics (Li et al., 2003). Additionally this method can be used for monitoring the long term behavior of cement in practice (Vipulanandan and Heidari, 2014).

2.9.1 Factors Effecting Resistivity of Cement

Electrical resistivity of cement is affected by a number of factors such as pore structure, pore solution composition, cementitious content, w/c ratio, moisture content and temperature (Polder et al., 2001). Electrical conduction occurs primarily due to ion transport through the pore solution in a cement-based system. It is strongly dependent on both pore solution conductivity and porosity (Wei and Li, 2012). Therefore chemical reactions and change in microstructure of cement during the hydration process affects the electrical resistivity response of the cement-based composites (Wei, 2014).

2.9.2 Factors Effecting Resistivity Measurements

As reported by Chung (2001), interfacial factors are important in obtaining electrical resistivity from electrical resistance. Due to the voltage present during electrical resistance measurement, electric polarization occurs as the resistance measurement is made continuously. The polarization results in an increase in the measured resistance. The conventional methods of measuring the electrical resistivity of cementitious materials can be categorized into direct-current (DC) methods and alternating-current (AC) methods, both of which require electrodes for their measurements. Therefore, there is the potential for contact problems between the electrodes and the matrix, which could completely affect the accuracy of the measurement (Zuo and Wei, 2014). Zhang (2014) suggested that replacing the DC measurement with the AC measurement can eliminate the polarization effect.

2.10 Piezoresistive Behavior

Banthia (1994) observed that strength and durability of concrete was improved by the addition of small amounts of fiber-reinforcement. Due to the fiber's high resistance to wear, heat, and corrosion, carbon fiber-reinforced concrete in particular has been shown to have excellent durability properties. Also, Chung (1996) reported that addition of carbon fiber to cement provided the strain-sensing ability and increased the tensile and flexural strengths, tensile ductility and flexural toughness, and decreased the drying shrinkage.

Chung (2001) studied the electrical resistivity of carbon fiber-reinforced cement paste and the electric polarization effect. By increasing the conductivity of the cement paste through the use of carbon fibers that were more crystalline the polarization effect

diminished. It was concluded that when the four-probe method was used, voltage polarity switching effects were dominated by the polarization of the sample itself, but when the two-probe method was used, voltage polarity switching effects were dominated by the polarization at the contact sample interface. Vipulanandan et al., (2004, 2006-2012) have studied the piezoresistive behavior of modified cementitious and polymer composites. The studies showed that the changes in resistivity with the applied stress were 30 to 50 times higher than the strain in the materials. Hence the change in resistivity has the potential to be used to determine the integrity of the materials.

2.11 Summary

Based on the review of literature related to oil well cement characterization and methods of monitoring the cementitous materials, the following can be summarized:

1. Various additives have been used to alter the setting time of cement slurry and also to improve early compressive strength, flexural strength of the cement mortar.
2. Silica fume is a common oil well cement additive which improved the compressive strength and the permeability of cement, and prevents the cement strength retrogression.
3. The most importance of using carbon fiber in cement was to enhance the pressure sensing ability of carbon fiber-cement composites.
4. Electrical resistivity is a good parameter to monitor the behavior of concrete and cement composites.
5. There have been no reports in the literature about characterization of oil well cement by electrical resistivity.

6. Accurate measurement of electrical resistivity is a challenge due to high interfacial factors.
7. Many researches have suggested the use of AC resistivity measurements to minimize the effect of polarization.
8. Modifying the cement with carbon fibers will turn it self-sensing materials which can be used in health monitoring of the structures.
9. Contamination of cement with oil based mud will reduce the compressive strength of cement and cause delays in drilling operations.

Chapter 3

MATERIALS AND METHODS

In this chapter, types of materials and testing methods used in this study are summarized. Fabrication of smart cement and cement testing is included. Sample preparation, density test, compression test, method of electrical resistivity measurement and the curing conditions are discussed.

3.1 Materials

In this study commercially available Class H oil well cement was used. A typical XRD pattern of Class H cement is shown in Fig. 1-1, where major constituents of the cement have been identified. The major constituents in the cement included tricalcium silicate (Ca_3SiO_5), dicalcium silicate (Ca_2SiO_4) calcium aluminoferrite (Ca_2FeAlO_5), calcium sulfate ($CaSO_4$) and magnesium sulfate ($MgSO_4$). Effect of carbon fiber modification to the cements with and without additives such as silica fume (SF) and polycarboxylate (PC) were investigated.

3.2 Smart Cement

Effect of carbon fibers on sensing properties of cementitious materials have been discussed by many researchers (Azhari et al. 2012, Baeza et al. 2013, Chung et al. 2000-2005, Vipulanandan et al. 2006-2014). Enhancement in sensing properties of oil well cement was achieved by mixing low percentages of lab modified carbon fibers with all the cement slurries. The concentration of carbon fibers was in the range of 0.1%-0.2% by the weight of cement (BWOC). The carbon fibers used in this study were pitch-based

fibers with diameter of 14.5μm, electrical resistivity of 148 μΩ.m and specific gravity of 1.62.

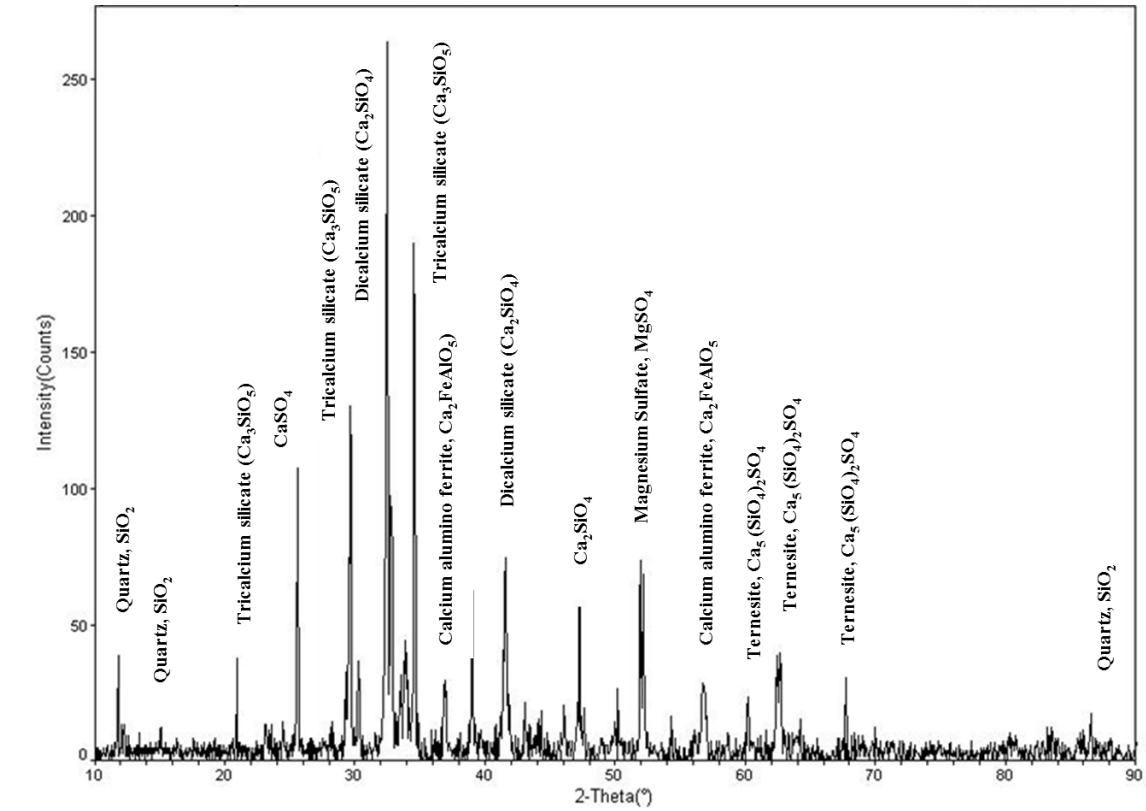

Figure 3-1. Typical X-ray-Diffraction (XRD) Pattern for Class H Oil Well Cement

3.3 Sample Mixture

The API practice recommendation was used in preparing the samples. The cement slurries were prepared using a high-shear blender type mixer with bottom driven blades according to the following procedure. First, the weighed amount of cement and the solid admixture were mixed in a container by hand or using a rod for about one minute. The mixing water was then poured into the blender. Then the required quantity of liquid additive (if any) was added into the mixing water using a needle, and the mixing started at a slow speed for about 15 seconds so that additives could be properly dispersed in the liquid solution. The cement solid additives were added to the liquids over a period of 15

seconds. Manual mixing was conducted for 15 seconds and a rubber spatula was used to recover material sticking to the wall of the mixing container to ensure homogeneity. Finally, mixing resumed for another 35 sec at high speed. This mixing procedure was strictly followed for all cement slurries. All mixing was done at an ambient room temperature of 23±2°C. The total time between the beginning of mixing and the start of the rheological and electrical resistivity tests was kept constant to avoid the effect of external variables on the results. The water-to-cement ratio in all formulation in this study was varied from 0.38 to 0.54.

3.4 Specimen Preparation

After mixing, specimens were prepared using cylindrical molds with diameter of 2 inches and a height of 4 inches. Two conductive wires were placed in all of the molds. The vertical distances between any two wires were the same. Embedment depth of the conductive wire was 1 inch, as shown in Fig. 3-2. In order to have consistent result, at least three specimens were prepared for each type of mix.

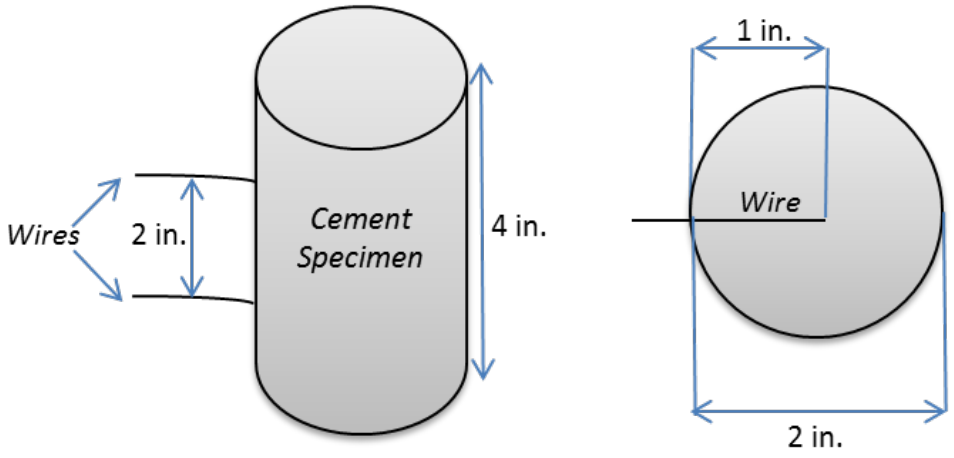

Figure 3-2. Schematic diagram of cement specimens

3.5 Curing Conditions

For each experiment one series of sample was selected as the baseline without any additives and was cured in room temperature. These specimens were air cured under the room temperature of 23±2˚C. In order to investigate the effect of temperature, a series of specimens were placed inside the oven with temperature of up to 85±2˚C, with and without putting in sealing conditions. Some of the high temperature cured specimens were kept in saturated sand to avoid the loss of water. The weight of specimens was measured during curing time to ensure the water loss was minimal.

3.6 Density

The density plays the major role in providing hydrostatic pressure in the wellbore. Density of slurries measured immediately after mixing using standard mud balance cup.

3.7 Rheological Properties

Rheological properties determine the pump ability and workability of cement. Workability of the cement is the energy required to handle and finish a cement mixture, and pump ability is related to the required energy to initiate the flow of the slurry.

The rheology tests were performed by utilizing a high speed viscometer as shown in Fig. 3-3. This device is a coaxial cylinder rotational viscometer, which employs a transducer to measure the induced angle of rotation of the bob by a fluid sample. Once the cement slurry is placed in annulus between the bob and the up, the viscous drag exerted by the fluid creates a torque on the bob, and is monitored by the transducer that measures the angular displacement of the bob. Using the angle of displacement of the bob, the processor calculates the output of the cement rheology characteristics.

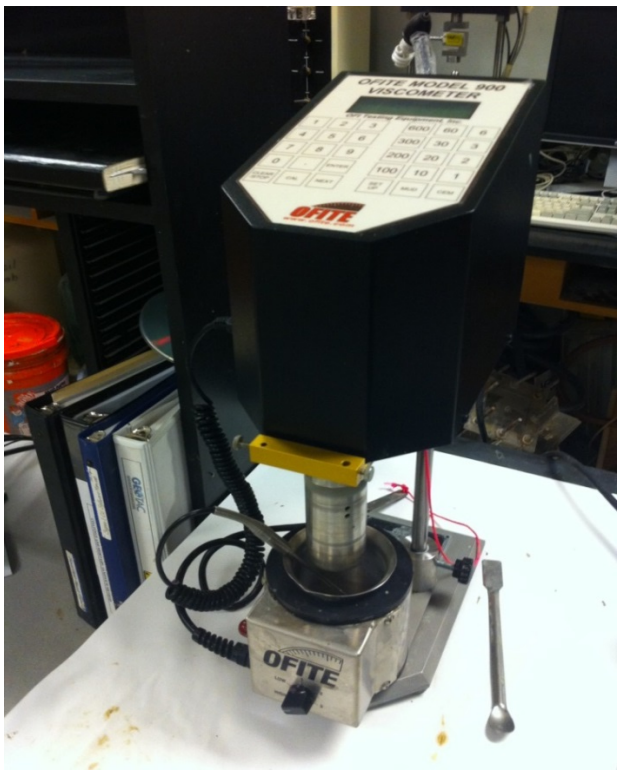

Figure 3-3. Digital high speed viscometer

The rheological properties of cement slurries were measured at room pressure and various temperatures at rpms ranging from 3 to 600, and related shear stresses were recorded. The speed accuracy of this device was 0.001 rpm. The temperature of the slurry was controlled through the predefined temperature threshold within the range of ±2˚C. The viscometer was calibrated using several standard solutions. All the rheological tests were performed after 10 minutes of mixing the cement slurries.

3.8 Electrical Resistivity

It was very critical to identify the sensing properties for the cement that can be used to monitor the performance. After numerous studies and based on the current study on oil well cements, electrical resistivity (ρ) was selected as the sensing property for cement-based materials (Vipulanandan et al., 2004-2013). Hence two parameters (resistivity and

change in resistivity) were used to quantify the sensing properties of cement. Electrical resistivity is given by

$$\rho = R(\frac{L}{A}) = R.K\ , \tag{3-1}$$

where R is electrical resistance, L is the linear distance between the electrical resistance measuring points, A is the effective cross sectional area and K is calibration parameter determined based on the resistance measurement method. Normalized change in resistivity with the changing conditions is represented as

$$\frac{\Delta\rho}{\rho} = \frac{\Delta R}{R}\ . \tag{3-2}$$

3.8.1 Initial Resistivity of Slurry

Different methods were used for resistivity measurements of OWC slurries. To assure the repeatability of the measurements, the initial resistivity was measured at least three times for each cement slurry and the average resistivity was reported.

a) Conductivity Probe

Commercially available conductivity probe was used to measure the conductivity (inverse of resistivity) of the fluids. In the case of cement, this meter was used during the initial curing of the cement. The conductivity measuring range was from 0.1μS/cm to 1000 mS/cm, representing a resistivity of 10,000 Ω.m to 0.1 Ω.m.

b) Digital Resistivity Meter

This device is used in the Petroleum industry to measure resistivity. It measures resistivity in the range of 0.01 Ω.m to 400 Ω.m.

3.8.2 Resistivity during Curing of Cement

Studies have shown that due to the voltage present during electrical resistance measurement, electric polarization occurs as the DC resistance measurement is made continuously. The polarization results in an increase in the measured resistance (Chung et al., 2001). In this study high frequency AC measurement was adopted to overcome the interfacial problems and minimize the contact resistances. Electrical resistance was measured using Agilent E4980A LCR meter during the curing time. This device has a least count of 1 μΩ for electrical resistance, and measures the impendence (resistance, capacitance, and inductance) in the frequency range of 20 Hz to 300 kHz. Each specimen was first calibrated using the same cement slurry to determine the parameter K and obtain the electrical resistivity (ρ) from the measured electrical resistance (R), based on the Eqn. 3-1. This calibration is needed to eliminate the errors in the measurements. Hence, L/A in equation 3-1 is replaced by an experimentally found calibration factor (K). The principle of measuring the resistivity during curing is shown in Fig. 3-4.

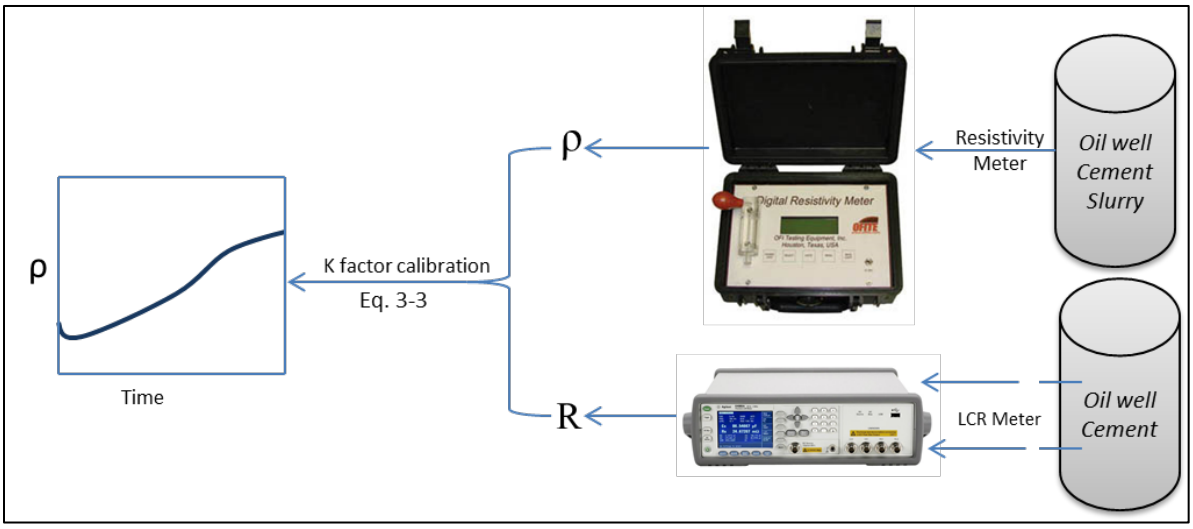

Figure 3-4. Schematic illustration of electrical resistivity measurements

In Fig. 3-5, variations of calibration parameter K are shown in logarithmic scale. Also a comparison between K parameter with DC and AC measurements is presented. It was evident that measuring the resistance with AC reduced the fluctuation in K parameter when using the two wire method. With AC measurement the variations in K parameter in two hours was 2300%, whereas for the same slurry, K value changed only 10% when the 300 kHz AC resistance measurement was adopted. Hence AC method can be used for calibration of the resistivity based on the resistance in two wire method.

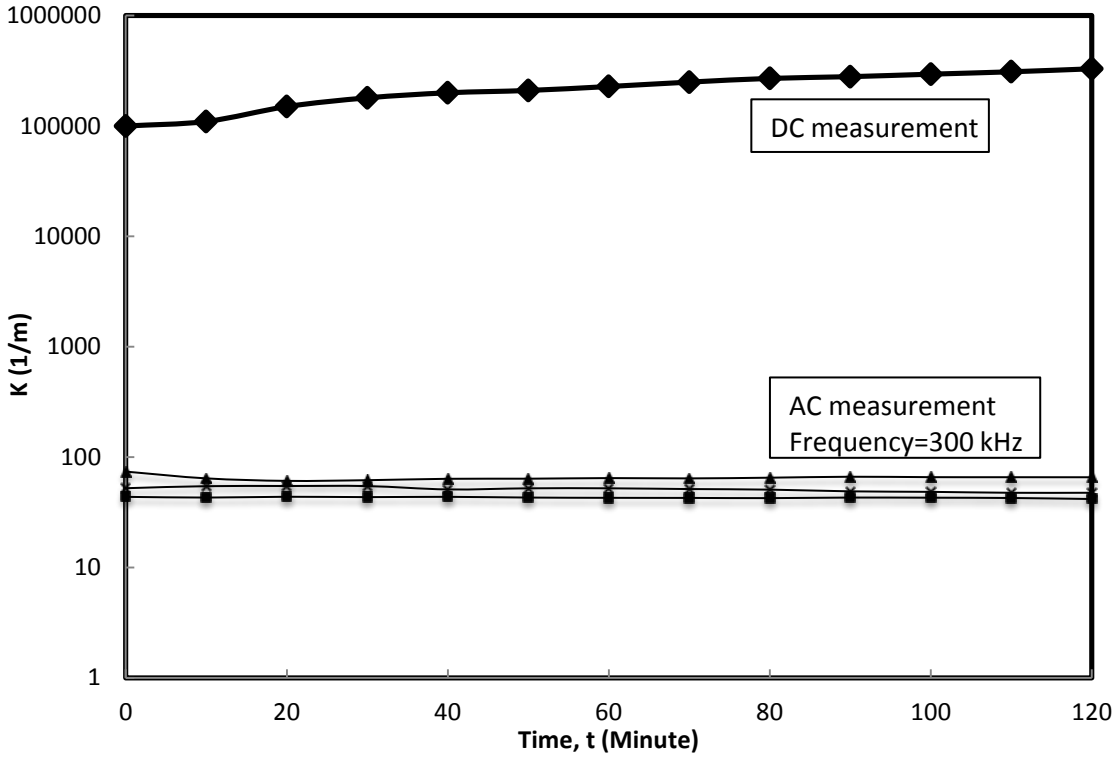

Figure 3-5. Typical variations of parameter K with AC and DC measurements

3.9 Compression Test (ASTM C39)

The cylindrical specimen was capped and tested at a predetermined controlled displacement rate. Ultimate compression load of the specimen could be determined from the test. The dimension of the specimen was measured using Vernier caliper and entered

into the computer as an input to calculate the stresses. Compression tests were performed on cement samples at various curing ages curing using at the room temperature (23 ±2˚C).

3.10 Piezoresistivity Test

Piezoresistivty describes the change in electrical resistivity of a material under pressure. Since oil well cement serves as pressure-bearing part of wells in real applications, the piezoresistivity of smart cement was investigated under compressive loading. During compression testing, electrical resistance was measured in the stress axis. To eliminate the polarization effect, AC resistance measurements were made using a LCR meter at frequency of 300 kHz. Then, change in resistivity was related to the applied stress.

3.11 Summary

Based on the above discussions following conclusions are advanced:

1. The rheological properties of cement slurries were measured using standard high shear viscometer and the rheological parameters were determined by analyzing the test data.
2. For measuring the resistance, AC measurements were performed from low to high frequency and the behavior of material was characterized based on the impendence response.
3. Standard electrical resistivity meter was used to calibrate each specimen to determine the true resistivity of cement.

4. Tinius olsen machine were used to perform compression test of oil well cement under room pressure and the room temperature conditions.
5. The piezoresistivity test was done for cement with various compositions and different curing conditions and piezoresistive sensitivities of various samples were evaluated.

Chapter 4

SMART CEMENT CHARACTERIZATION

The main purpose of this chapter is to characterize the behavior of smart cement, in order to monitor the chemi-resistive behavior of oil well cement initially, during setting, and after hardening. Cement with various water/cement ratios was and cured in different conditions to investigate the effect of these parameters on the smart cement. Cement with various water-to-cement ratios was tested at low and high temperatures to evaluate the effect of w/c and temperature on electrical, rheological and physical properties of smart OWC. Silica fume was used as a modifying agent to confirm the sensing properties of smart cement in the presence of additives. Also compressive piezoresistive behavior of oil well cement was investigated as the sensing property.

4.1 Density

The average density of each specimen was measured immediately after mixing. From the Table 4-1, the average density of oil well cement slurry with water-to-cement ratio (w/c) of 0.38 was 16.36 ppg or 1960 kg/m^3. The density with the addition of 0.1% carbon fibers was 16.47 ppg; hence the addition of 0.1% of carbon fibers (CF) had minimal effect on the density. The density of 10% silica fume (SF) slurry was 4% more than the normal oil well cement. This difference was because of the higher density of silica fume compared to the oil well cement. It was found that increasing the water-to-cement ratio from reduced the density of the cement. The density of the slurry with water-to-cement ratio 0.54 was 3% lower compared to the slurry with the water-to-cement ratio of 0.38.

Table 4-1. Densities of class H oil well cement with different w/c ratios and additives (ppg)

Time	W/C = 0.38						W/C= 0.44	W/C= 0.54	Remarks
	0% CF	0.1% CF	5.0% SF	10% SF	15% SF	20% SF	0.1% CF	0.1% CF	
After mixing	16.36	16.48	16.85	16.99	17.12	17.36	16.12	15.78	Density varied from 15.84 to 17.36
Remarks	Minimal effect on density		Addition of Silica fume increased the slurry density				Increasing the w/c ratio reduced the density		

4.2 Rheological Properties

The rheological properties of an oil well cement (OWC) slurry determines the quality of the final product and helps predicting its end use performance and physical properties during and after processing. Rheological measurements can determine the flow properties of the cement slurry such as its plastic viscosity, yield point, frictional properties and gel strength. Rheology studies the flow of fluids and deformation of solids under stress and strain. In shear flows, imaginary parallel layers of liquid move over or past each other in response to a shear stress to produce a velocity gradient, referred to as the shear rate, which is equivalent to the rate of increase of shear strain (Douglas et al., 1995).

The viscosity, μ, of a fluid is the ratio of the shear stress, τ, to the shear rate, $\dot{\gamma}$ as given by

$$\mu = \frac{\tau}{\dot{\gamma}} \ . \tag{4-1}$$

In common oilfield units, the unit of viscosity is the centipoises (cp) and in SI unit, it is the Pascal-sec (Pa.s).

4.3 Rheological Models

Three rheological models have been applied in characterization of rheological properties of drilling fluids and cement slurries: Bingham plastic, power law, and Herschel-Bulkley (HB). These models cover various ranges of the yield-stress values that will be encountered in the field. Generally, in terms of rheological properties, fluids are classified into two groups: Newtonian and non-Newtonian. Newtonian fluids follow the Newtonian model represented by Eq. 4-1, in which the shear stress is proportional to the shear rate. To characterize the behavior of these models Bingham plastic model was introduced as

$$\tau = \tau_0 + \mu_p \dot{\gamma}, \tag{4-2}$$

where τ_0 is the yield point and μ_p is the plastic viscosity or the slope of the straight line in Fig. 4-1.

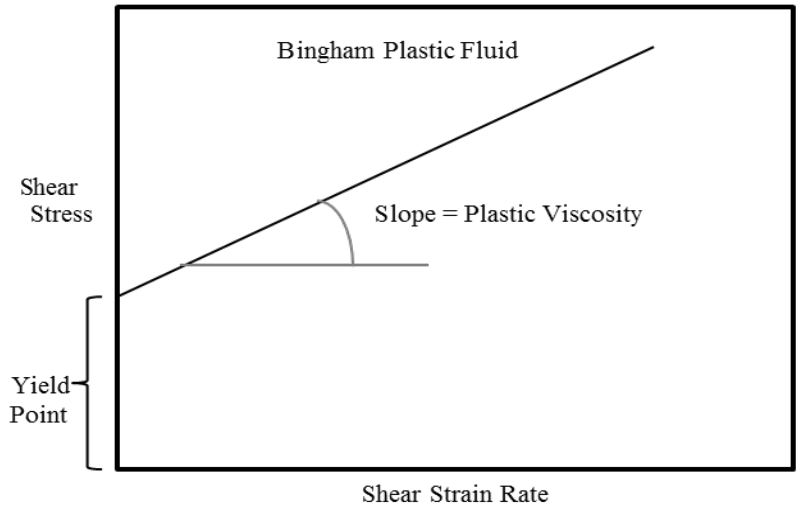

Figure 4-1. Typical shear stress-shear rate relationship for a Bingham-Plastic fluid

Unlike Newtonian fluids, the viscosity of non-Newtonian fluids depends on the applied shear rate and the time during which the shear rate is applied. The fact that the viscosity depends on the shear rate means that the tested sample does not have a constant viscosity. Thus, the relationship between shear stress and shear rate is not linear as shown in Fig. 4-2.

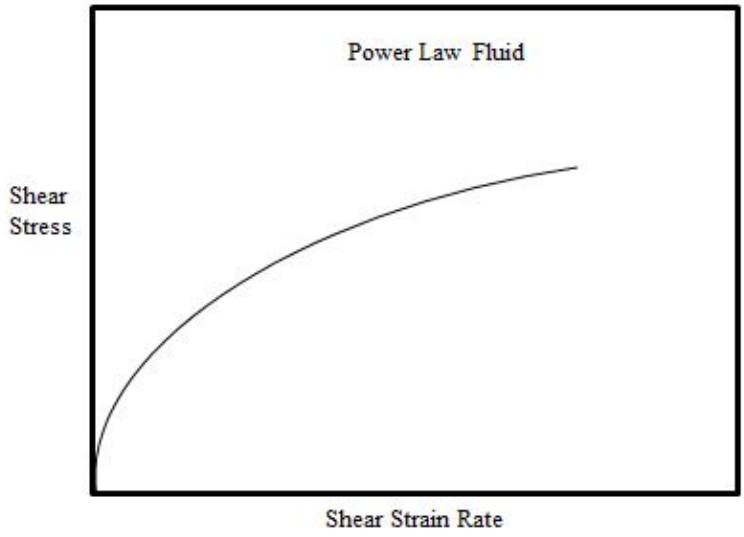

Figure 4-2. Shear stress- strain rate relationship for power law fluid with n<1

The Power-law fluids curve passes through the origin and is described by the Eq. 4-3:

$$\tau = k\dot{\gamma}^{n}, \tag{4-3}$$

where $\tau, \dot{\gamma}$, k and n represent the shear stress, consistency, shear rate, and power law exponent, respectively. The power law represents the case of zero yield stress, while at the Bingham plastic model covers the case where the yield stress (τ_o) equals the yield point (Power et al., 2003).

Herschel-Bulkley model combines Power-law and Bingham plastic behaviors of fluids through the equation 4-4, as

$$\tau = \tau_o + k\dot{\gamma}^n , \tag{4-4}$$

where τ, $\dot{\gamma}$, k and n are the same as the power law model and τ_o presents the yield stress (the shear stress at zero strain rates). Cement slurries are considered shear-thinning when exponent n is less than 1, which means the viscosity reduces at higher shear strain rates, or the slope of shear stress – strain rate curve decreases with increasing the shear stress (Fig 4-3).

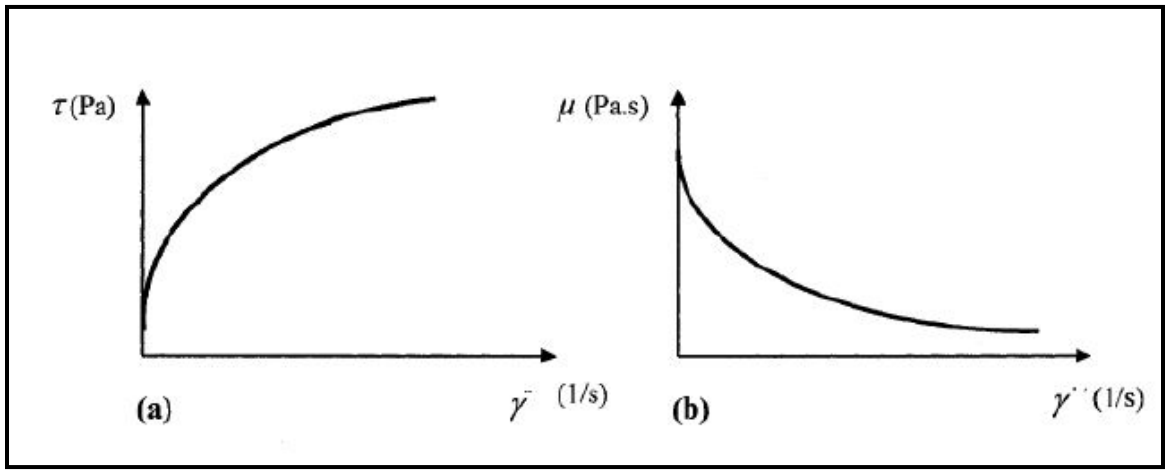

Figure 4-3. Typical shear thinning behaviour: (a) shear stress vs. shear strain rate, and (b) Viscosity vs. shear strain rate.

Various rheological models used to oil and gas industry to describe cement slurry rheology are summarized in Table 4-2 and the remarks are noted. Based on the table 4-2, it was found that required characterization of the rheological behavior of the cement slurry and prediction of the yield stress is highly sensitive to the model selection. The appropriate model can be selected based on the rheological data from the experiment results.

Table 4-2. Various rheological models of cement slurries

Model	Equation	Remarks
Newtonian Model	$\mu = \frac{\tau}{\dot{\gamma}}$	Does not consider the non-Newtonian behavior.
Bingham Plastic Mode	$\tau = \tau_0 + \mu_p \dot{\gamma}$	Cannot predict the shear in nonlinear flow behavior.
Power Law Model	$\tau = k\dot{\gamma}^n$	Does not consider the yield stress at zero strain rates.
Herschel-Bulkley Model	$\tau = \tau_o + k\dot{\gamma}^n$	Limited to a range of shear strain rates.

4.4 Rheology of Smart Cement Slurry

4.4.1 Effect of Carbon Fibers

The effect of carbon fiber additive on plastic viscosity and yield point of API class H cement slurries was studied. All additives were weighed by weight of cement. Standard API high speed mixer was used at 4000 and 1200 rpm to mix the slurries. Slurries were mixed without and with 0.1% carbon fiber based on weight of cement (BWOC). FANN standard viscometer (strain rate of 512 and 1024 sec^{-1}) was used to determine the shear stress – strain rate relationships for the various cement mixes and the responses are summarized in Table 4-2.The Bingham plastic relationships (Eq. 4-1) for cement with and without carbon fibers are compared in Fig. 4-1. Addition of 0.2% carbon fiber to the cement slurry with a w/c ratio of 0.38 increased the plastic viscosity by 2 cps and reduced the yield point by 4.5 $lb/100ft^2$ (Table 4-1). Also the ratio of τ_o / μ_p reduced from 0.34 to 0.27. With 0.1% carbon fiber the effects on the rheological properties were slightly reduced but the ratio of τ_o / μ_p remained unchanged.

Table 4-3. Effect of Carbon Fiber Addition on the Rheological Properties of Cement

Composition	Carbon Fiber (BWOC)	Plastic Viscosity (μ_p) (cp)	Yield Point (τ_o) ($lb/100ft^2$)	τ_o / μ_p ratio	Remarks
Class H Cement	0% CF	71	24	0.34	**Minor changes in the plastic viscosity.** **Reduced the YP.**
W/C = 0.38	0.1% CF	65	22	0.34	
	0.2% CF	73	20	0.27	

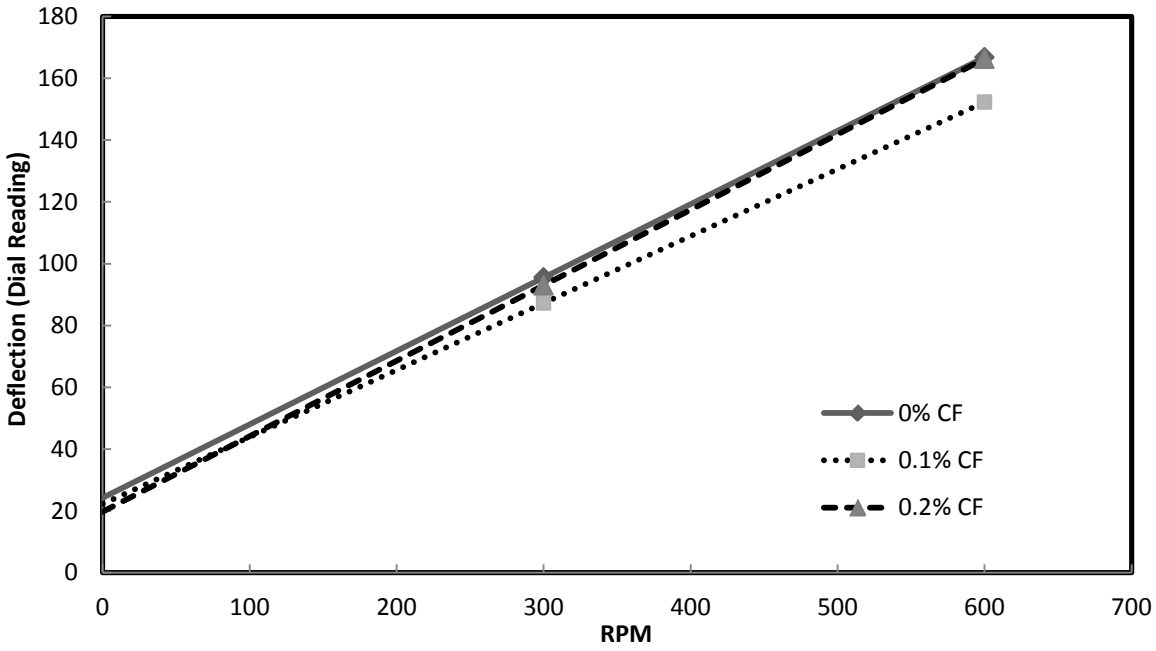

Figure 4-4. Variation of shear stress- strain rate Bingham relationships for cement with and without carbon fibers

4.4.2 Rheology Behavior of OWC

Fig. 4-2 shows the shear stress – strain rate of cement with water-to-cement ratio 0.38. Based on the experimental results the trends of shear stress with shear rate were non-linear. It was observed that the oil well cement behaved as a shear-thinning material; meaning the slope of shear stress-strain curve reduced with increasing the strain rate. Viscosity reduces with increasing the shear rate. Relationship between shear stress and shear strain rate of cement modified with varying amount admixtures was investigated.

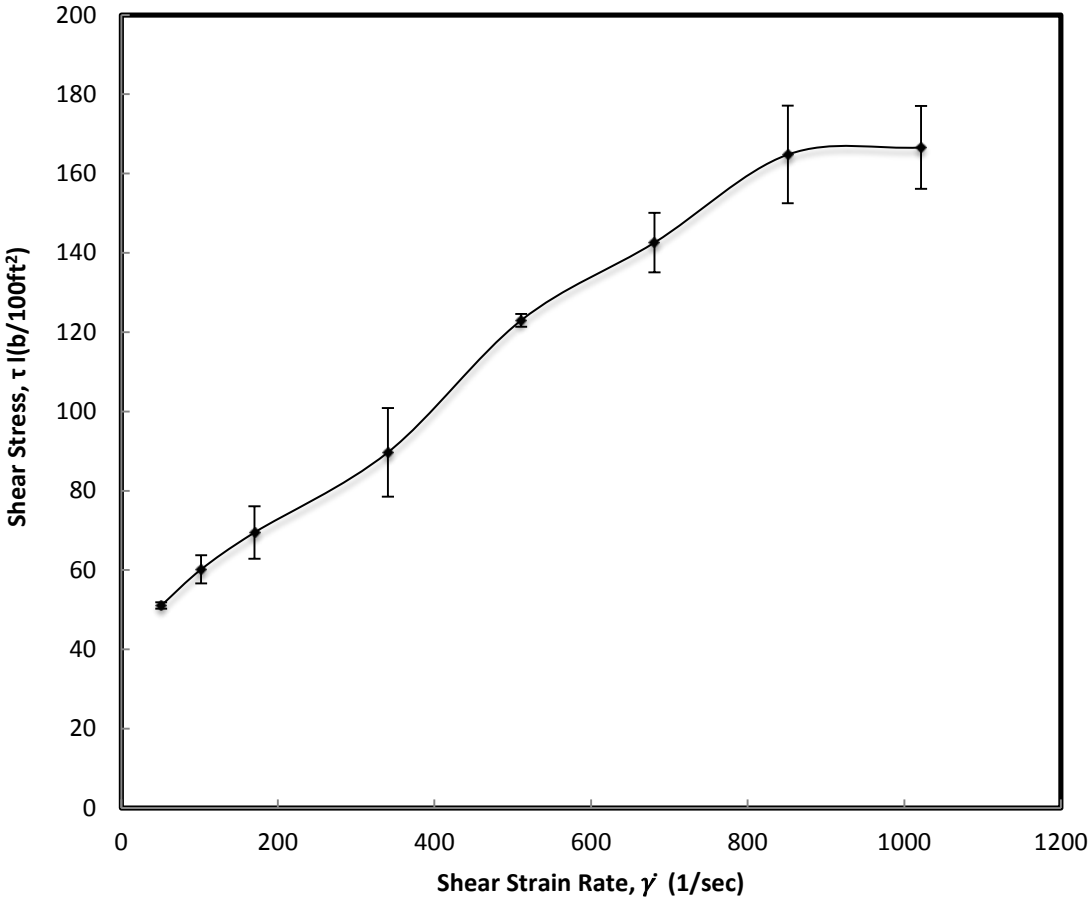

Figure 4-5. Relationship between shear stress and shear strain rate for class H oil well cement

4.4.3 Model Development

The amount of shear stress varies in different parts of the displacement system. For example the shear rate is high at the bottom of the hole and lower in the annulus. Hence, cement viscosity reduces by thinning in higher shear stresses (Dyke et al., 2000). Therefore accurate modeling of this behavior becomes very important.

Based on the inspection of the test data and shear-thinning nature of the rheological behavior of OWCs a hyperbolic relationship is proposed as

$$\tau - \tau_o = \frac{\dot{\gamma}}{a + b\dot{\gamma}}, \tag{4-4}$$

where:

τ_o is the yield stress,

a and b are model parameters, and

$\dot{\gamma}$ is the shear strain rate (sec^{-1}).

Relationship proposed in Eq. (4-4) can be used to represent various linear and nonlinear trends based on the values of the parameters a and b. When parameters a and b are positive the relationship was hyperbolic as

$$\frac{d\tau}{d\dot{\gamma}} > 0 \Rightarrow \frac{(a + b\dot{\gamma}) - b\dot{\gamma}}{(a + b\dot{\gamma})^2} = \frac{a}{(a + b\dot{\gamma})^2} > 0 \Rightarrow a > 0 \tag{4-5}$$

and

$$\frac{d^2\tau}{d\dot{\gamma}^2} < 0 \Rightarrow \frac{-ab}{(a + b\dot{\gamma})^2} < 0 \Rightarrow b > 0. \tag{4-6}$$

In Fig. 4-6, the model prediction of smart cement with water-to-cement ratio of 0.38 is shown.

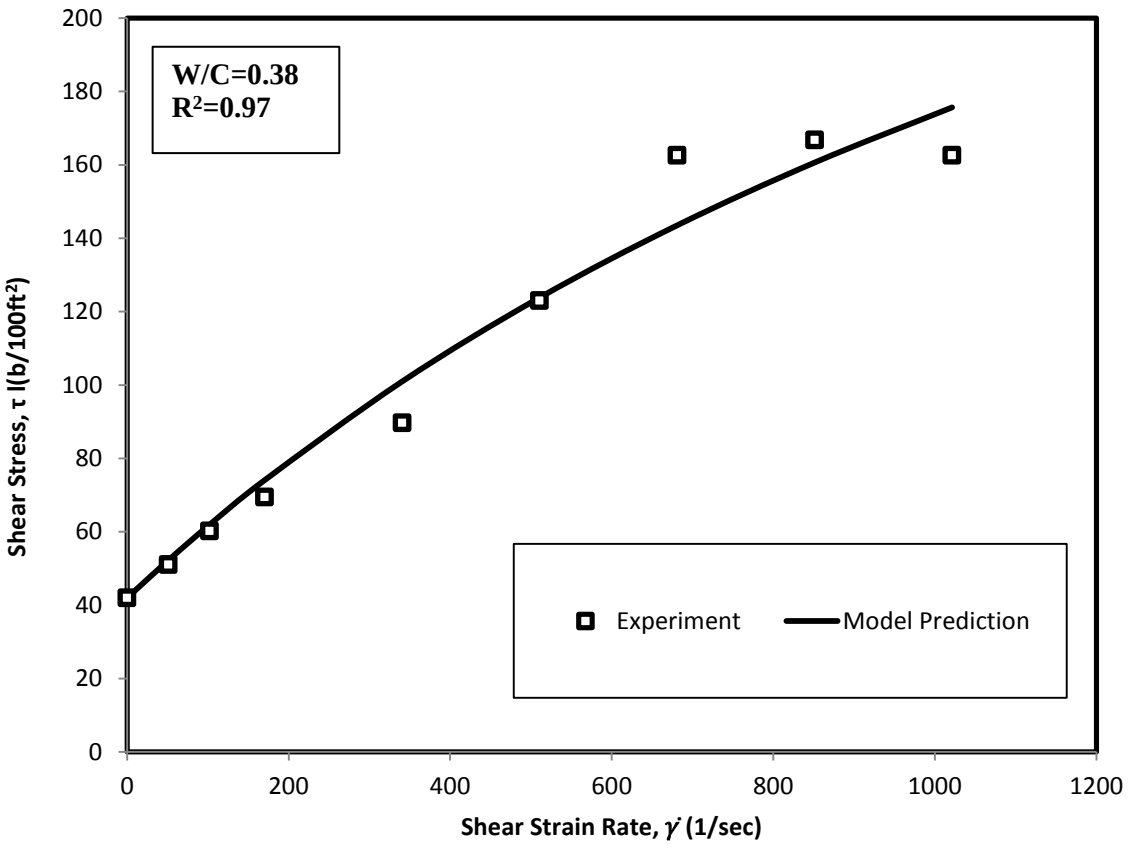

Figure 4-6. Hyperbolic prediction of shear stress vs. shear strain rate in class H oil well cement

4.4.4 Comparison with Existing Models

Due to the non-linear curvature of the rheological data of OWCs (Fig. 4-2), and limiting shear stress in high strain rates, not all cement slurries can be well described by the Bingham plastic and Herschel-Bulkley models. The hyperbolic model did not suffer such limitations. The advantage of the proposed model was the ability to predict the viscosity in higher shear strain rates, and considering the non-linear behavior of shear stress-shear strain relationship quite well within an unlimited strain rate range. HB model

over predicted some of the shear stresses in the higher shear strain rates. Whereas, the proposed model had a limiting value in very high shear strain rates. For instance, if the shear strain rate in the HB model approached infinity the shear rate would also be infinite as illustrated by

$$\dot{\gamma} \to \infty \Rightarrow \ \tau \to \infty . \tag{4-4a}$$

Whereas in the proposed hyperbolic model (Eqn. 4-4), in infinite shear strain rates, the shear stress is limited to

$$\dot{\gamma} \to \infty \Rightarrow \ \tau = \tau_o + \frac{1}{b}. \tag{4-4b}$$

The root mean squared error (RMSE) (Eqn. 4-7) and coefficient of determination (R^2) values were calculated for the above-mentioned models by

$$RMSE = \sqrt{\frac{\sum_{i=1}^{N} (Yi - \widehat{Yi})^2}{N}}, \tag{4-7}$$

where *Yi* is the shear stress based on the experimental data, $\widehat{Yi}$ is the model prediction of shear stress at each shear strain rate and *N* is the number of data. Since RMSE is scale dependent, it was a good measure of accuracy to compare forecasting errors of different rheological models for estimating the shear stress variable.

In Fig. 4-7, comparison of the proposed model with the Herschel-Bulkley model for predicting shear stress-strain relationship of class H cement with water-to-cement ratio of 0.44 is shown. The rheological properties and model parameters for Bingham plastic, Herschel-Bulkley and Hyperbolic models are summarized in Table 4-3. Based on the

trends from various experiments Based on trends from various experiments and both RMSE and R^2 values, it was found that hyperbolic model had a higher accuracy in predicting the flow behavior of cement slurries. The coefficient of determination for all models was varied from 0.90 to 0.99. The RMSE was 10.32 lb/100ft^2 for hyperbolic model, 4.54 lb/100ft^2 for HB model and 28.42 lb/100ft^2 by using the Bingham-Plastic model. The yield stress (τ_o) of cement with water-to-cement ratio of 0.44 was 12.50 lb/100ft^2 with the proposed hyperbolic model. For the same cement slurry, the Hurschel-Bulkley and Bingham Plastic model predicted the yield stresses of 6.21 lb/100ft^2 and 88.14 lb/100ft^2, respectively.

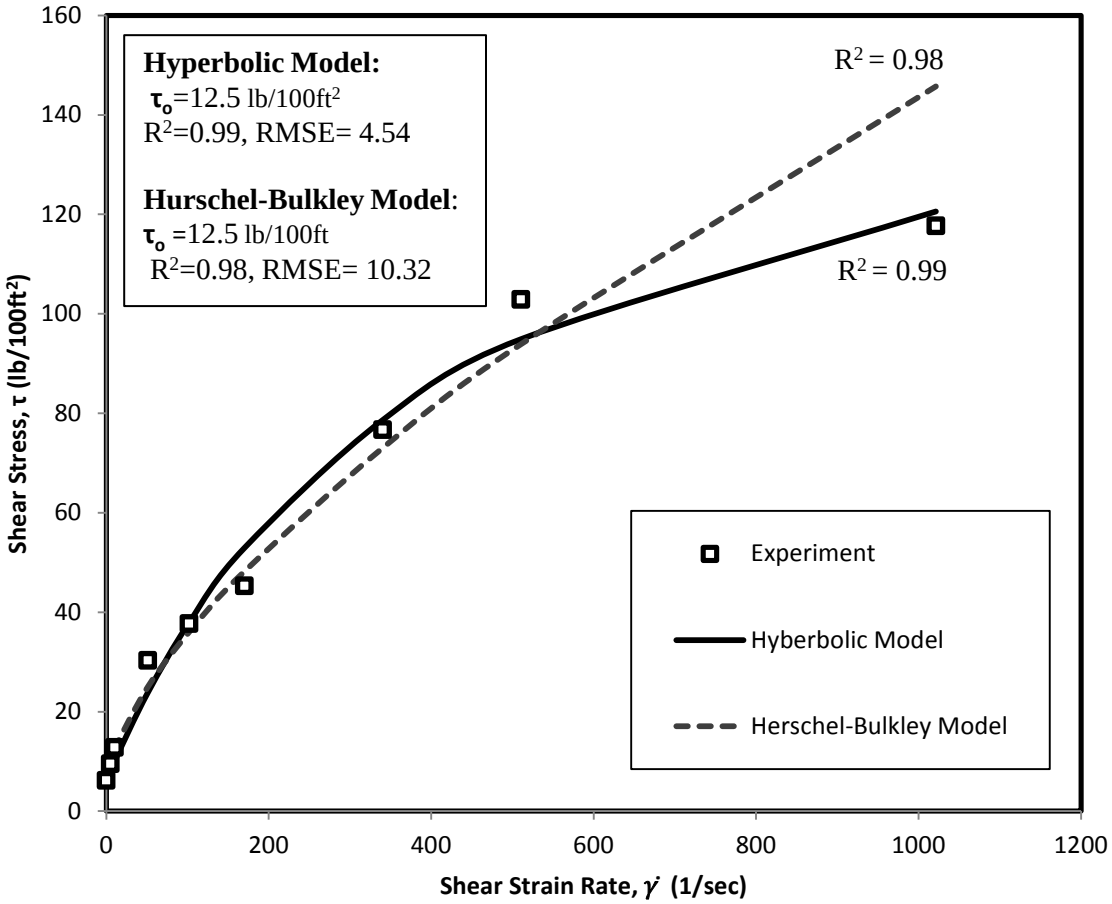

Figure 4-7. Prediction of rheology behaviour of cement with Hyperbolic model and the Herschel Bulkley model

Table 4-4. Bingham Plastic, Herschel Bulkley and Hyperbolic model parameters for smart OWC

Bingham Plastic Model (Eqn. 4-2) R^2=0.90 RMSE=28.4 lb/100ft^2		**Herschel-Bulkley Model (Eqn. 4-3) R^2=0.98 RMSE=10.32 lb/100ft^2**			**Hyperbolic Model (Eqn. 4-4) R^2=0.99 RMSE=4.54 lb/100ft^2**		
τ_o (lb/100ft^2)	**μ_p (cP)**	**τ_o (lb/100ft^2)**	**k**	**n**	**τ_o (lb/100ft^2)**	**a**	**b**
88.14	13.86	6.21	1.35	0.67	12.50	2.67	0.0062

4.5 Electrical Properties

Electrical properties were measured to obtain the sensing properties of Smart OWC. In this study, electrical properties such as impendence spectroscopy (IS), initial electrical resistivity and change in resistivity during curing and under compression loading were determined and correlated to other properties of cement.

4.5.1 Impendence Characterization of Cement

In order to understand the self-sensing ability of cement, the material properties of cement were characterized under AC measurement using two-wire method. The selection of two wire method was due to simplicity and practicality of this method in the field. However, measuring the resistance using two-wire method was associated with contact resistances at the interface of the wires and cement (Chung, 2006). Hence quantifying contact resistance and the bulk resistance was important to obtain the bulk resistance from the apparent resistance and determine the sensing properties.

4.5.1.1 Theory

Identification of the most appropriate equivalent circuit to characterize the electrical properties of a material is essential in order for the material's properties to be further understood (West et al., 1997). In this study, an equivalent circuit to represent the smart cement was required for better characterization through analysis of the IS data. There were many challenges associated with choosing a correct equivalent circuit. It was necessary to somehow make a connection between the different elements in the circuit and the different regions in the impedance data of the corresponding sample (West et al., 1997). Given the difficulties and uncertainties, researchers tend to use a pragmatic approach and adopt a model that is believed to be the most appropriate based on their knowledge of the expected behavior of the material under study, and they then demonstrate that the results are consistent with the circuit used. In this study, based on the past research studies (Vipulanandan & Prashanth, 2013) two possible equivalent electrical circuits for cement-based materials were analyzed in order to find the most suitable equivalent circuit to represent the smart cement measured responses.

Case1: General Bulk Material—Resistance and Capacitor

In the equivalent circuit for case 1, the contacts were connected in series, and both the contacts and the bulk material were represented using a capacitor and a resistor connected in parallel (Fig. 4-8). In the equivalent circuit for case 1, Rb and Cb are the resistance and capacitance of the bulk material, respectively, and Rc and Cc are the resistance and capacitance of the contacts, respectively.

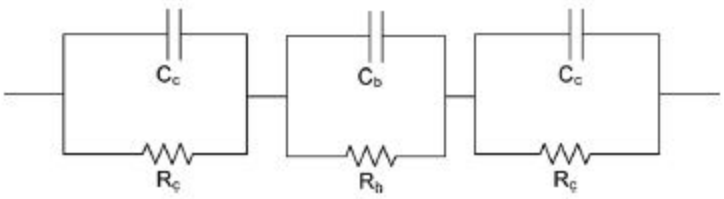

Figure 4-8. Equivalent circuit for case 1, (Vipulanandan & Prashanth, 2013)

The total impedance of the equivalent circuit for case 1 (Z_1) can be given by (Vipulanandan & Prashanth, 2013)

$$Z_1 = \frac{R_b}{1+\omega^2 R_c^2 C_c^2} + 2\frac{Rc}{1+\omega^2 R_c^2 C_c^2} - j\left\{\frac{2\omega R_c^2 C_c}{1+\omega^2 R_c^2 C_c^2} + \frac{\omega R_b^2 C_b}{1+\omega^2 R_b^2 C_b^2}\right\}. \quad (4\text{-}8)$$

In Eq. 4-8, ω is the angular frequency of the applied signal. When the frequency of the signal is very low, $\omega \to 0$ then $Z_1=R_b+2R_c$, and when it is very high, $\omega \to \infty$ then $Z_1 = 0$.

Case 2: Special Bulk Material—Resistance Only

Case 2 is a special case of case 1 in which the bulk capacitance of the material (C_b) was assumed to be negligible (Fig. 4-9).

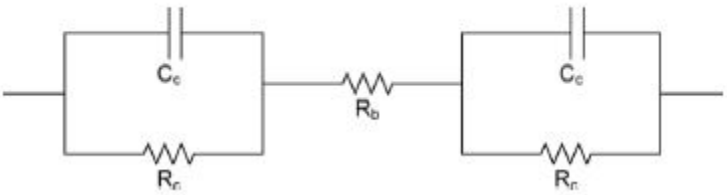

Figure 4-9. Equivalent circuit for case 2, (Vipulanandan & Prashanth, 2013)

The total impedance of the equivalent circuit for this case (Z_2) is presented as (Vipulanandan & Prashanth, 2013)

$$Z_2 = R_b + 2\frac{Rc}{1+\omega^2 R_c^2 C_c^2} - j\left\{\frac{2\omega R_c^2 C_c}{1+\omega^2 R_c^2 C_c^2}\right\}. \quad (4\text{-}9)$$

When the frequency of the applied signal is very low, $\omega \to 0$ and $Z_2=R_b+2R_c$ and when it is very high $\omega \to \infty$ and $Z_2= R_b$.

A comparison of the typical responses of equivalent circuits for case 1 (Fig. 4-8) and case 2 (Fig. 4-9) is shown in Fig. 4-10.

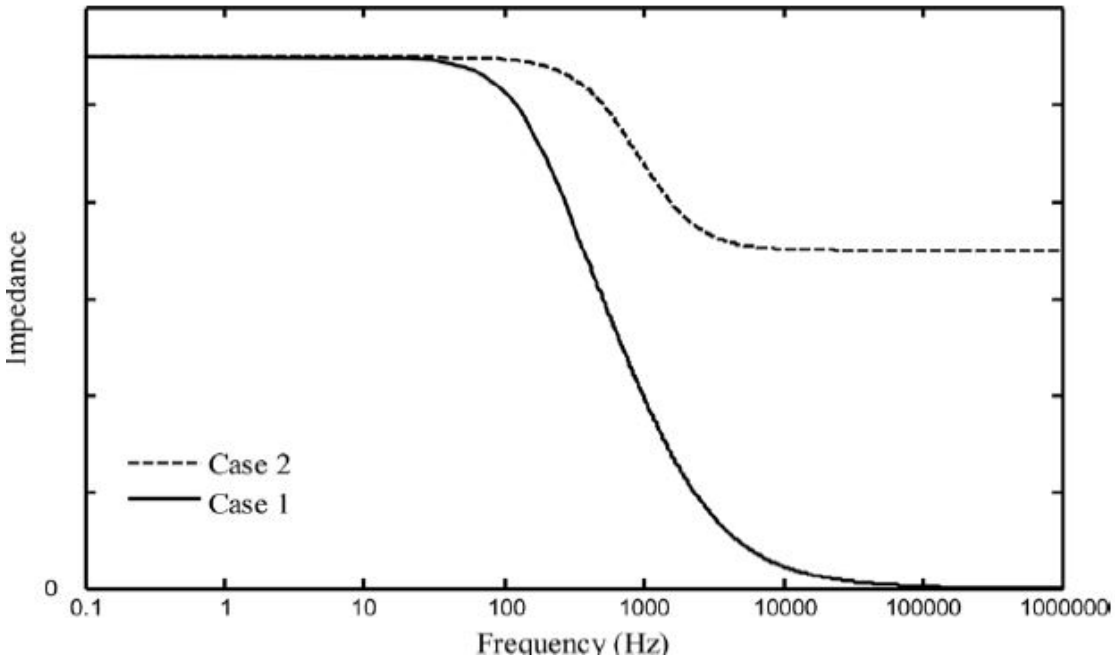

Figure 4-10. Comparison of typical responses of equivalent circuits for case 1 and case 2 (Vipulanandan & Prashanth, 2013)

4.5.1.2 Characterization of the Smart OWC

The impedance spectroscopy (IS) test was performed on the cement samples to quantify the bulk and contact resistances at various curing ages. During the experiment, the frequency of the constant amplitude AC signal was varied from 20 Hz to 300 kHz,

and the corresponding impedance responses of the smart cement were measured using an LCR meter. The IS test results for the cement slurry right after mixing and after 28 days of curing are shown as in Fig. 4-11 The IS experimental results trend was identical to the equivalent circuit for case 2 (Fig. 4-10). Therefore, case 2 (Resistance only material) was selected as the most suitable one to represent the smart cement.

The model predictions of the IS using Eq. 4-9 are plotted with the experimental data in Fig.4-11. From the model (Eq. 4-9), the bulk resistance (R_b) of the fresh cement slurry were obtained as 89 Ω.; whereas the bulk resistance of the hardened cement after 28 days of curing was increased to 936 Ω. The contact resistances for the fresh slurry and hardened cement were 374 Ω and 491 Ω, respectively. Hence the bulk and contact resistances increased with the curing time. The contact capacitance (Cc) of the fresh cement slurry was estimated as 7.1 μF. For the hardened cement Cc was 8.6 μF.

The tests indicated that both contact resistance and bulk resistance increased with increase in the curing time (age of the cement). It was also found that the measured resistance at high frequency converged to the bulk resistance (R_b) from the Eq. 4-9. The variation of the bulk resistance obtained from the model was less than 9% of the measured resistance at 300 kHz frequency for both fresh cement slurry and the hardened cement. For the cement used in this experiment, the measured resistance at high frequency converged to the value of bulk resistance. Therefore, the bulk resistance of the cement slurry and hardened oil well cement can be determined by measuring the resistance at 300 kHz frequency.

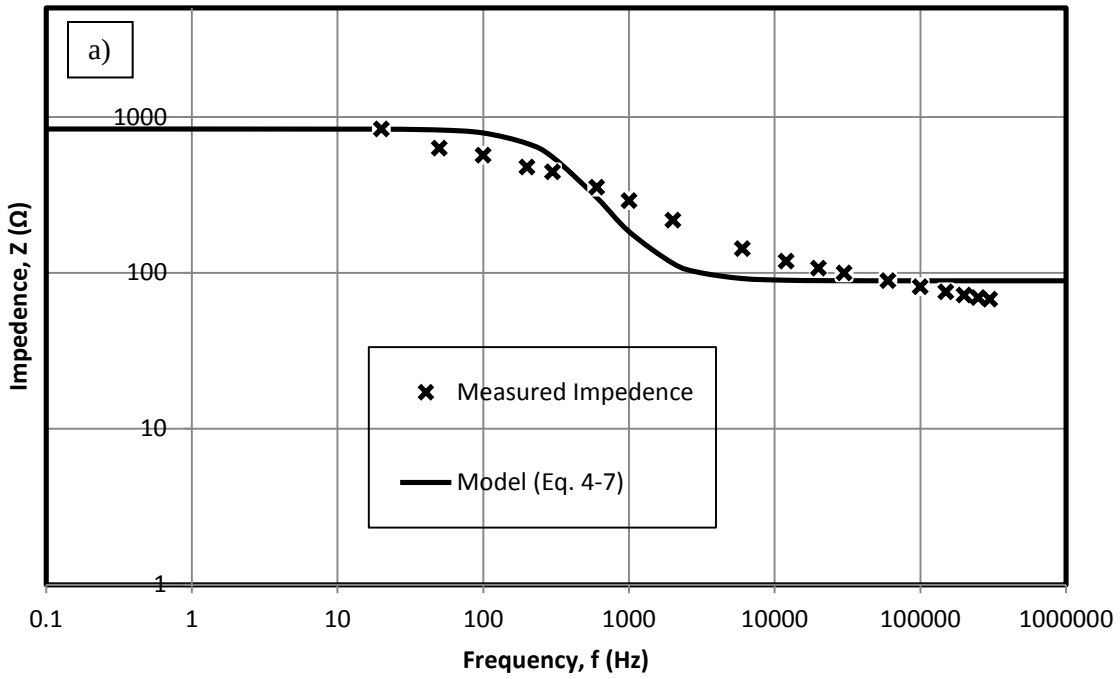

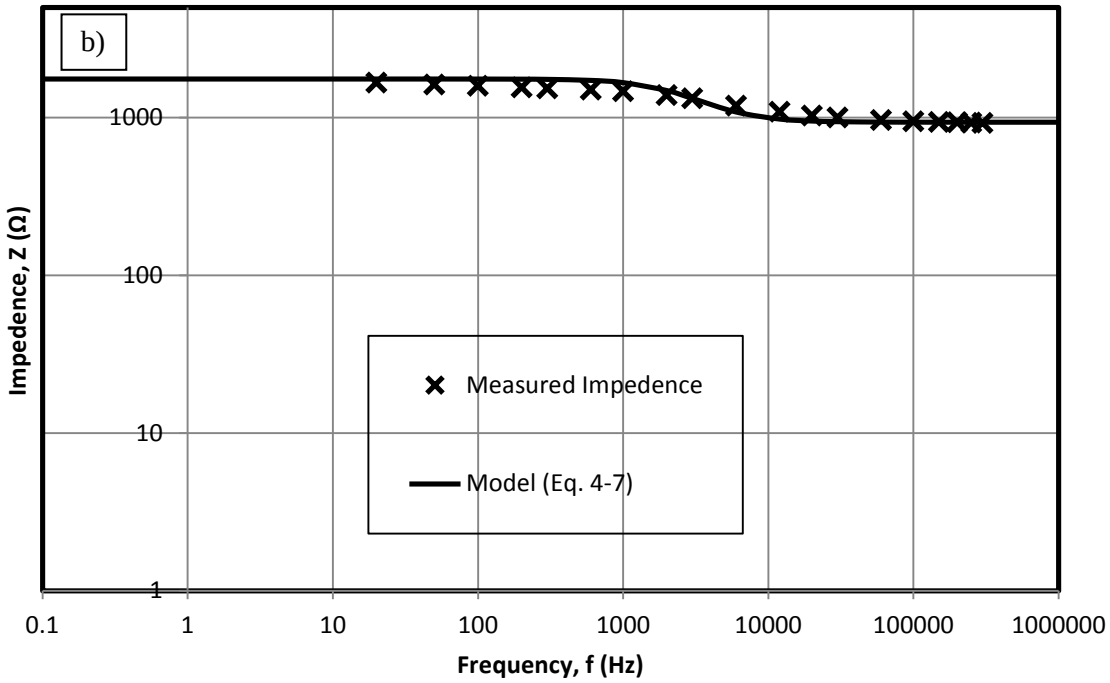

Figure 4-11. Impedance versus frequency for a) Cement slurry after mixing b) Hardened Cement after 28 days of curing

4.5.2 Initial Resistivity of OWCs

The resistivity of cement slurry with water-to-cement ratio of 0.38 and 0.01% carbon fiber (BWOC) is shown in Fig. 4-12. The resistivity was measured after mixing using the standard resistivity meter and the conductivity meter during two hours of curing time for various cement slurries. It was found that the initial resistivity of cement slurry was varied from 0.96 Ω.m to 1.15 Ω.m and the average resistivity was 1.06 Ω-m. From Fig. 4-11, the resistivity decreased gradually until it reached a minimum point. This trend was observed in all of the resistivity responses of the cement samples. The decrease in resistivity immediately after mixing was due to dissolution of conductive ions (K^+, Na^+, Ca^{2+}, SO_4^{2-}) from the cement particles after cement is mixed with water. The dissolving process of the ions causes the resistivity decrease during early period. When the transform reaction between the two phases is in equilibrium, the increase in the degree of cement hydration caused the resistivity rate to increase (Xiao & Li, 2008).

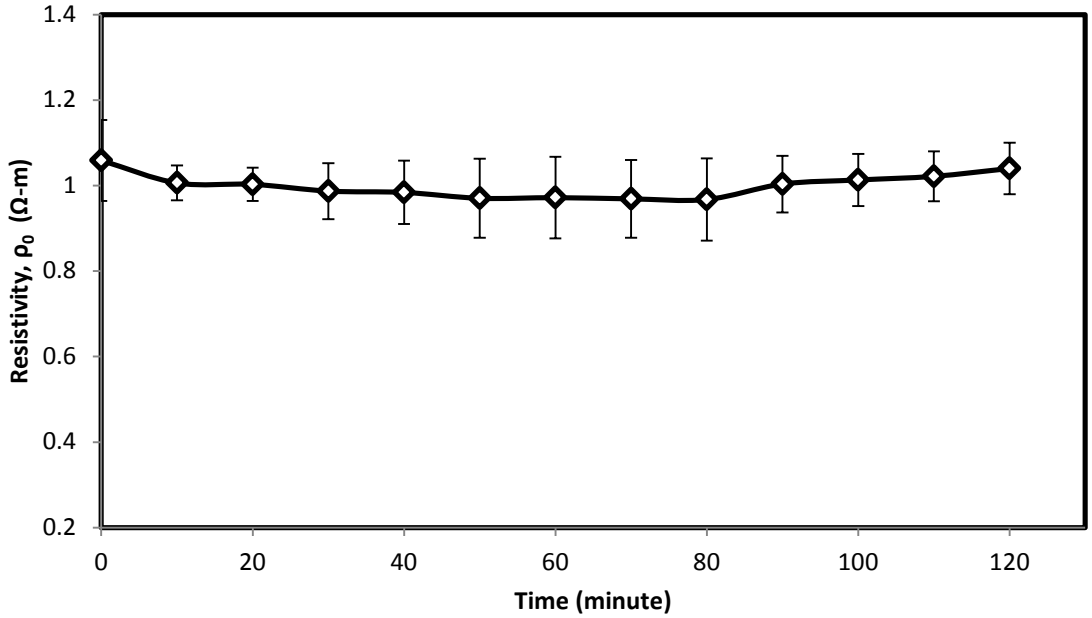

Figure 4-12. Initial resistivity of OWC with w/c of 0.38

4.5.2.1 Effect of Admixtures on Initial Resistivity

Effect of admixtures on the initial resistivity was investigated by adding various admixtures to the base cement slurry. Neat class H cement with water-to-cement ratio of 0.38 was chosen as the base slurry, and the concentration of the admixtures were reported based on the weight of cement (BWOC). As shown in Fig. 4-13, addition of 0.1% and 0.2% of carbon fiber (CF) to class H oil well cement with w/c ratio of 0.38 reduced the resistivity to 0.98 and 0.94 Ω.m, a 15% and 18% reduction from the neat cement, respectively. With 10% silica fume (SF), the initial resistivity was 1.11 Ω.m, a 5% decrease in resistivity compared to the base OWC slurry. The initial resistivity increased 70% to the value of 1.97 Ω.m when 4% barite was mixed with the base slurry. When 2.5% bentonite was added to the slurry, the initial resistivity was 1.26 Ω.m, a 9% increase in resistivity compared to the baseline. Finally 5% fly ash (FA) and cement with w/c ratio of 0.38 had an initial resistivity of 0.83 Ω.m, which was 28% less than the resistivity of the cement only mix.

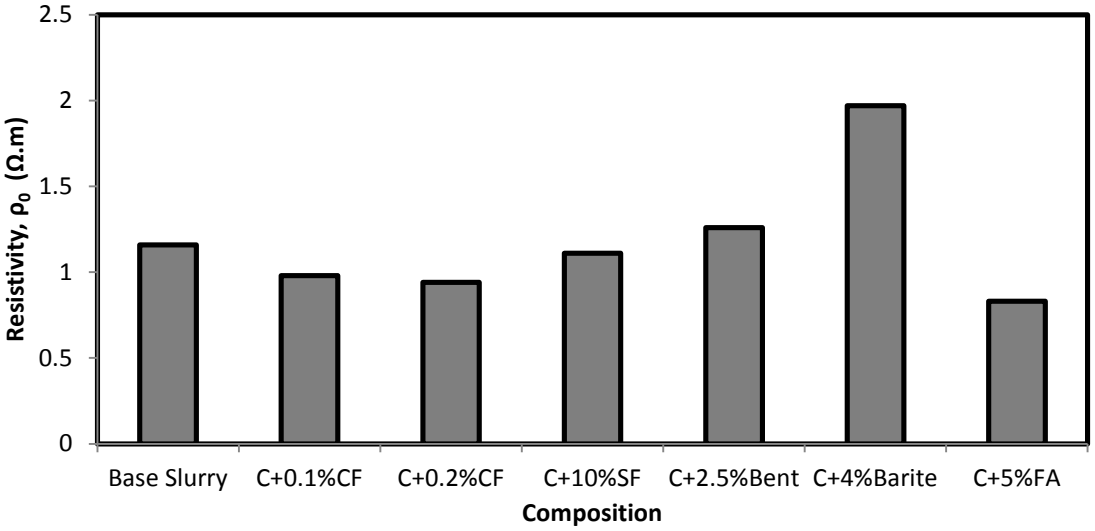

Figure 4-13. Effect of various admixtures on initial resistivity of OWC

4.5.3 Resistivity during Curing

4.5.3.1 Theory

Li and Wei (2006) investigated the change in resistivity with time as a fingerprint of hydration process. Figure 4-13 illustrates the change in electrical resistivity (ρ) during curing time for cement. It was observed that the resistivity curves from the various samples followed a similar trend. The electrical resistivity dropped to a minimum value, and then gradually increased with time. Initially after mixing cement with water, resistivity decreased to a minimum value (ρ_{min}), and the corresponding time to reach the minimum resistivity was t_{min}, as shown in Fig. 4-14. t_{min} can be used as an index of speed of chemical reactions and cement set times. Experimental results by Wei (2012) indicated that the electrical resistivity is predominated by the conductivity of the pore solution and the connectivity of pores. Fig. 4-15 depicts the relationship between the formation in hydration products and change in resistivity. As shown in Fig. 4-15a right after mixing, the pores are connected and more conduction paths are formed between cement particles. After 24 hours of curing the hydration products block the conduction path and tortuosity increases as shown in Fig. 4-15b. The decrease of connectivity of pores results in a sharp increase in the resistivity curve. Meanwhile, the porosity decreases due to the increase and accumulation of the hydration products that also resulted in the gain and increase in compressive strength (Wei, 2012). Finally, with the slowdown of hydration process the resistivity increased with a lower rate up to 24 hours, and reached a value of ρ_{24} (Fig. 4-14). Change in electrical resistivity with respect to minimum resistivity $[(\rho_{24}-\rho_{min})/\rho_{min}]$, quantifies the formation of solid hydration products. Therefore by tracking the change in

resistivity of well cement, a clear understanding of hydration process and strength development can be obtained, which would be valuable in determining the wait on cement (WOC) times.

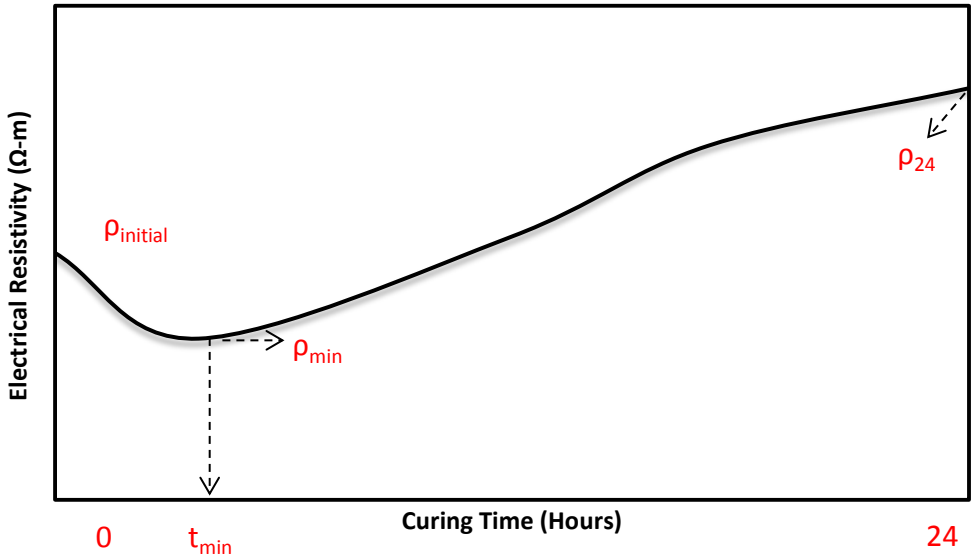

Figure 4-14. Typical bulk resistivity development with curing time

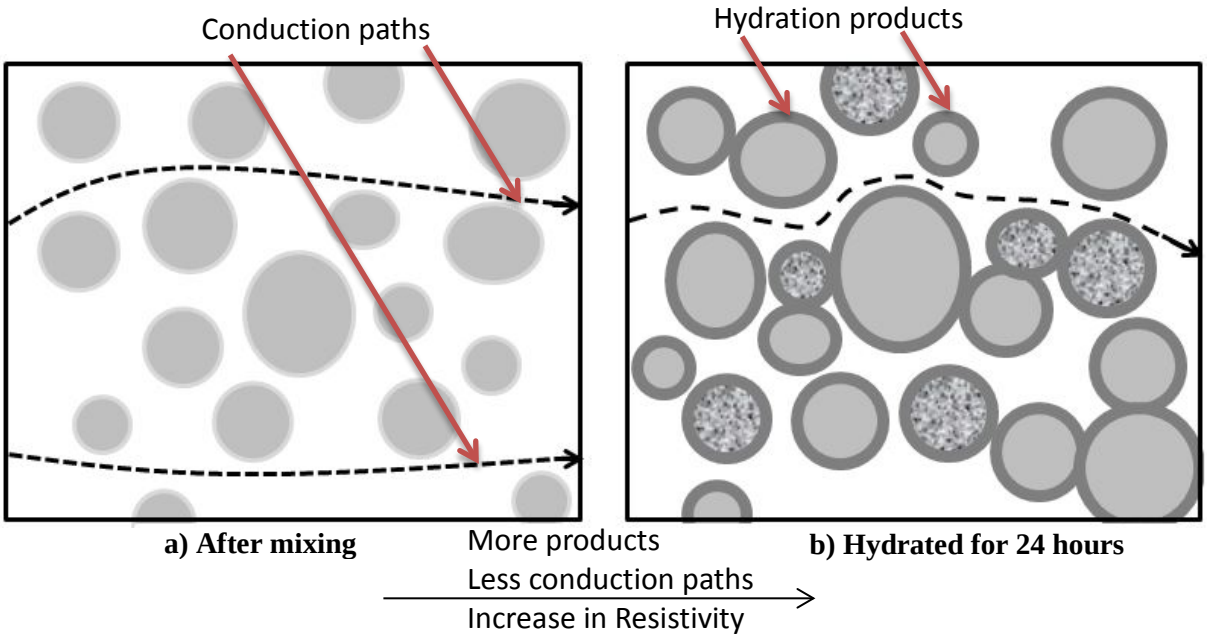

Figure 4-15. The schematic presentation of conduction paths for a cement paste

4.5.2 Monitoring the Resistivity of Smart Cement during Curing

As outlined above several characteristic parameters can be used in monitoring the curing (hardening process) of the cement. The parameters are initial resistivity ($\rho_{initial}$), minimum resistivity (ρ_{min}), time to reach the minimum resistivity (t_{min}) and percentage of maximum change in resistivity [$(\rho_{24}-\rho_{min})/\rho_{min}$]. Fig. 4-16 shows the change in bulk resistivity of cement with water-to-cement ratio of 0.38 up to 24 hours of curing by using AC measurements. The characteristic parameters are summarized in Table 4-5. The Resistivity of cement was 1.15 Ω.m initially and reduced to reach the ρ_{min} resistivity of 0.97 Ω.m after 90 minutes (t_{min}). As the cement hydration products were formed and cement started hardening, the resistivity increased with a sharp rate up to 18 hours, and then increment in resistivity was with a lower rate. The 24 hour resistivity (ρ_{24}) of this sample was 4.38Ω.m, which indicated that the maximum change in resistivity in 24 hours was more than 351%. The test showed the high sensitivity of AC resistivity measurements for characterizing the changes in smart cement during the curing process (hardening of the cement).

Table 4-5. Summary of electrical resistivity development for cement with water-to-cement ratio of 0.38 after 1 day of curing

Initial resistivity (Ω.m)	**ρ_{min} (Ω.m)**	**t_{min} (Minute)**	**ρ_{24} (Ω.m)**	**$[(\rho_{24}-\rho_{min})/\rho_{min}]$ (%)**
1.15	0.97	90	4.38	351.23

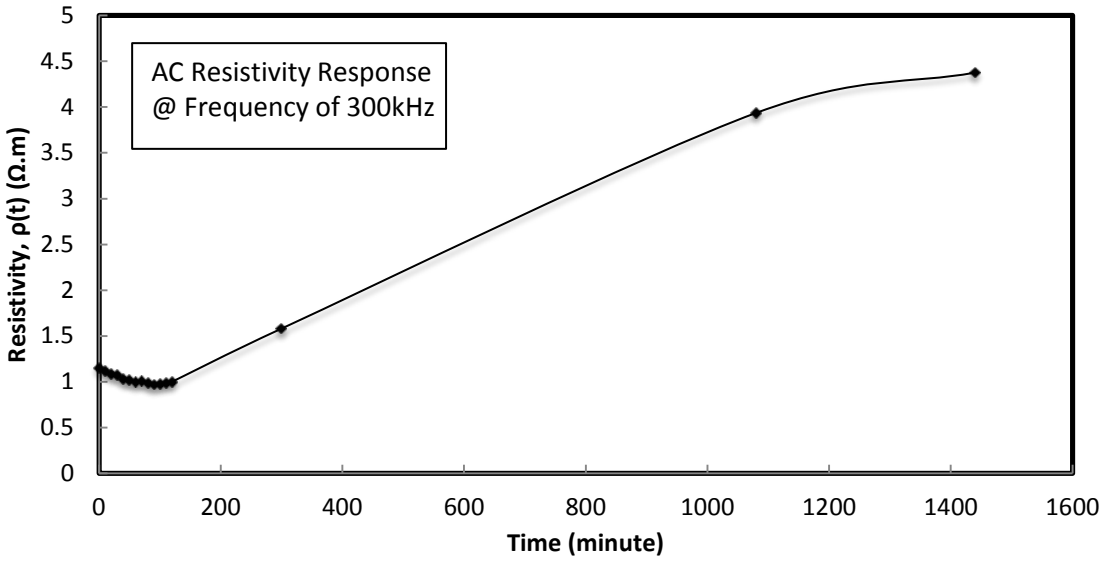

Figure 4-16. Bulk electrical resistivity development of OWC up to 24 hours of curing

4.5.3 Effect of Admixtures (DC)

The DC resistivity responses from various cement compositions are summarized in Table 4-6. The time to reach the minimum resistance was reduced by 30 minutes when the w/c ratio increased from 0.38 to 0.44. The maximum change in resistivity for cement with w/c ratio of 0.38 and 0.44 were 67% and 306% respectively.

Carbon Fiber (CF): The maximum change in resistivity in the first 24 hours with 0.2% CF was 52% and the time to reach the minimum resistivity was 70 minutes. Addition of CF to the cement with a w/c ratio of 0.44 had minimal effect on the initial resistivity but reduced the maximum change in resistivity after 24 hours (Table 4-6).

Silica fume (SF): The time to research minimum resistivity was 50 minutes and was not affected by the addition of up to 0.2% CF. The maximum resistivity change was 87%. With and without CF, the observed trends were similar; hence addition of carbon fibers had minimal effect on the curing of the cement with 10% silica fume.

Bentonite (Bent): Addition of 0.1% CF did not affect the initial resistivity in the bentonite sample. The time to reach minimum resistivity was 190 minutes and adding 0.1% CF reduced it to 90 minutes. The maximum resistivity change was 120%. With 0.1% CF, the maximum resistivity change was 214%. Hence adding carbon fibers influenced the resistivity of the curing cement with 2.5% bentonite.

Barite: The time to research minimum resistivity was 40 minutes and was not affected by the addition of 0.1% CF. The maximum resistivity change was 111% and with carbon fiber addition it was 124%. Addition of carbon fiber influenced the resistivity changes in the curing cement with 4% barite.

Fly ash (FA): Addition of 0.1% and 0.2% CF increased the initial resistivity. The time to research minimum resistivity was 30 minutes and adding CF didn't affect the time to research the minimum resistivity. The maximum resistivity change was 255%. With 0.1% and 0.2% of CF, the maximum resistivity change was reduced to 135% and 128% respectively.

These observed trends in Table 4-6 clearly indicated the sensitivity of resistivity to the changes occurring in the curing of cement. However, due to the contact resistances present at the interface of the electrical leads and cement required DC measurements no consistency and repeatability were found in the patterns for modeling and relating the resistivity trends to the properties of oil well cement slurries and hardened cement samples. Therefore, based on section 4.3.1.2, AC resistance with high frequency which allowed the measurement of bulk resistivity of the cement was replaced with the DC measurements.

Table 4-6. Resistivity change during curing time for oil well cement with various additives

Mix proportions		ρ_{min} (Ω-m)	t_{min} (min)	1Hour resistivity (Ω-m)	ρ_{24} (Ω-m)	$(\rho_{24}-\rho_{min})/\rho_{min}$ (%)
W/C=0.38	Cement (C)	0.86	70	0.87	1.43	67%
	C+0.2%CF	0.85	70	0.88	1.30	52%
	C+10%SF	0.94	50	1.01	1.75	87%
	C+10%SF+0.1 CF	0.96	50	0.96	1.84	91%
	C+10%SF+0.2 CF	0.98	50	1.00	1.79	82%
W/C=0.44	Cement (C)	1.06	40	1.13	4.30	306%
	C+0.1%CF	1.20	40	1.26	2.66	121%
	C+0.2%CF	1.04	70	1.23	2.26	118%
W/C=0.38	C+2.5%Bent	1.13	190	1.16	2.48	120%
	C+2.5%Bent+ 0.1%CF	1.00	90	1.02	3.14	214%
	C+4%Barite	1.91	40	1.95	4.03	111%
	C+4%Barite+ 0.1%CF	1.24	40	1.28	2.77	124%
	C+4%Barite+ 0.2%CF	1.28	50	1.30	2.70	112%
	C+5%FA	0.83	30	1.07	2.96	255%
	C+5%FA+0.1 %CF	0.82	30	0.83	1.93	135%
	C+5%FA+0.2 %CF	0.95	30	0.99	2.17	128%

4.6 Piezoresistivity

4.6.1 Theory

Piezoresistivity can be defined as the ability of the body to exhibit change in the resistivity values on being subjected to stress. Thus, if

$$\Delta\rho/\rho = f(\sigma), \tag{4-10}$$

then the material is considered to be a piezoresistive material. The four-probe method and

the two-probe method are the two mostly commonly used approaches to capture the resistance of a material. The difference between two and four probe methods is the presence of contact resistances at the interface of wires. However in this study based on the concept described in the section 4.5.1, AC measurement with the frequency of 300 kHz was employed to eliminate the contact problems.

4.6.2 Piezoresistivite Behavior of Smart Cement

Fig. 4-17 and 4-18 shows the piezoresistive behavior of cement with w/c of 0.38 after 1 day and 7 days of curing, respectively. Because there was minimal change in electrical resistivity before applying the load, the smart cement showed piezoresistive behavior after the once compressive loading was applied. It was found that for both curing ages, the change in electrical resistivity was increased with increasing the applied load. It is reported that oil well cement had a maximum strain of 0.2 to 0.3% at failure. The change in electrical resistivity at failure for cement after 1 day of curing was 780%. However, the piezoresistive sensitivity was reduced with the curing time. For the cement cured for 7 days the change in electrical resistivity at failure was 146%.

The cracks were detected by visual and auditory observations from the cement samples during the testing. Fractional change in electrical resistivity during compressive loading ($\Delta\rho/\rho$) was sensitive to cracks at low and high compressive stresses. It was evident from Figs. 4-17(b) and 4-18(b) that there was a sharp increase in the $\Delta\rho/\rho$ with the formation of cracks and a sharper increase with the formation of major cracks. In almost the entire piezoresistivity tests, there was a great increase in change in resistivity when the sample reached its ultimate stress.

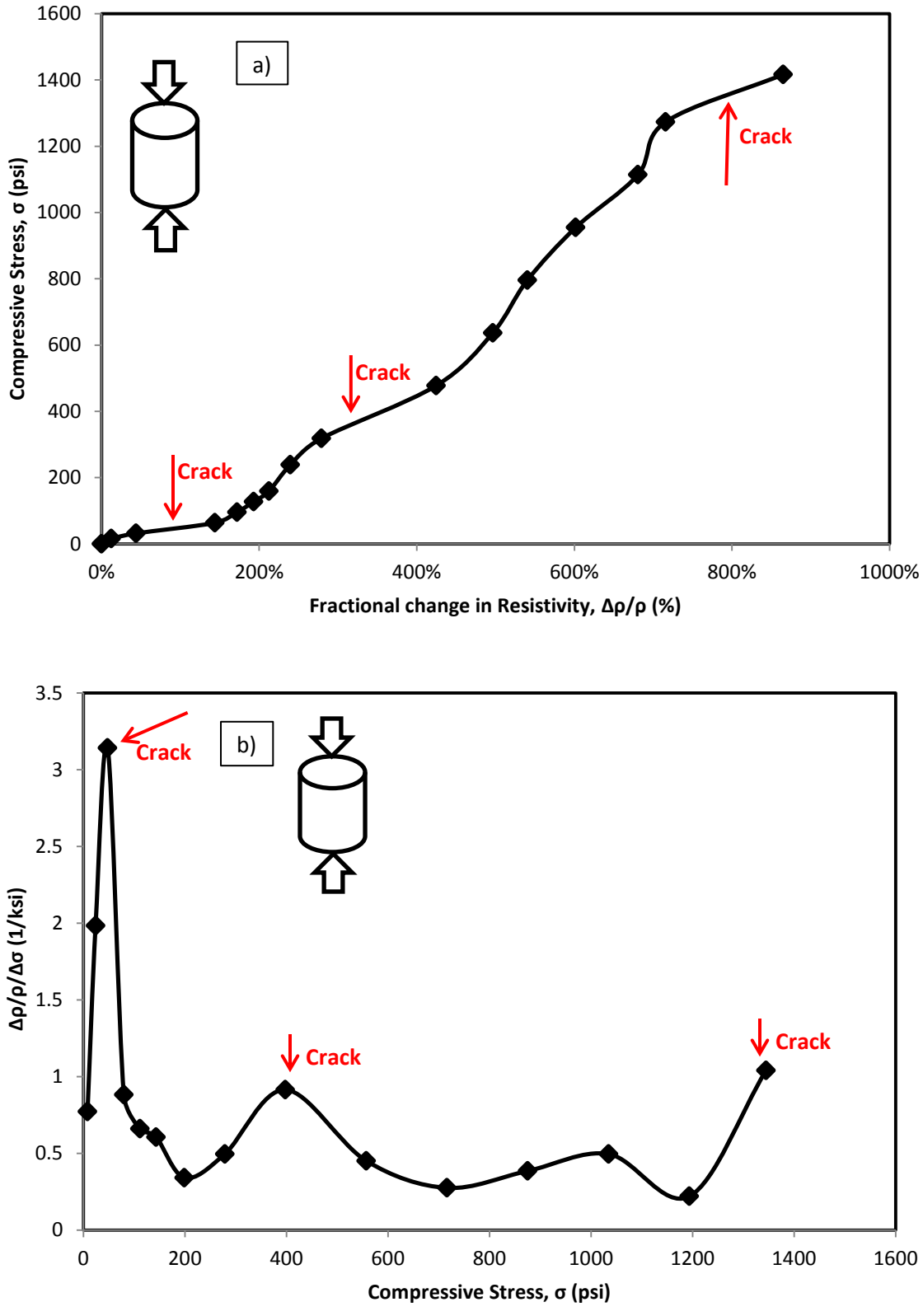

Figure 4-17. Piezoresistive behavior of cement after 1 day a) Compressive stress vs. change in resistivity b) Change in resistivity normalized by change in stress vs. compressive stress

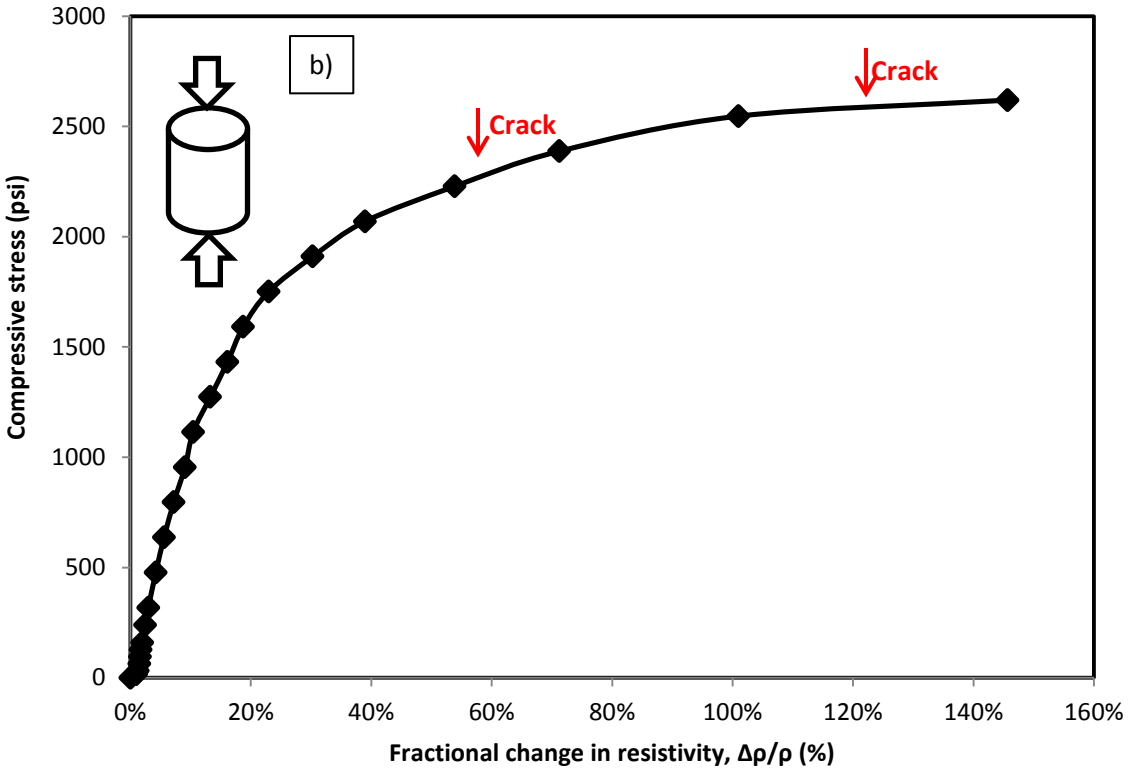

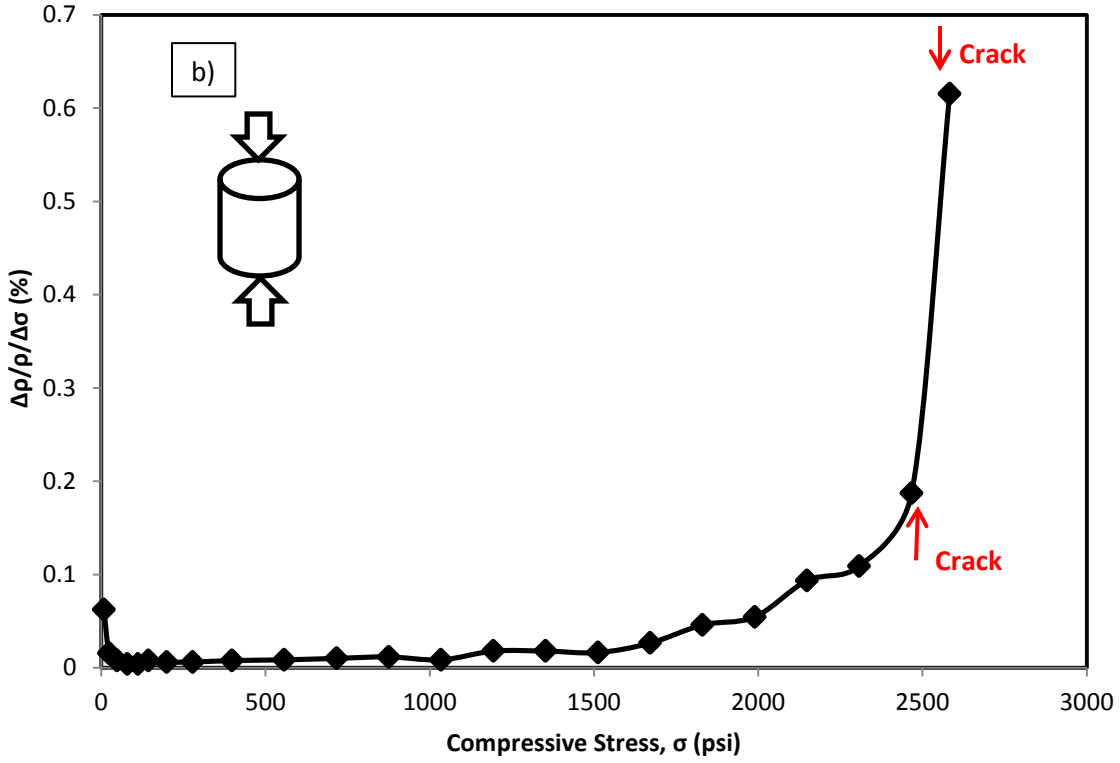

Figure 4-18. Piezoresistive behavior of cement after 3 days a)Compressive stress vs. change in resistivity b) Change in resistivity normalized by change in stress vs. compressive stress

4.6 Effect of W/C and Temperature on Properties of Smart Cement

Class H cement with water-to-cement (w/c) of 0.38, 0.44 and 0.54 was used in this study. The cement samples were prepared according to the API standards. To make the cement a piezoresistive material, 0.1% (BWOC) of modified carbon fibers was mixed with all the samples as the base modification (smart cement). In order to investigate the effects of the w/c and temperature on OWC rheology, smart oil well cement slurries without any admixtures were tested. The effect of temperature was investigated by performing the rheological tests at 23°C and 85°C using the digital high shear viscometer.

4.6.1. Rheological Properties

Cement slurries with different w/c at various temperatures showed significantly different rheological properties. However, regardless of the w/c and temperature, all slurries exhibited non-Newtonian and shear-thinning behavior as shown in Fig. 4-18 and Fig. 4-19.

From Fig. 4-19(a), it was evident that increasing the w/c reduced the apparent viscosity of cement. The viscosity of cement with w/c of 0.38 at a shear strain rate of 100 (1/sec) was 196 cp. At the same shear strain rate, cement with w/c ratio of 0.44 and 0.54 had viscosity of 153 cp and 129 cp, respectively. Fig. 4-18 (b) illustrates the viscosity of slurry with w/c of 0.38 at different temperatures. For the slurries with the same w/c ratio, the apparent viscosity increased with increasing the temperature. It was found that at the same shear strain rate, the apparent viscosity of cement at 85°C was 184% higher than the viscosity of cement at room temperature (23°C).

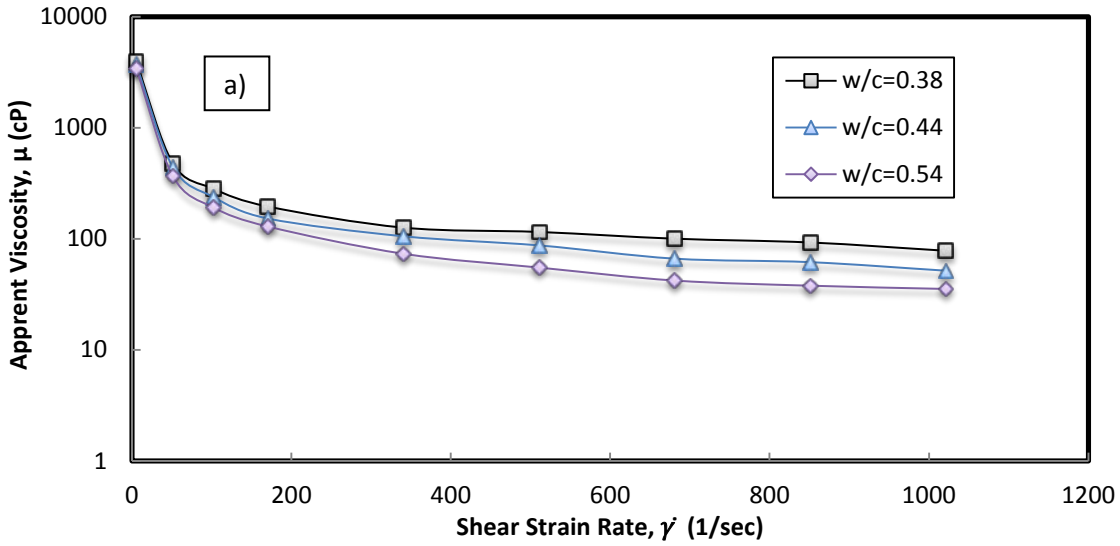

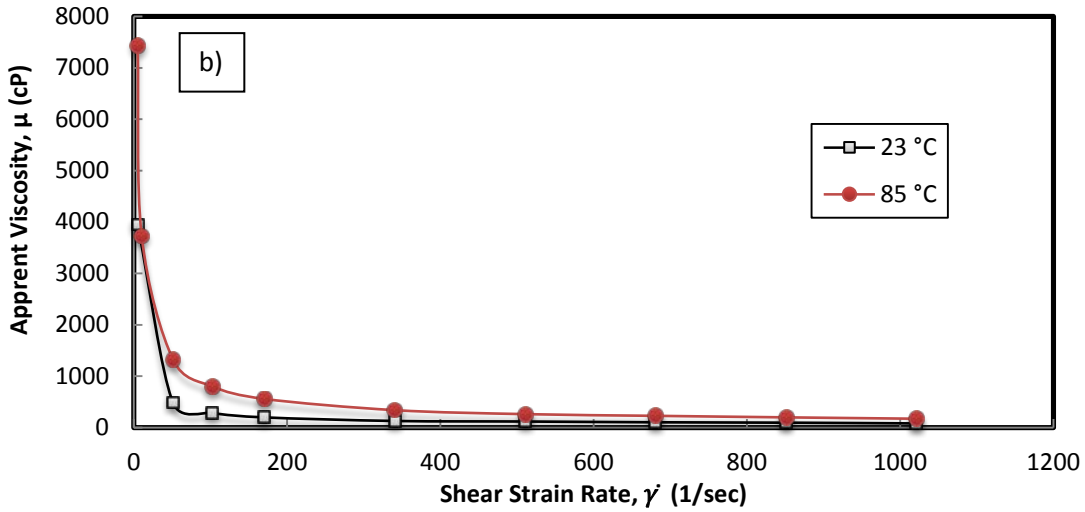

Figure 4-19. Apparent viscosity of cement a) with variable w/c ratios b) at different temperatures

Fig. 4-20 shows the shear stress- strain rate relationship of cement slurries with various w/c ratios at low and high temperatures. It was clear that increasing the water-to-cement ratio reduced the shear stress at the same strain rates, which indicates the improved flow properties of cement with higher w/c ratios. The same trends were found in several similar studies in literature. The reduction in the shear stress (i.e., reduction in

viscosity and yield stress) was related to decrease in the volume fraction of solids for slurries with higher w/c ratios (Anjuman et al., 2011). Effect of temperature is also illustrated in Fig. 4-20. At 85 °C, the high shear stress occurred at very low shear strain rate which confirmed the formation of gel structure due to the chemical reactions at the high temperatures.

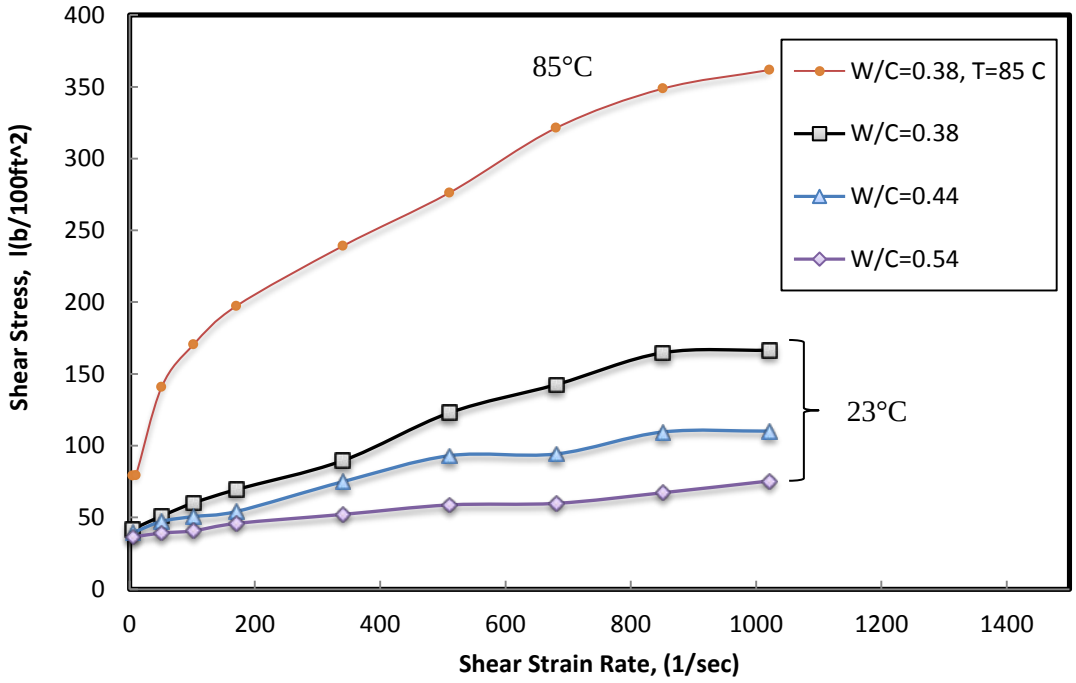

Figure 4-20. Shear stress- strain relationship for OWC with various w/c at 23℃ and 85℃

4.6.1.2 Modeling

Based on the shear thinning behavior observed from the rheological tests, the proposed hyperbolic model (Eq.4-4) was adopted for modeling of the rheological properties of cement with w/c ratio of 0.38, 044, and 0.54 as show in Fig. 4-21. The hyperbolic model predicted the shear stress-strain fitted well with the all series of experimental data, and the coefficient of determination was varied from 0.96 to 0.98.

The model parameters for hyperbolic model are summarized in Table 4-7. A comparison of the hyperbolic with Herschel-Bulkley (HB) model (Eq. 4-3) is also presented. From the table, it was found that the accuracy of the prediction of flow properties was improved using the hyperbolic model compared to the HB model. It was also found that the yield stress value (τ_o) was dependent upon the model selection. Generally, compared to the HB model, the yield stress values were lower using the hyperbolic model. For cement with w/c of 0.38 the yield stress was 41.98 lb/100ft^2 using the hyperbolic model. For the same water-to-cement ratio, HB model predicted the yield stress value of 38.24 lb/100ft^2.

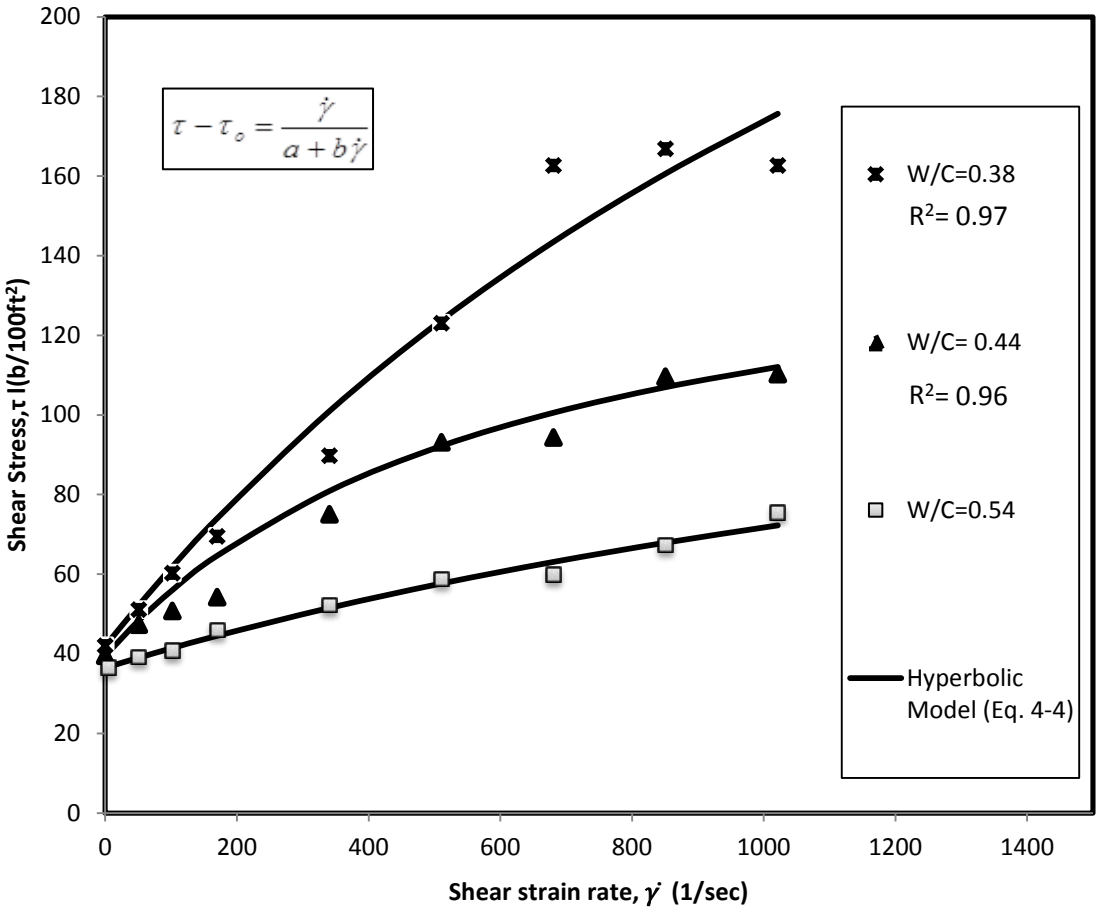

Figure 4-21. Experimental data and Hyperbolic model prediction for oil well cement with various w/c ratios

Table 4-7. Herschel Bulkley and Hyperbolic model parameters for various w/c

	Hyperbolic Model (Eq. 4-4)				Herschel-Bulkley Model (Eq. 4-3)			
W/C ratio	**τ_o (lb/100ft^2)**	**a**	**b**	**R^2**	**τ_o (lb/100ft^2)**	**K**	**n**	**R^2**
0.38	41.98	4.84	0.0027	0.97	38.24	45.01	0.148	0.67
0.44	39.53	5.29	0.0082	0.96	33.12	41.18	0.109	0.64
0.54	36.51	19.69	0.0087	0.98	29.47	25.34	0.133	0.82

The effect of w/c ratio on the yield stress is presented in Fig. 4-22(a). As was expected, increasing the water-to-cement ratio reduced the yield stress. The slurry with lower w/c ratio had fewer volume fraction of solids; hence exhibited lower yield stress. From Fig. 4-22(b) it was evident that increasing the temperature increased the yield stress. This was likely due to the gelling of cement at 85°C which indicated that initially more energy was required to make the slurry flow at a higher temperature.

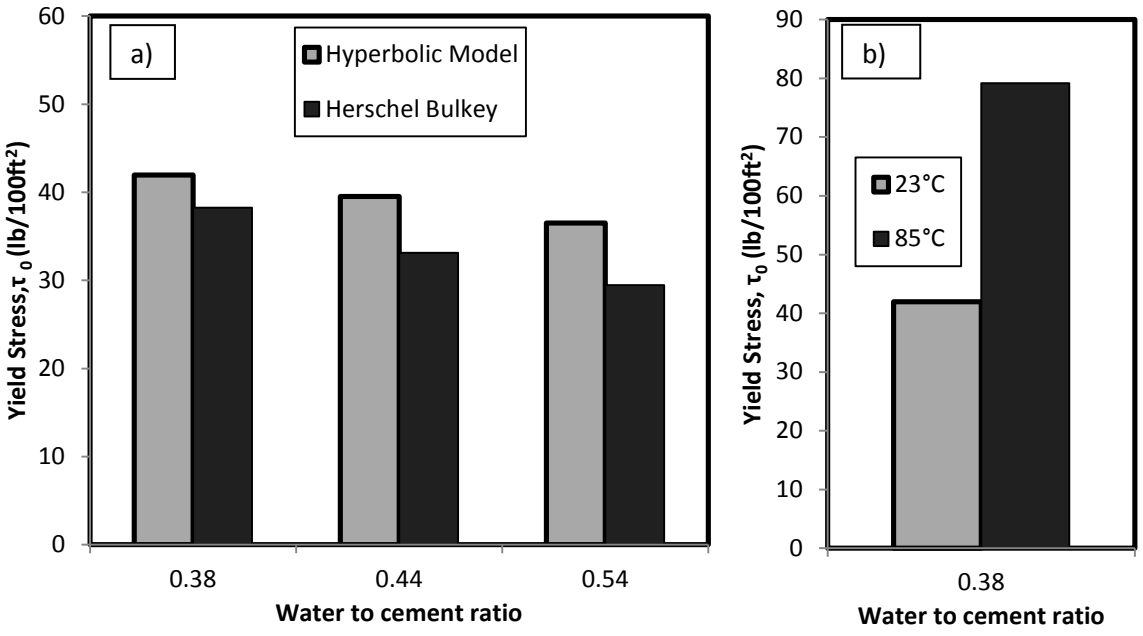

Figure 4-22. Variation of yield stress of oil well cement slurry with a) w/c ratio

4.6.2 Electrical Resistivity

4.6.2.1 Initial Resistivity and Density

The average density of the modified cement was 16.55 lb/gal (ppg). The densities of cement slurries with various w/c ratios are summarized in Table 4-8. Since the density of water is lower than that of the cement, increasing the water-to-cement ratio reduced the density of cement slurries.

Table 4-8. Effect of w/c ratio on density of cement slurries

Water-to-cement Ratio	Density (lb/gal)
0.38	16.5
0.44	16.1
0.54	15.8

Fig. 4-23 shows the initial electrical resistivity of cement with different water-to-cement with variations of temperature. It was evident from figure that initial electrical resistivity of slurries was reduced by increasing the w/c and the curing temperature. The higher the water-to-cement ratio the lower was the electrical resistivity. For cement with water-to-cement of 0.54, initial electrical resistivity was 0.88 Ω.m in room temperature. At the same water-to-cement electrical resistivity was reduced 35% for the slurry cured at 85°C. A comparison of change in initial electrical resistivity and change in density with variation of w/c ratio is presented in Fig. 4-24. Reducing the water-to-cement ratio from 0.54 to 0.38 increased the density of slurry by less than 5%, whereas, the initial electrical resistivity was incremented by more than 45%. Hence, compared to the density, electrical

resistivity was a more sensitive parameter for controlling the initial quality of cement slurry after mixing.

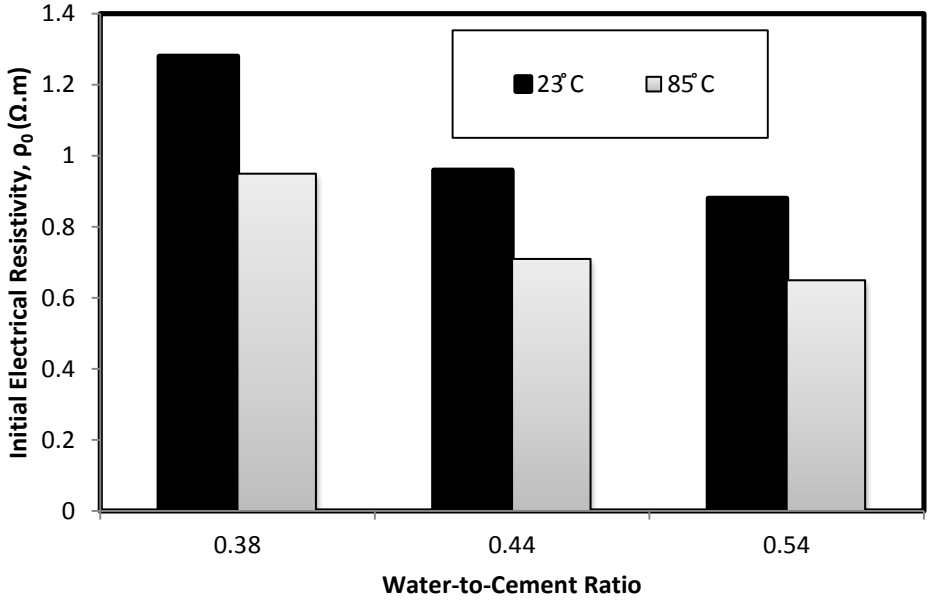

Figure 4-23. Effect of w/c ratio and temperature on initial electrical resistivity of OWCs

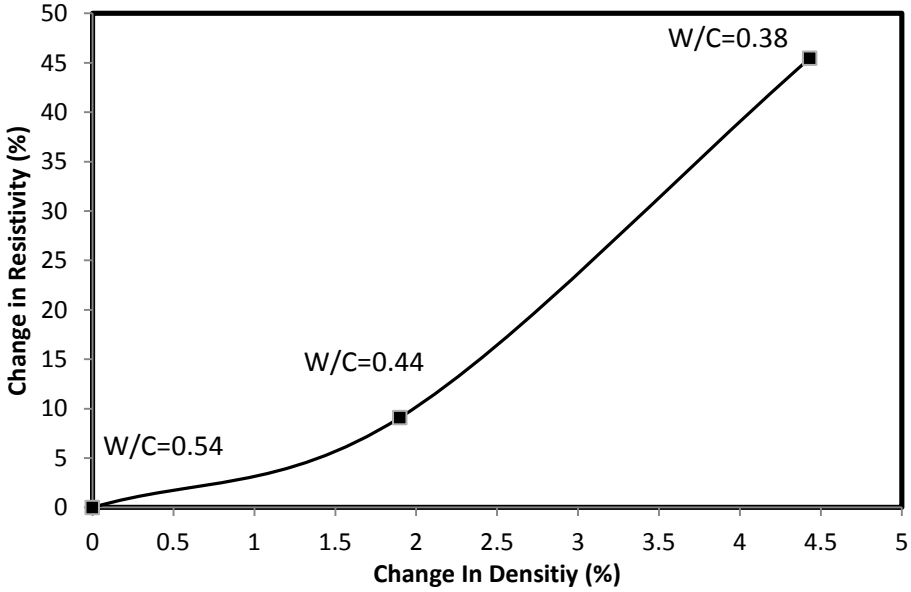

Figure 4-24. Change in resistivity vs. change in Density for cement with various w/c ratios at room temperature (23 °C)

4.6.2.2 Resistivity during Curing

The same approach as outlined in section 4.5.3 was used to characterize the cement slurry during the setting process. Fig. 4-25 shows the resistivity response of cement with various w/c from after mixing to 24 hours of curing. Electrical resistivity development for all the samples followed the same pattern. From the figure and Table 4-9, increasing the w/c reduced the minimum resistivity of smart cement. Also increasing the w/c increased the t_{min} value and reduced the maximum change in resistivity. In order to better quantify the resistivity change in 24 hours, resistivity index (RI_{24}) is defined as the maximum percentage change in resistivity with respect to minimum resistivity. The RI_{24} for cement wit w/c of 0.38 was more than 351%. The RI_{24} were 119% and 99% for slurries with w/c of 0.44 and 0.54 (Table 4-9). This was due do the less relative volume fraction of solids and consequently production of less hydration in products in cement with lower higher water-to-cement ratio.

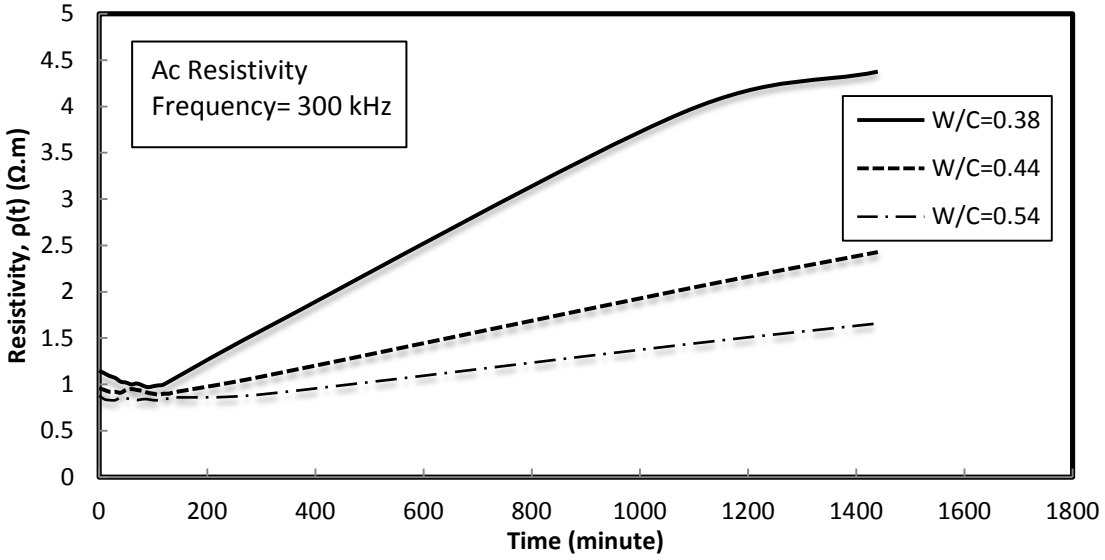

Figure 4-25. Bulk electrical resistivity development of OWC with various water-to-cement ratios up to 24 hours of curing

Table 4-9. Summary of bulk resistivity parameters for cement with various w/c ratios

W/C	Initial resistivity (Ω.m)	ρ_{min} (Ω.m)	t_{min} (Minute)	ρ_{24} (Ω.m)	$RI_{24\ hours}$ (%)	$RI_{10\ Days}$ (%)
0.38	1.28	0.97	90	4.38	351.2	571
0.44	0.96	0.89	110	1.95	119.3	523
0.54	0.88	0.83	110	1.66	99.8	433

4.6.2.3 Model Development

The resistivity curves were shifted to the time t_{min}, and the hyperbolic function was used to model the development of resistivity during curing time as

$$\rho(t) = \rho_{min} + \frac{t - t_{min}}{A + B(t - t_{min})}, \tag{4-11}$$

where ρ_{min} is the minimum resistivity, t_{min} is the corresponding time to reach the minimum resistivity and A and B are model parameters. Fig. 4-26 shows the resistivity responses from the experiment and the model predictions after 10 days of curing.

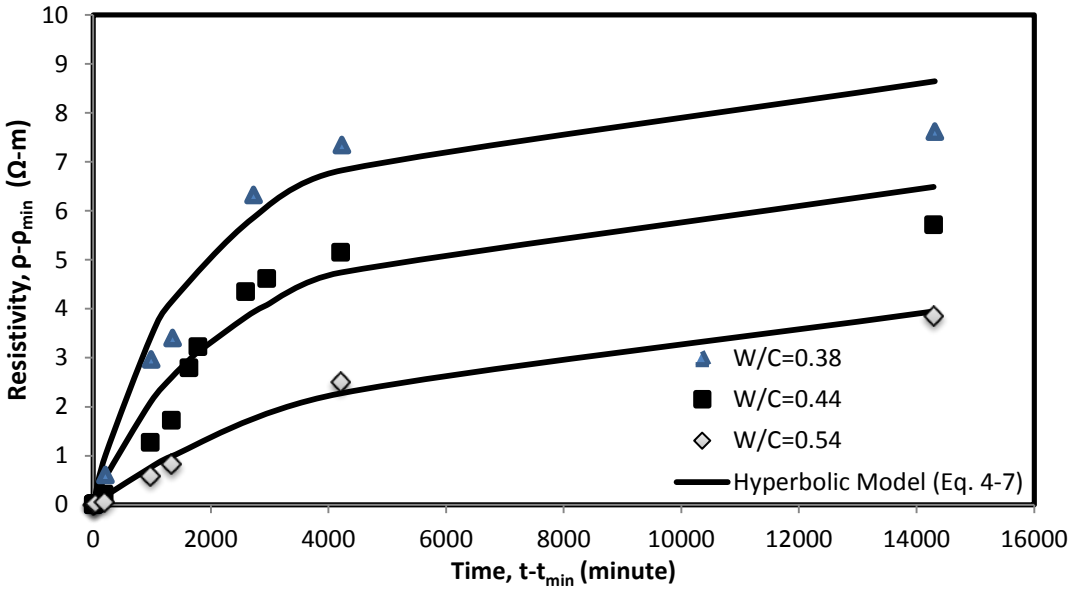

Figure 4-26. The hyperbolic prediction of the resistivity curves for various w/c ratios

The model parameters are summarized in Table 4-10. The ultimate resistivity in the Table 4-10 demonstrates the value of resistivity when t in Eq. 4-11 approaches infinity.

Table 4-10. Hyperbolic model parameters and ultimate resistivity for cement with various w/c ratios

W/C	A	B	R^2	Ultimate Resistivity (Ω.m)
0.38	191	0.11	0.97	10.4
0.44	381	0.15	0.95	7.7
0.54	1113	0.18	0.99	6.5

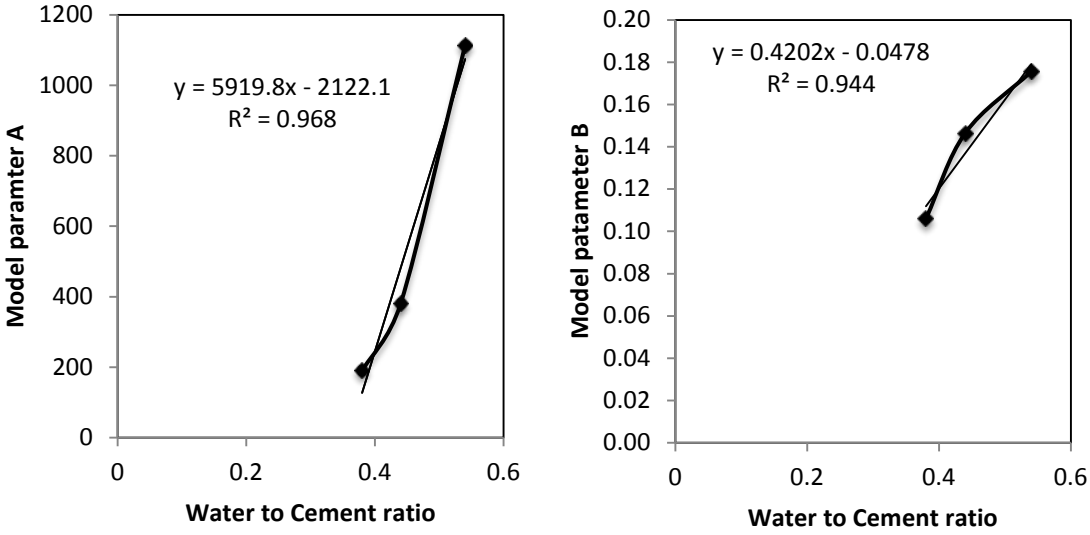

Figure 4-27. Relationship between w/c and A and B parameters of Eq. 4-7

Therefore parameters A and B were determined as shown in Eq. 4-12 and 4-13 given by

$$A = 5919(\frac{W}{C}) - 2122 \quad \text{and} \tag{4-12}$$

$$B = 0.4202(\frac{W}{C}) - 0.0478. \tag{4-13}$$

Where A and B are model parameters of Eq. 4-11 and W/C is the water-to-cement ratio. Based on the Table 4-9, it was found that the w/c ratio can be deduced from the initial resistivity value. It was apparent that the relationship between water-to-cement ratio and the initial resistivity (ρ_0) followed a power law. The correlation between water-to-cement ratio and initial resistivity is given by Eq. 4-14, as

$$(\frac{W}{C}) = 0.458\rho_0^{-0.831} \quad . \tag{4-14}$$

Therefore by only knowing the w/c the initial resistivity can be estimated. Moreover the electrical resistivity development of smart cement during curing time could be predicted by using the proposed formulations. It is necessary to note that the equations 4-11, 4-12, 4-13 and 4-14 is valid in the water-to-cement ratio range of 0.38 to 0.54.

4.6.3 Compressive Strength

Fig. 4-28 illustrates the effect of water-to-cement ratios and temperature variations on the compressive strength of cement. In general, compressive strength was reduced by increasing the w/c ratio. The fact that less amount of solids was present in the cement with lower w/c ratio, led to a lower compressive strength development in those slurries, compared to the cement with higher w/c ratios. Based on the Figure, 3-day compressive strength of the cement with w/c of 0.38 and 0.54 were 6.30 ksi and 2.55 ksi, respectively. Curing the cement at a higher temperature increased the compressive strength of cement. The increase of compressive strength for the high temperature-cured cement samples was related to the acceleration in the rate of hydration at high temperatures. For cement with w/c of 0.38 the compressive strength was 49% more when it was cured at 85°C for 3 days compared to the cement cured in the room temperature.

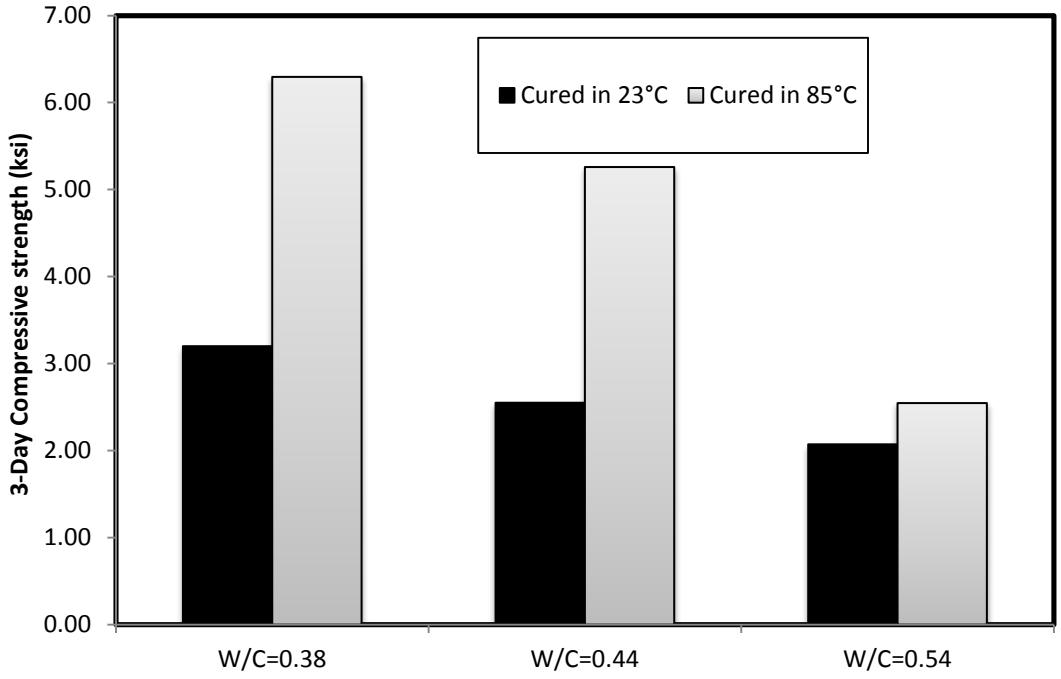

Figure 4-28. Compressive strength of cement with different w/cs after 3 days of curing

4.6.4 Relationship between Resistivity and Compressive Strength

During the entire cement hydration process both the electrical resistivity and compressive strength of the cement increased gradually with the curing time. For cement pastes with various w/c ratios, the change in resistivity was varied during the hardening. For example, the cement paste with a lower w/c ratio had a higher electrical resistivity change (RI_{24}) than cement with higher w/c ratio (Table 4-9). Ma and Li (2014) computer stimulation indicated that the porosity of cement was inversely proportional to the degree of hydration. They found that the porosity of the cement paste with a lower w/c ratio was less than that with a higher w/c ratio. Therefore, both electrical resistivity and compressive strength was relatively higher in cement with a lower w/c ratio after certain days of curing. The relationship between compressive strength and change in electrical resistivity is schematically illustrated in Fig. 4-29. There was a linear relationship

between the compressive strength and the percent change in resistivity during 24 hours of curing (RI_{24}), as shown in Fig. 4-30.

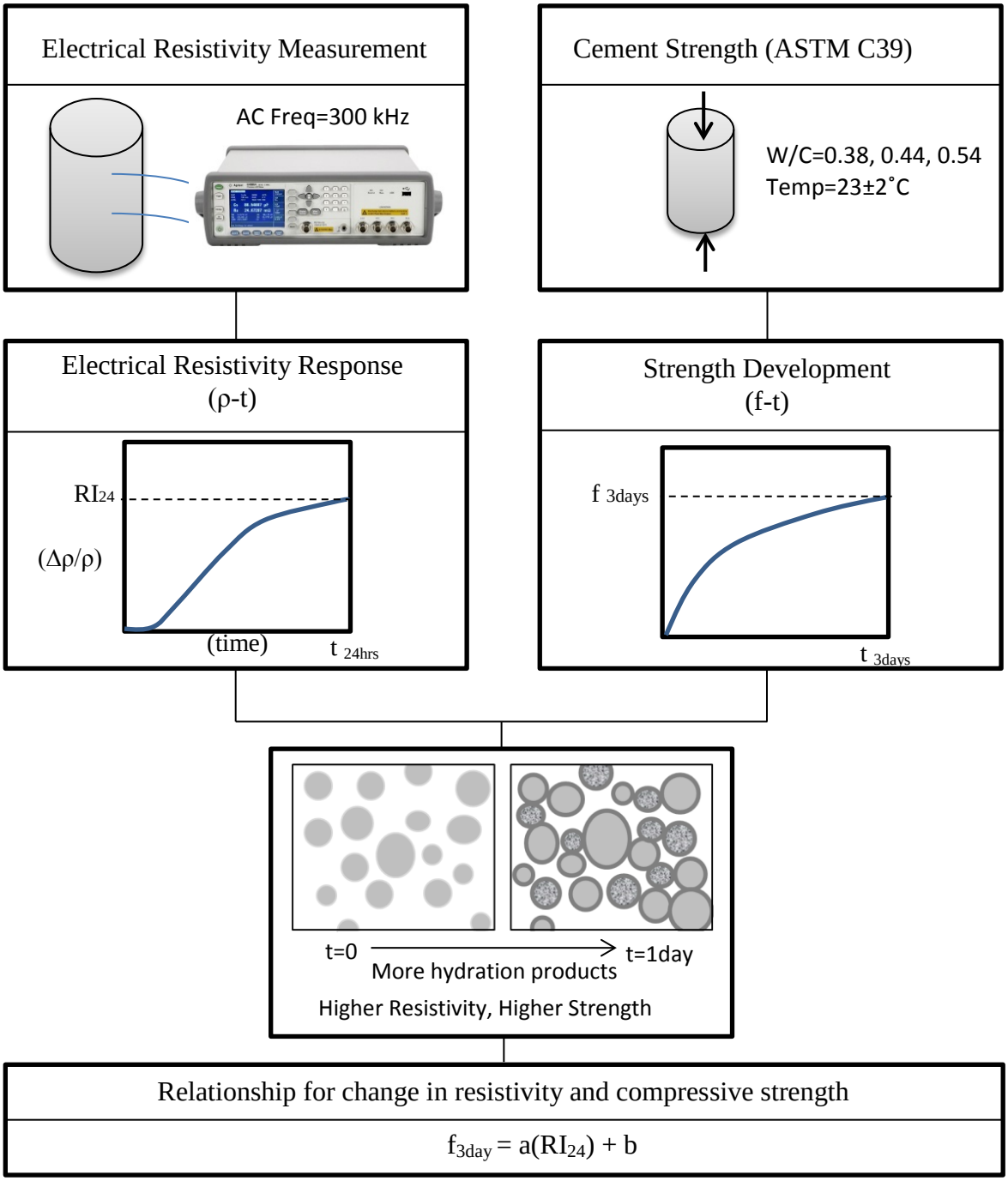

Figure 4-29. Schematic presentation of determination of relationship between the change in resistivity and the compressive strength

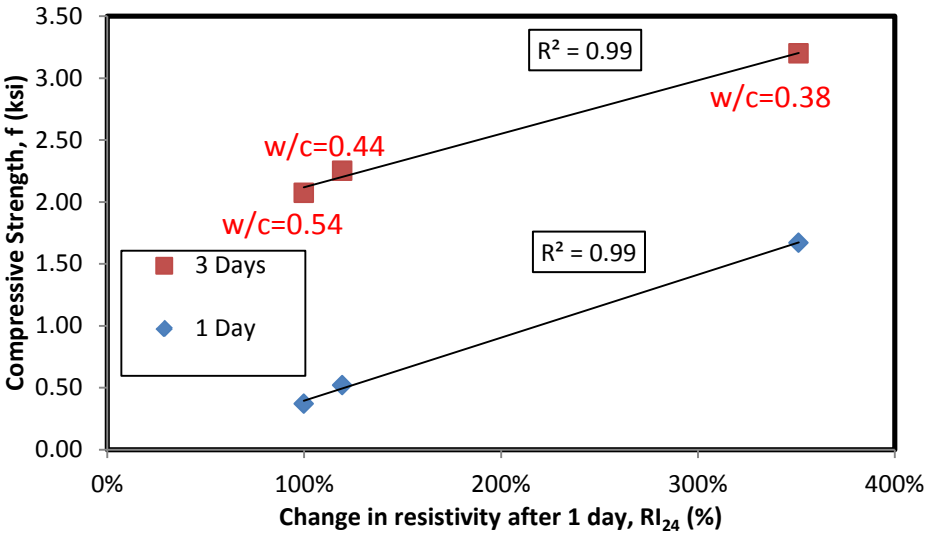

Figure 4-30. Relationship between bulk resistivity change (RI24) and compressive strength of cement

From Fig. 4-30 the relationship between RI_{24} and the 1-day and 3-day compressive strength was

$$f_{1day} = 0.508 \times RI_{24} - 0.11 \text{ and} \tag{4-14}$$

$$f_{3day} = 0.378 \times RI_{24} + 1.88, \text{ respectively.} \tag{4-15}$$

For drilling applications, knowledge of the strength development of cement is important since it affects the wait on cement (WOC) times. Several tests indicated that the electrical resistivity development correlated with the compressive strength development of the cement. Therefore, monitoring the resistivity of the cement was a reliable method to reflect the compressive strength development and determining the WOC times.

4.6.5 Piezoresistive Behavior

Piezoresitive response of specimens is presented in Fig. 4-31. It was found that change in electrical resistivity during compressive loading was more in cement with

higher water-to-cement ratio. Cement slurries that were cured in high temperature showed less piezoresistivity at the same water-to-cement ratio. For example at the compressive stress of 1000 psi which is marked by dashed line in Fig. 4-31, the change in resistivity for cement with w/c of 0.44 was 15% and 30% when the cement was cured at 23°C and 85°C, respectively. At the same compressive stress, change in resistivity was 3 times more for cement with w/c of 0.38 compared to cement with w/c of 0.44. The fractional change in resistivity at failure for 3-day cured sample with water-to-cement ratio of 0.38 was more than 250% which indicated the high piezoresistive sensitivity of smart cement.

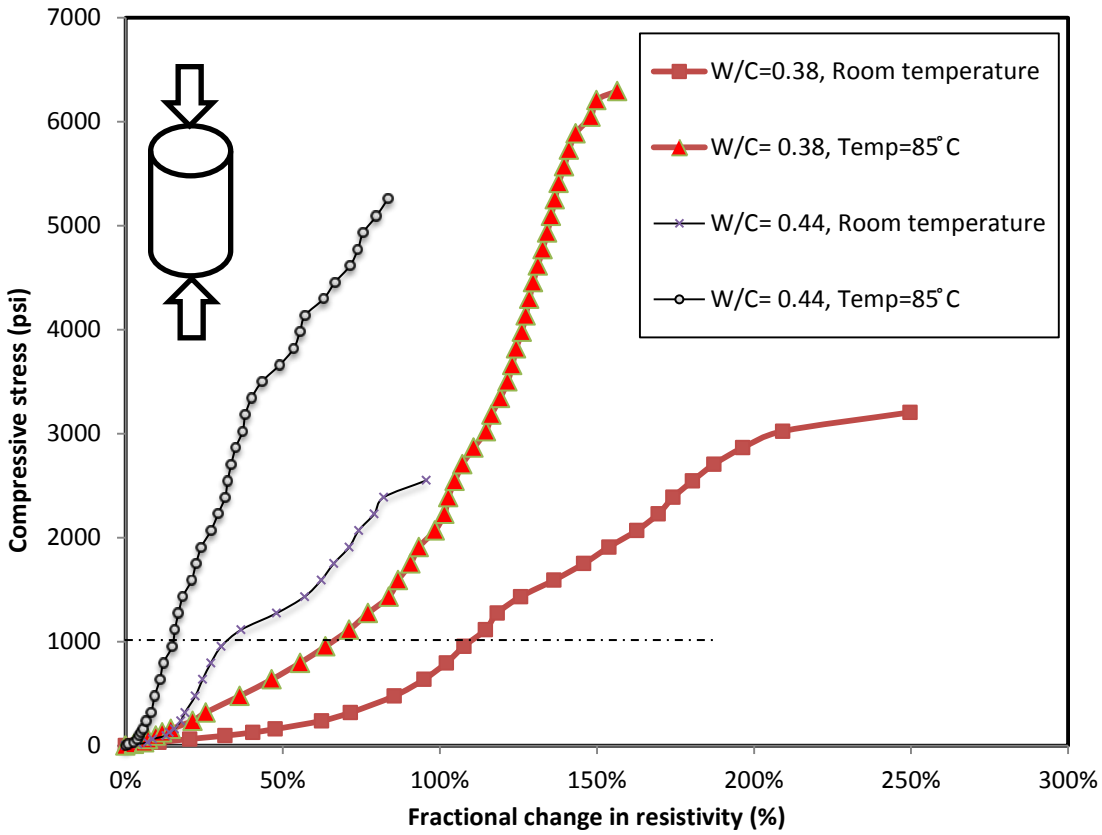

Figure 4-31. Piezoresistive behavior of cement with different w/cs and temperature variations

4.7 Effect of Silica fume on Properties of Smart Cement

In this section, effect of silica fume on smart cement was investigated by addition of 5%, 10%, 15% and 20% (BWOC) of silica fume to cement. The silica fume was replaced by cement and water to solid (cement and silica fume) ratio of 0.38 was remained the same in all the samples. All the cement slurries were mixed with 0.1% of carbon fibers (BWOC) as the base modification.

4.7.1 Electrical Resistivity

Effect of silica fume on initial resistivity of smart cement is illustrated in Fig. 4-32. It was evident that addition of silica fume increased the initial resistivity of cement. The silica fume has micro filling property which means that silica particles fill the pores in the cement paste (Page et al., 1996). The pore solution is the main conduction phase for the cement. Therefore, silica fume increased the initial resistivity of smart cement by filling the pores inside the cement matrix.

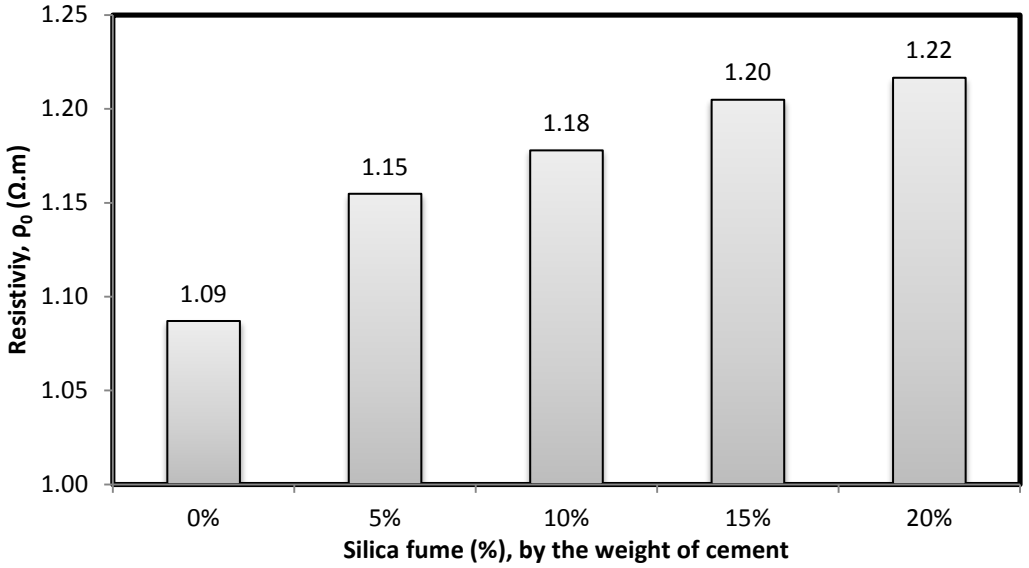

Figure 4-32. Effect of silica fume on initial resistivity of cement

The relationship between the initial resistivity and the silica fume content is given by

$$\rho_0 = 0.0308(SF)^{0.484} + \rho_{neat\ cement}\ , \tag{4-16}$$

where ρ_0 is the initial electrical resistivity of cement and silica fume slurry with water to solid ratio of 0.38. SF is the amount of silica fume replacement with cement, by the weight of cement in percentage and $\rho_{neat\ cement}$ is the initial resistivity of cement with w/c of 0.38 without any silica fume. The prediction of ρ_0 based on various SF concentrations is presented in Fig. 4-33.

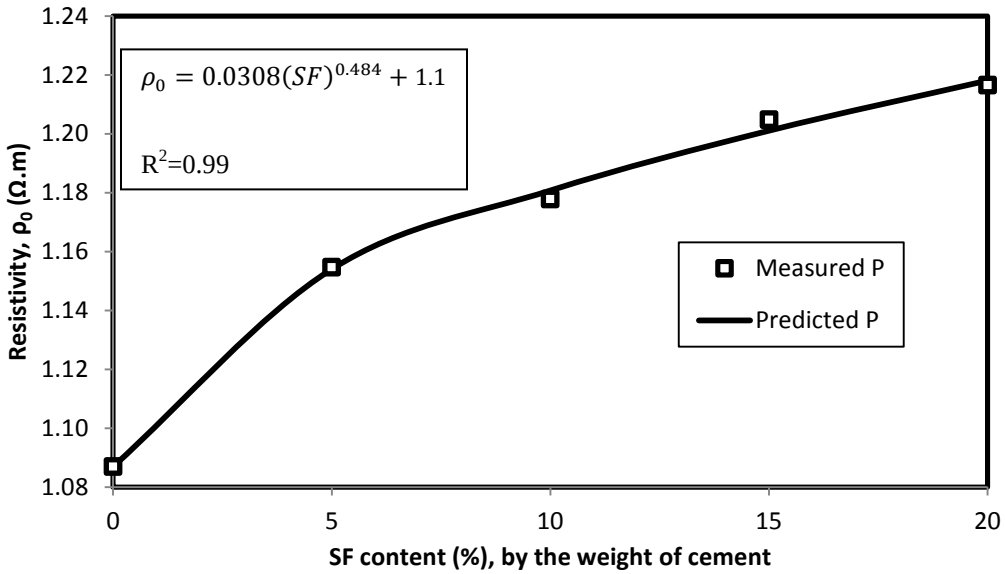

Figure 4-33. Relationship between initial resistivity and percentage of silica fume

4.7.1 Rheological Properties

The stress-strain rate relationship for cement with various amount of silica fume is shown in Fig. 4-34. It was evident that increasing the amount of silica fume increased the viscosity of the cement at all of the shear strain rates. Addition of SF also increased the area of shear stress- strain curves, which showed that the slurries with higher amount of silica fume required higher energy to be pumped. The yield stress was also increased with

increasing the SF content. Increasing the silica fume from 5% to 20% led to a 200% increase in the yield stress. The studies of Mueller (2013) showed that silica fume had a higher surface area compared to oil well cement (about 3 to 4 times). Therefore, it was expected that replacement of cement by silica fume would result in increase in the viscosity and the yield stresses by increasing the friction. The hyperbolic model (Eq. 4-4) prediction is also presented in Fig.4-34. The coefficient of determination (R^2) for the model was in the range of 0.98 to 1 which verified the high accuracy of the hyperbolic model predictions. The hyperbolic model parameters are shown in Table 4-11.

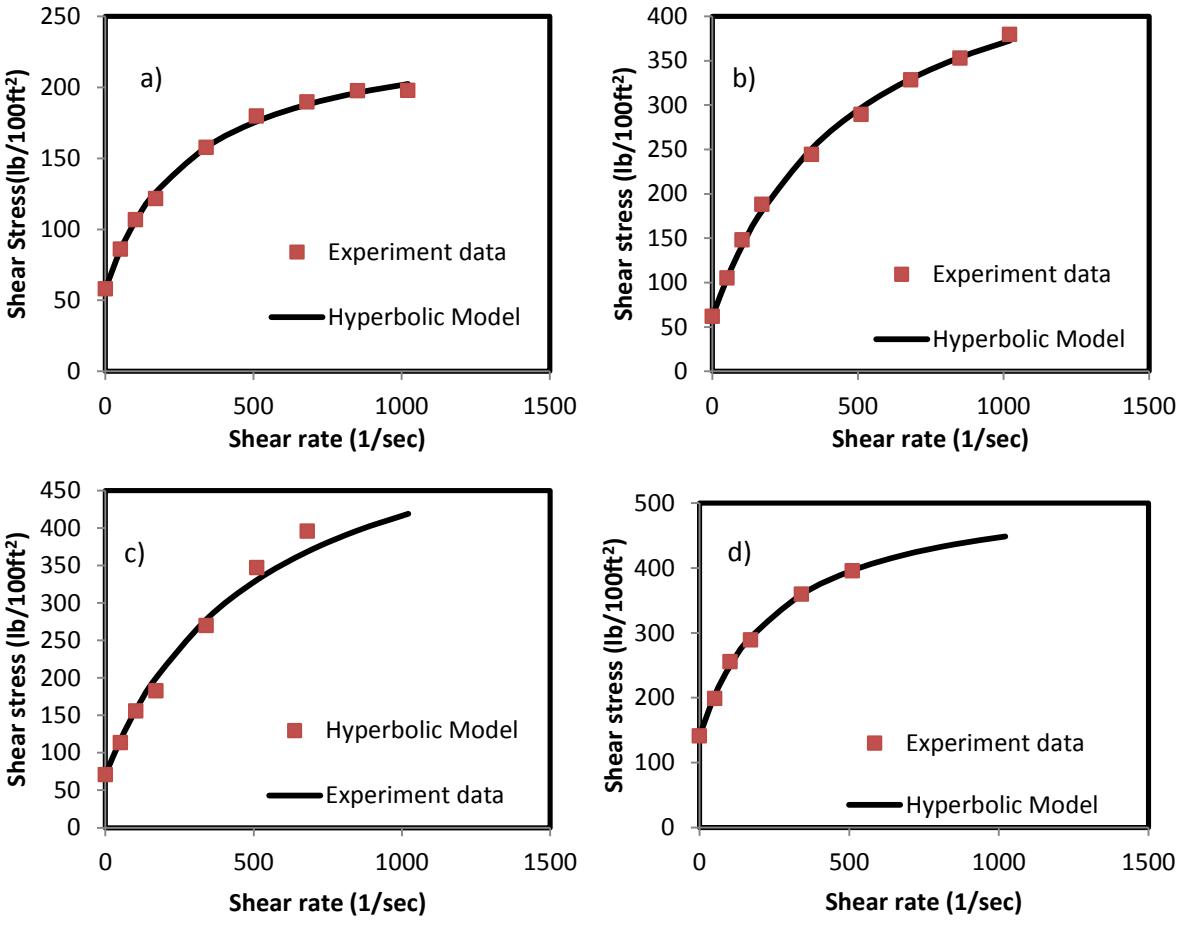

Figure 4-34. Shear stress- strain relationship and hyperbolic model prediction of cement with a) 5% b) 10% c) 15% d) 20% Silica fume

Table 4-11. Hyperbolic model parameters for cement with various amount of silica fume replacement

Silica fume (% BWOC)	*τ_o (lb/100ft^2)	*a	*b	R^2
0	42	4.839	0.0027	0.98
5	58	1.585	0.0053	1
10	62	1.062	0.0021	1
15	71	0.999	0.0018	0.99
20	130	0.564	0.0031	0.98

* τ_o is the yield stress and a and b are hyperbolic model parameters from Eq. 4-4.

Figure 4.35 illustrates the yield stress values for OWC slurries incorporating various dosages of silica fume. It can be observed that compared to the control mixture, the yield stress was increased by up to 69% with increasing the amount of silica fume to 15%. Beyond that point, the yield stress was increased by more than 198% when 20% silica fume was replaced by the cement.

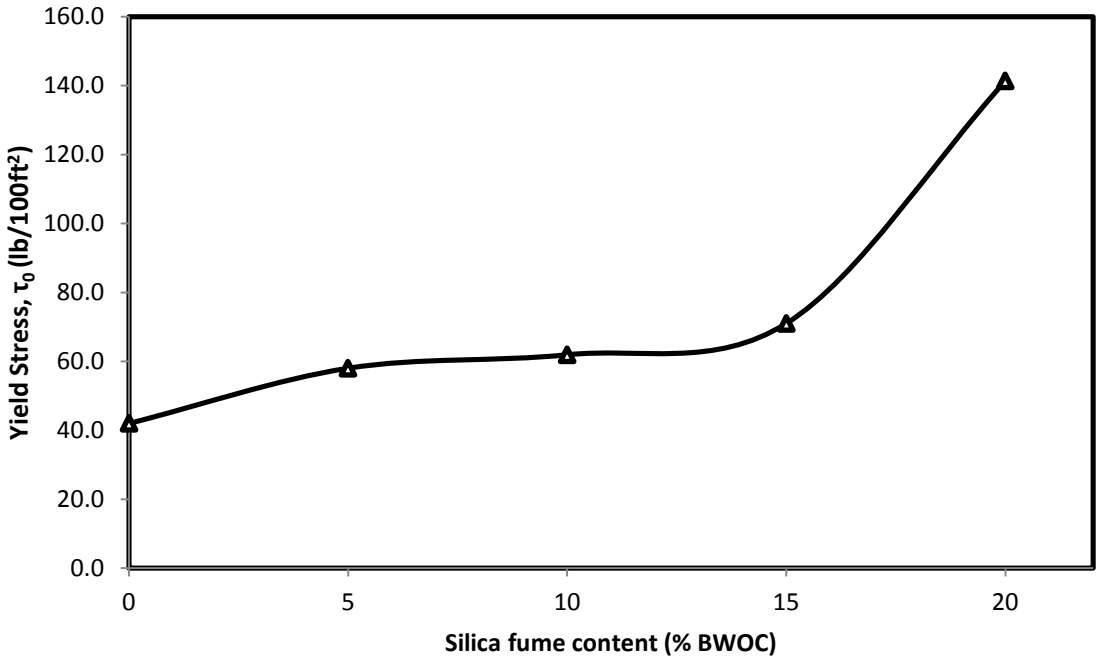

Figure 4-35. Effect of silica fume on yield stress of OWC slurries

4.8 Using External Power to Accelerate the Cement Hydration

In this section, a series of experiment had been performed to investigate the effect of external electrical current on hydration of cement. The electrical current was applied through the wires that were already embedded in the cement. The amplitude of the voltage applied was 10 volts. The specimens were placed inside the calorimeter and the change in temperature was monitored at 1 minute intervals. In order to investigate the effect of the applied electrical power on cement hydration, another calorimetric test was performed on control cement sample without any external power. Fig. 4-36 presents the calorimetric analysis of two cement samples with and without external electrical power.

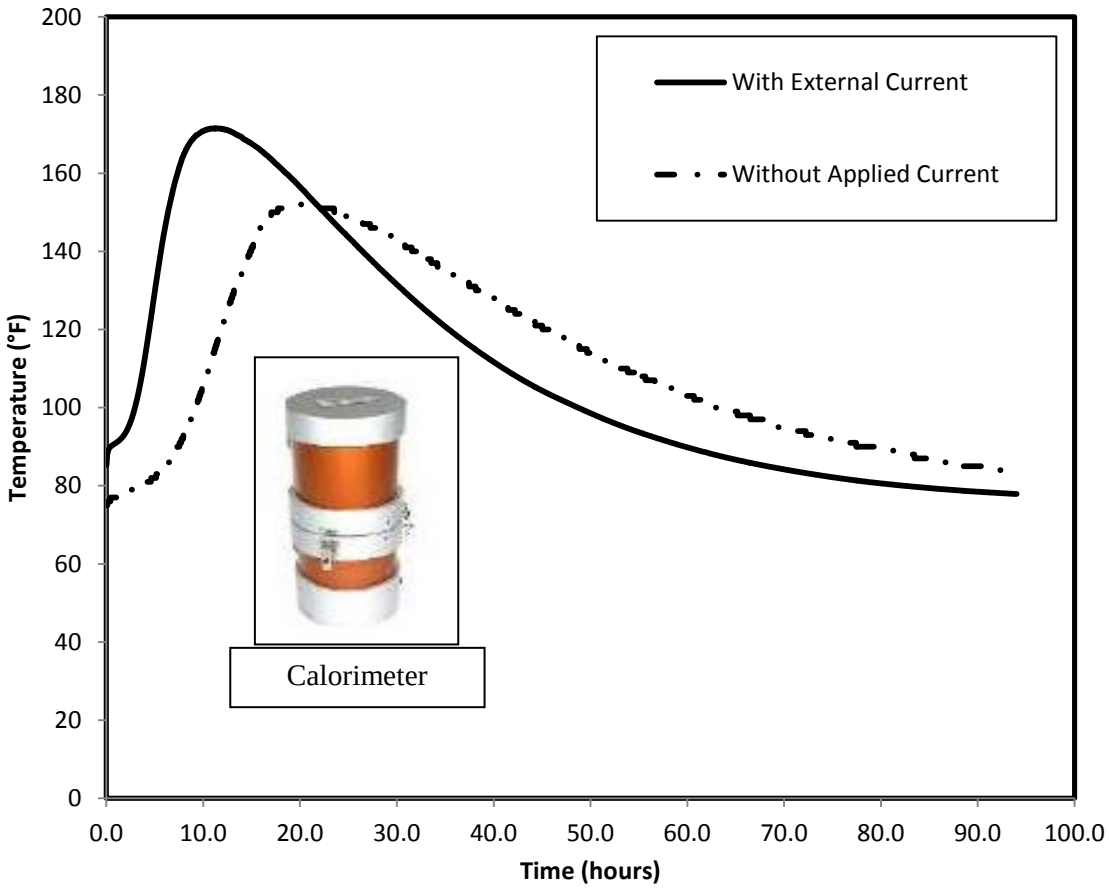

Figure 4-36. Calorimetry of cement with and without the presence of external power

It was observed that applying power to the cement accelerated the hydration. The time to reach the peak temperature for the sample with applied current was 11.5 hours after mixing the slurry. The sample without applied current reached the peak in 22 hours (Table 4-12). It was also clear from the figure and Table 4-12 that the peak temperature for cement with and without external power were 152 °F and 171°F, respectively. This can be explained by the Joule's law for a resistive material, given by

$$Q = I^2 Rt\,, \tag{4-17}$$

where Q is the heat generated, I is the current, R is the electrical resistance of cement and t is the time. According to Eq. (4-17), when the current is applied to a resistor such as cement, a portion of the electrical energy will be converted to the heat and flow out to the material. Applying current to the cement, increased the thermal energy and hence the temperature generation during the hydration. It is reported in the literature that increasing the temperature increases the speed of chemical reactions and the rate of hydration (Pane et al., 2005). In this test, the peak temperature was shifted to the left when the power was applied to cement which confirms the acceleration in the hydration.

Table 4-12. Summary of the calorimetric test for the cement with and without applied current

Condition	Peak temperature (°F)	Time to reach the peak (Hours)	Area under the curve up to peak
Without Applied power	152	22	112,412
10 V DC power applied	171	11.5	103,568

Electrical resistivity of the two samples was monitored during the calorimetric test. Weight lost was also monitored to assure that the changes in resistivity were only due to the effect of the applied current. The resistivity responses during 110 hours of curing are

presented in the Figs. 4-37(a) and 4-37(b). According to the figures the change in electrical resistivity for the cement with external power was more than 400 times higher compared to the control sample, when the weight loss in both specimens was minimal. This is another indicator that shows the acceleration in the rate of hydration with the applied electrical current.

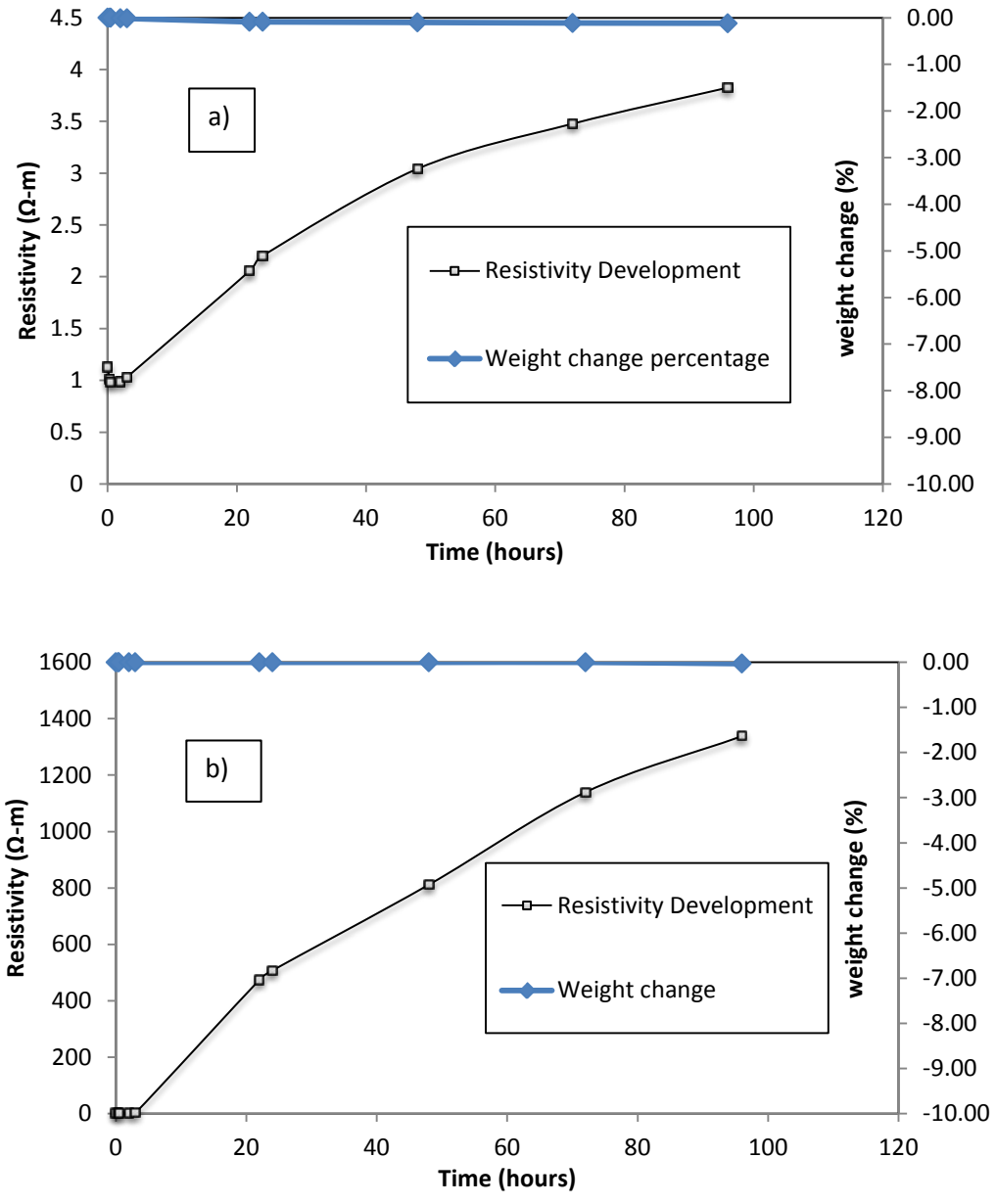

Figure 4-37. Resistivity response for a) Control sample b) Cement with applied power

4.10 Summary

In this chapter the smart cement was characterized. The effects of various mineral admixtures on the sensing properties of API Class H oil well cement slurries were investigated. Experiments were done to evaluate the effect of various w/c ratios and curing temperatures on properties of smart OWC. Finally colorimetric tests were performed to investigate the effect of applied current on the hydration of smart cement. Based on the experimental results the following conclusions can be drawn:

1. It was found from Impedance spectroscopy tests that smart cement was a resistance-only material, the resistance of cement at 300 kHz frequency was in the range of the bulk resistance of the material.
2. Addition of carbon fibers increased the piezoresistive sensitivity of the cement without compromising the rheological or mechanical properties.
3. Initial electrical resistivity with various admixtures was sensitive to the composition of the slurry.
4. The electrical resistivity responses during curing for various samples followed the same trend. Resistivity reduced to a minimum point, increased sharply and then increased gradually with a lower rate. Therefore, electrical resistivity was a sensitive parameter to monitor the changes during curing of cement
5. Cement with various w/c ratios had different resistivity responses. The change in resistivity was higher for cement with lower water-to-cement ratios.

6. A correlation was found between percentage change in electrical resistivity and the compressive strength and of cement with different water-to-cement ratios after 3 days of curing.
7. The rheological test showed that class H cement had shear-thinning behavior and a hyperbolic model was proposed to predict shear stress- strain relationship. The model was fitted with the experimental data for cement with several compositions.
8. The study revealed that both yield stress and apparent viscosity increased with reducing the water-to-cement ratio and increasing the temperature.
9. Smart cement exhibited piezoresistive behavior and the change in electrical resistivity at failure was varied from 60 to more than 780%.
10. It was found that the piezoresistive sensitivity was affected by water-to-cement ratio, age of the cement and the temperature in which the sample was cured.
11. Calorimetric tests proved that applying external power to cement led to increase in the rate of hydration.

Chapter 5

SMART CEMENT CONTAMINATED WITH OIL BASED MUD

In this chapter contamination of smart cement with oil based drilling mud was investigated. Two series of cement slurries were prepared, uncontaminated, and contaminated with oil based drilling mud (OBM). Vegetable oil based mud was used to prepare the mud sample with oil to water ratio of 4:1 and 1% chemical surfactant. Contaminated cement samples included 0.1%, 1%, and 3% OBM, BWOC. In order to simulate the contamination in the wellbore, OBM was added to the cement slurry after 10 minutes of mixing. The rheological tests were performed to examine the effect of contamination of flow properties of cement. The shear stress-strain relationship was determined using a hyperbolic model. Compression tests were performed to evaluate the OBM contamination impact on strength of cement, and electrical resistance was measured during the compressive loading to obtain the piezoresisive behavior of smart cement contaminated with OBM.

5.1 Density

The average density of the modified cement was 16.36 ppg. Since the density of OBM was lower than that of the cement, OBM contamination reduced the density of cement slurries. Densities of samples are summarized in Table 5-1. The density of 0.1% and 3% OBM contaminated cement were reduced by 0.98% and 5.5%, respectively. The

decrease in density was due to the increased amount of air voids that was visible in contaminated samples.

Table 5-1. Effect of OBM contamination on density of cement samples

OBM contamination	Density (ppg*)
Uncontaminated	16.36
0.1% OBM Contaminated	16.20
1.0% OBM Contaminated	16.02
3.0% OBM Contaminated	15.50

*1 ppg = 1lb/gal = 119.83 kg/m^3

5.2 Rheological Properties

5.2.1 Effect of Contamination

It was evident from the rheological tests that both contaminated and uncontaminated cement slurries have shear-thinning behavior. OBM contamination reduced the rheological properties of modified cement. For instance, the viscosity of uncontaminated cement at a shear strain rate of 100 (1/sec) was 282 cp. At the same shear strain rate 0.1% OBM contaminated sample had viscosity of 204 cp. Contamination of cement with up to 3% OBM reduced the viscosity by more than 30% at the shear strain rate of 100 (1/sec). The viscosity was also reduced at higher shear strain rates with OBM contamination. The yield point of 0.1%, 1% and 3% OBM contaminated cement slurries was reduced by more than 37%, 25% and 22% respectively. The Bingham plastic relationship for uncontaminated and contaminated cement also shows a reduction in both yield point and plastic viscosity (Table 5-2). This is because of the lower friction in contaminated slurries due to the lubricating effect of OBM.

5.2.2 Modeling

Due to the shear-thinning behavior of the cement slurries Bingham plastic model was not an accurate model to estimate the shear strain rate – shear stress relationship. To predict the shear stress versus the shear strain rate, a hyperbolic model was proposed and fitted with the experimental data. The developed hyperbolic model is presented in Eq. 5-1 as

$$\tau = \tau_{\circ} + \frac{\dot{\gamma}}{A+\dot{\gamma}B} \ , \tag{5-1}$$

where τ_0 is the yield stress at 0 shear strain rate (lb/100 ft^2), $\dot{\gamma}$ is the shear strain rate (1/sec) and A and B are the hyperbolic model parameters. Experimental observations and hyperbolic prediction for two cement slurries are shown in Fig. 5-1. The advantage of the proposed model is its higher accuracy especially at higher strain rates. A comparison of the proposed model with the Herschel-Bulkey model (Eq.4-4) which is widely being used in industry is also illustrated in Fig. 5-2. A Summary of the rheological parameters for Bingham plastic, Herschel-Bulkey and the proposed hyperbolic model is provided in Table 5-2.

Table 5-2. Summary of rheological model parameters

	Hyperbolic Model				**Herschel-Bulkley**				**Bingham Model**		
OBM contamination	$\boldsymbol{\tau_0}$	**A**	**B**	**R^2**	$\boldsymbol{\tau_0}$	**K**	**n**	**R^2**	**YP**	**PV**	**R^2**
0	42.0	4.8	0.0027	0.99	36.5	0.25	0.91	0.98	83.4	39.6	0.65
0.1%	19.0	3.5	0.0129	0.98	17.5	1.48	0.56	0.97	51.8	17.0	0.54
1%	19.6	4.1	0.0128	0.98	16.3	2.10	0.49	0.98	62.4	8.4	0.34
3%	21.8	2.2	0.0111	0.99	19.7	4.495	0.419	0.98	64.9	17.1	0.47

$\boldsymbol{\tau_0}$ is the yield stress in lb/100ft^2, a and b are hyperbolic model parameters, K and n are HB model parameters and PV is the plastic viscosity in centipois (cp).

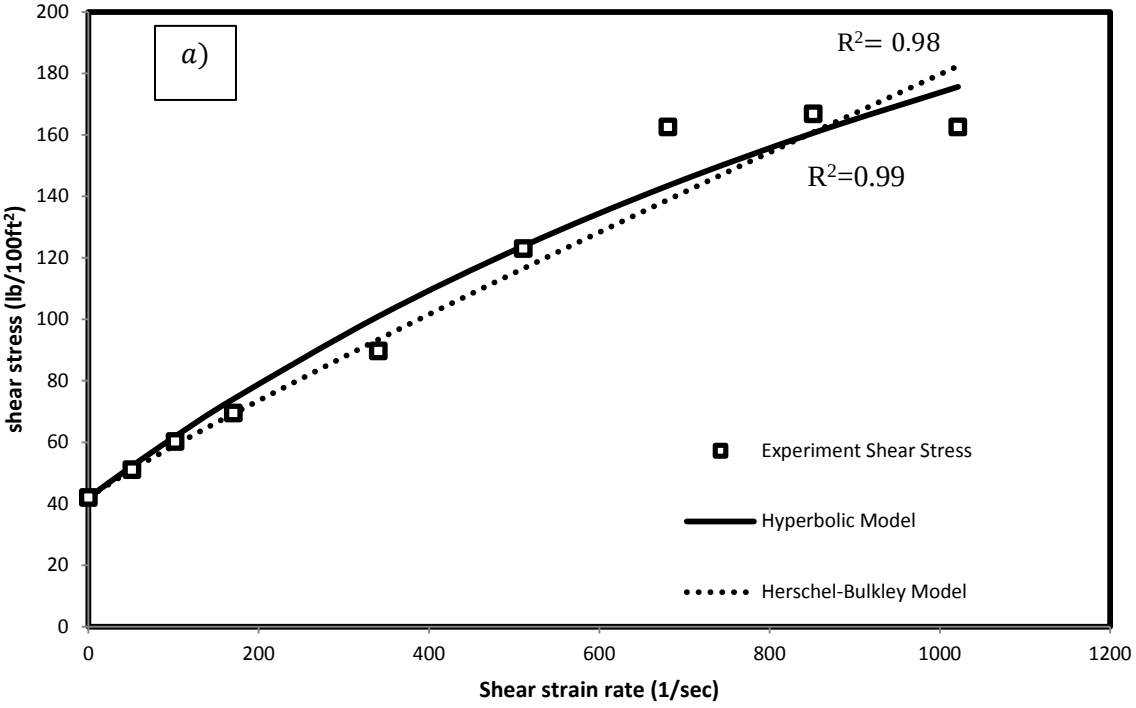
a)
R²= 0.98
R²=0.99
shear stress (lb/100ft²)
Shear strain rate (1/sec)
Experiment Shear Stress
Hyperbolic Model
Herschel-Bulkley Model
0
20
40
60
80
100
120
140
160
180
200
0
200
400
600
800
1000
1200

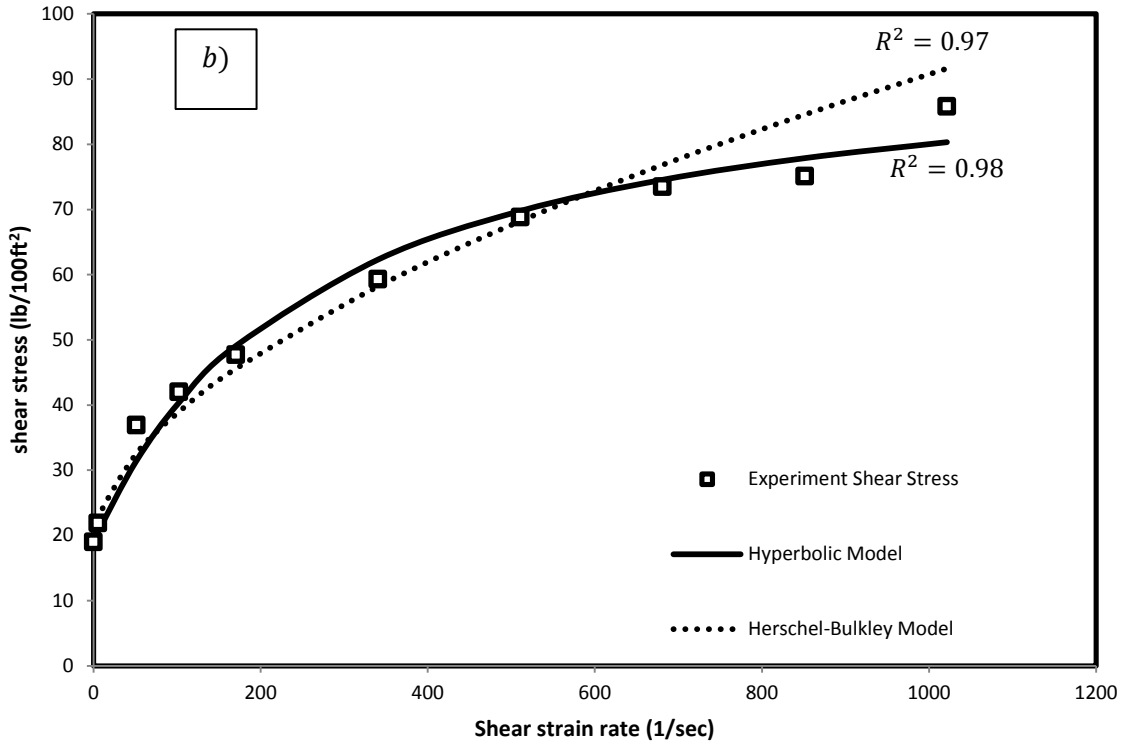
b)
$R^2 = 0.97$
$R^2 = 0.98$
shear stress (lb/100ft²)
Shear strain rate (1/sec)
Experiment Shear Stress
Hyperbolic Model
Herschel-Bulkley Model
0
10
20
30
40
50
60
70
80
90
100
0
200
400
600
800
1000
1200

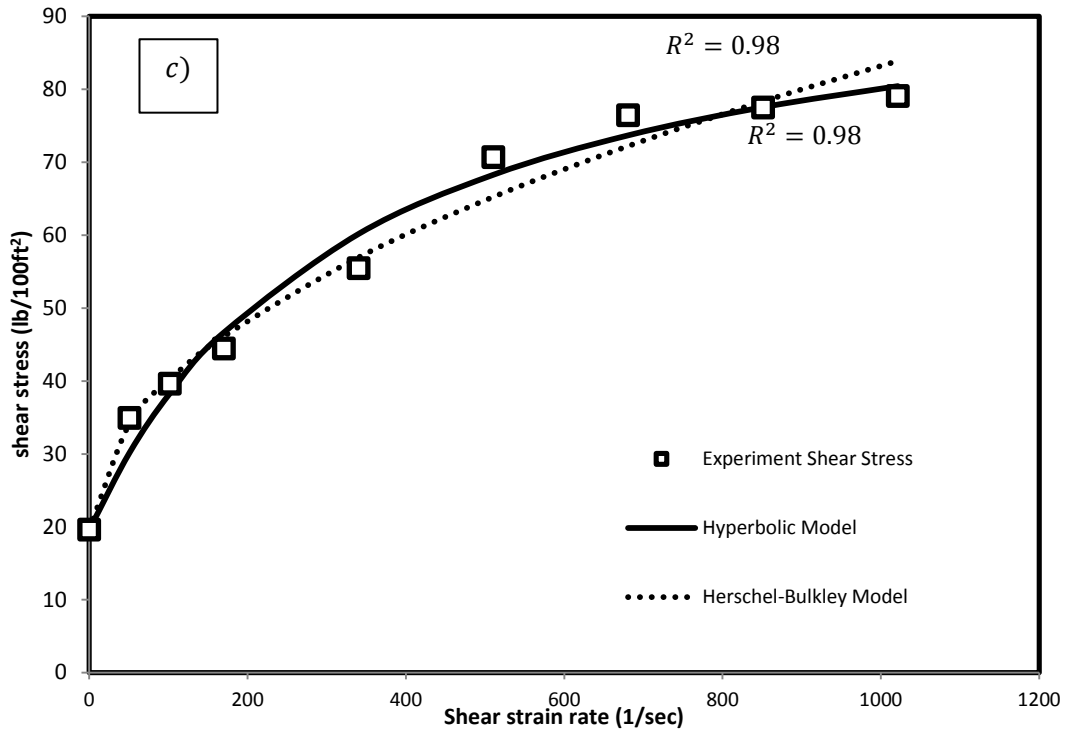

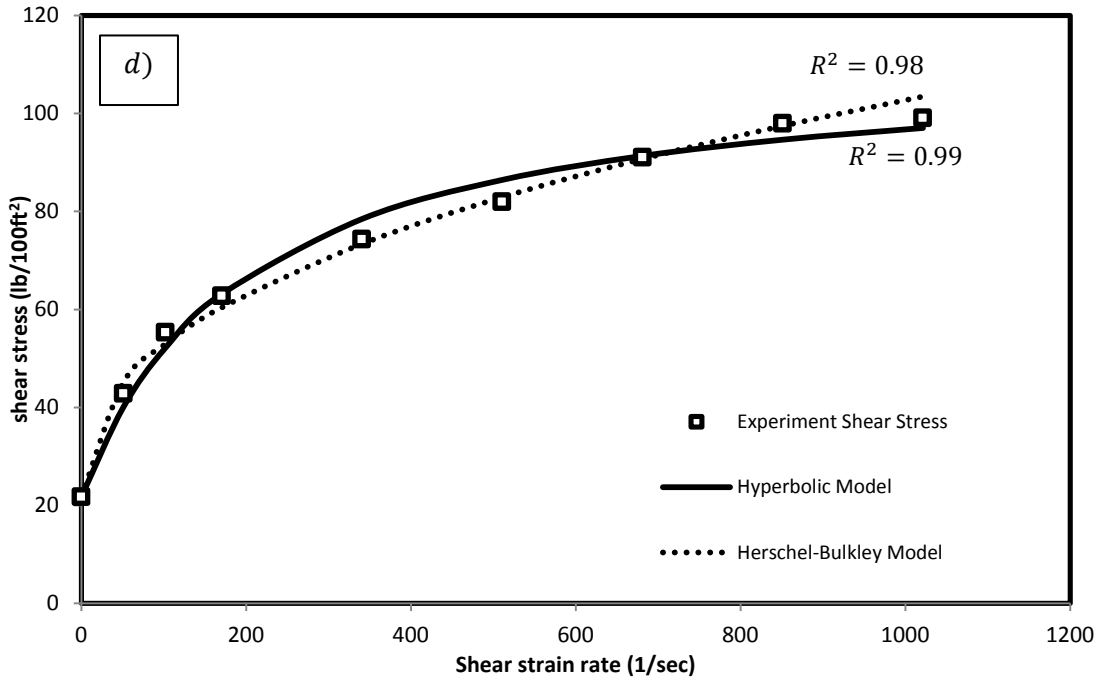

Figure 5-1. Experimental data, hyperbolic model and Herschel-Bulkley model prediction of shear stress vs. shear strain rate for a) Uncontaminated b) 0.1% OBM Contaminated c) 1% OBM Contaminated d) 3% OBM Contaminated slurries

5.3 Electrical Resistivity

5.3.1 Initial Resistivity

Electrical resistivity of uncontaminated and contaminated cement immediately after preparing the sample is shown in Fig 4. As shown in the figure, the initial electrical resistivity of the modified cement increased with increasing the mud contamination. The average initial electrical resistivity of modified uncontaminated cement was 1.06 Ω.m. contaminating the cement with only 0.1% of OBM increased its electrical resistivity to 1.95 Ω.m which is 84% more than the uncontaminated cement. When cement was contaminated with 1% and 3% OBM the increment in initial electrical resistivity was more than 216% and 304%, respectively. From the figure the initial Density was slightly reduced when cement was contaminated with OBM. Contamination of cement with 0.1%, 1% and 3 Percent OBM increased initial electrical resistivity more than 84%, 216% and 304%, respectively. Hence, electrical resistivity was highly sensitive to OBM contamination, and initial electrical resistivity of cement is one of indicators to detect of OBM contamination.

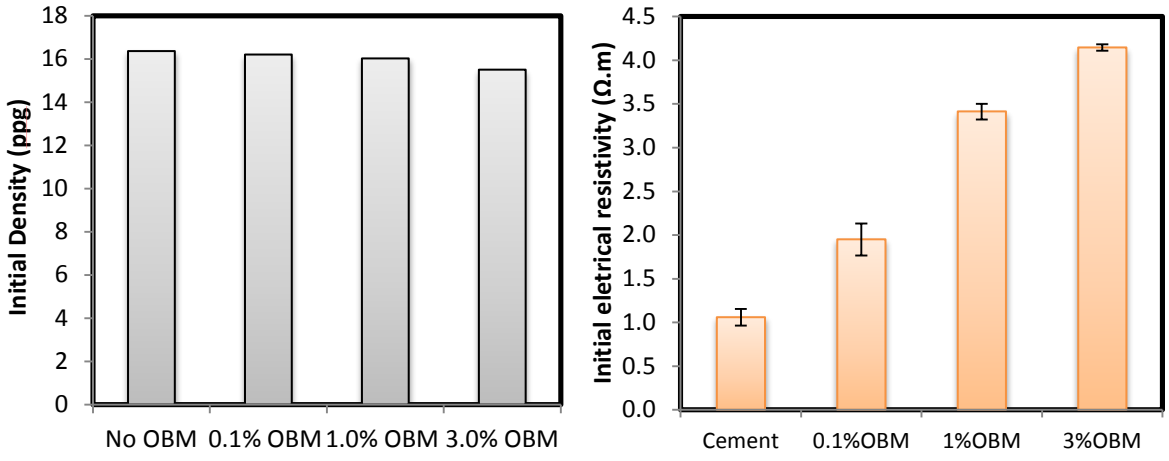

Figure 5-2. Initial density and resistivity of the cement slurries with OBM contamination

5.3.2 Resistivity during Curing Process

As outlined in chapter 4 electrical resistivity could be used as a fingerprint of curing process. Figure 5-3 illustrates the change in electrical resistivity (ρ) during curing time for modified uncontaminated cement with w/c of 0.38. It was observed that the electrical resistivity of cement with and without contamination had the same characteristics. The electrical resistivity dropped to a minimum value, and then gradually increased with time. The minimum resistivity value (ρ_{min}) and the corresponding time to reach the minimum resistivity was t_{min}, as shown in Fig.5-3. Change in electrical resistivity with respect to minimum resistivity was significantly varied when cement was contaminated with even low concentrations of OBM. Therefore tracking the change in resistivity of cement reflected a clear understanding of hydration process and strength development of cement with different OBM contaminations.

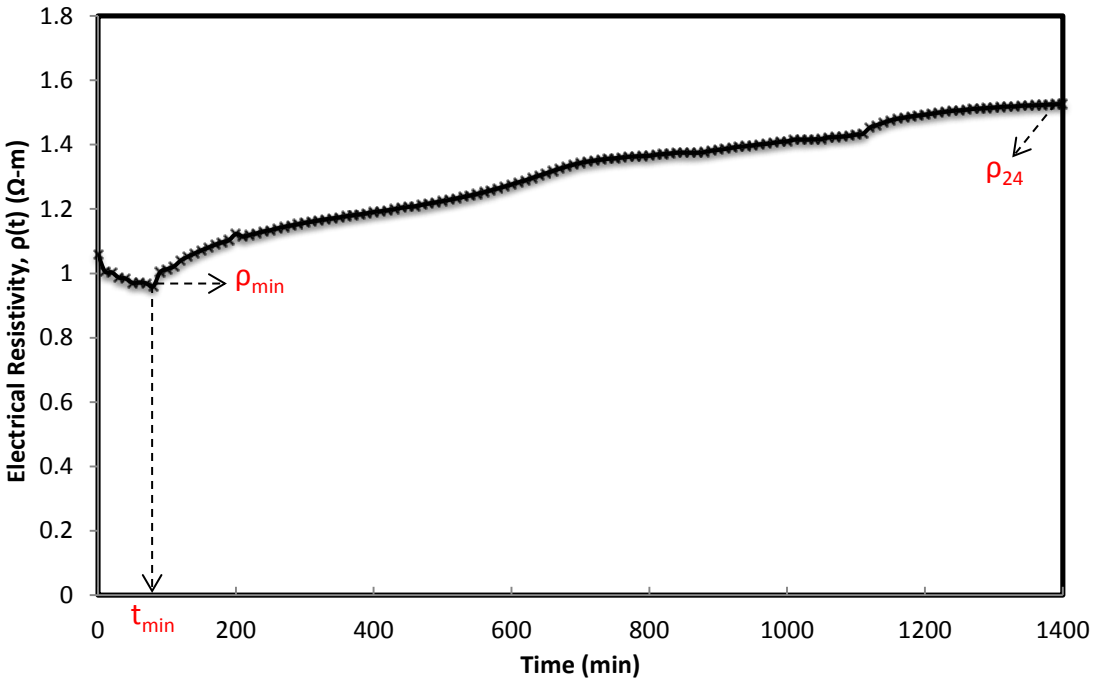

Figure 5-3. Electrical resistivity response of uncontaminated cement with w/c of 0.38

Variations of electrical resistivity with time for samples with different OBM contaminations using DC measurement are summarized in Table 5-3. OBM contamination increased the minimum resistivity of cement (ρ_{min}). With 0.1% contamination the minimum resistivity of cement increased from 0.96 Ω.m to 1.89 Ω.m, a 96 percent increase. Subsequently, higher OBM contamination increased the $t_{min,}$ and decreased the change in resistivity. In order to better quantify the resistivity change in 24 hours, resistivity index (RI_{24}) is defined as the maximum percentage change in resistivity with respect to minimum resistivity. RI_{24} in uncontaminated cement was 59.1% (Table 5-3). With 3% OBM contaminated RI_{24} was reduced to 22.4%. Change in electrical resistivity indicates that, less hydration products developed in a contaminated cement system than that developed in an uncontaminated cement system.

Table 5-3. Electrical resistivity response of uncontaminated and OBM contaminated cement

	Initial resistivity (Ω-m)	**ρ_{min} (Ω-m)**	**t_{min} (minute)**	**ρ_{24} (Ω-m)**	$\frac{(\rho 24 - \rho min)}{\rho min}$
Uncontaminated	1.06	0.96	70	1.53	59.11%
0.1% OBM	1.95	1.89	70	2.92	54.74%
1.0% OBM	3.35	3.28	80	4.34	32.21%
3.0% OBM	4.28	4.14	100	5.07	22.40%

5.4 Compressive Strength

5.4.1 Effect of Contamination

The compressive strength of uncontaminated cement was 1.1 ksi and 3.2 ksi after 1 day and 28 days of curing. As shown in Fig. 5-4 compressive strength of OBM contaminated cement is depended on the amount of contamination. Compressive strength appears inversely proportional to concentration of OBM. For instance, 3% OBM contamination reduced the 1-day compressive strength of cement by more than 77% compared to the uncontaminated modified cement. For the same sample the 28 day compressive strength was 32% lower than that of uncontaminated sample.

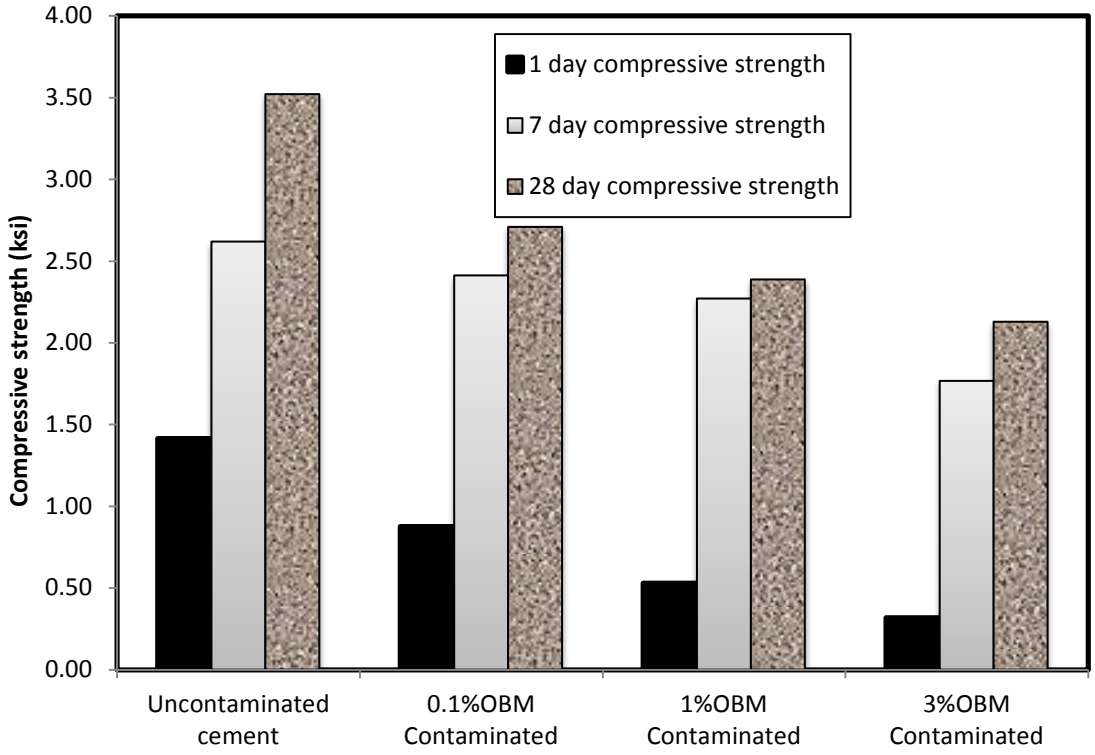

Figure 5-4. Compressive strength development of OBM contaminated cement at 1, 7 and 28 days of curing

5.4.2. Relationship between Resistivity and Compressive Strength

A similar observation was found in 1-day resistivity change with increasing the contamination. Compressive strength and electrical resistivity development depends on the hydration process. OBM contamination reduced the compressive strength and the change in electrical resistivity (RI_{24}) in all of the samples studied. Of the various resistivity parameters RI_{24} had a direct correlation with the compressive strength of cement for each curing time (1, 7 and 28 days) with and without contamination. The relationship between the change in electrical resistivity and compressive strength is shown in Fig. 5-5. It was clearly shown that by monitoring the changes in electrical resistivity of modified smart cement, an estimation of strength development can be obtained.

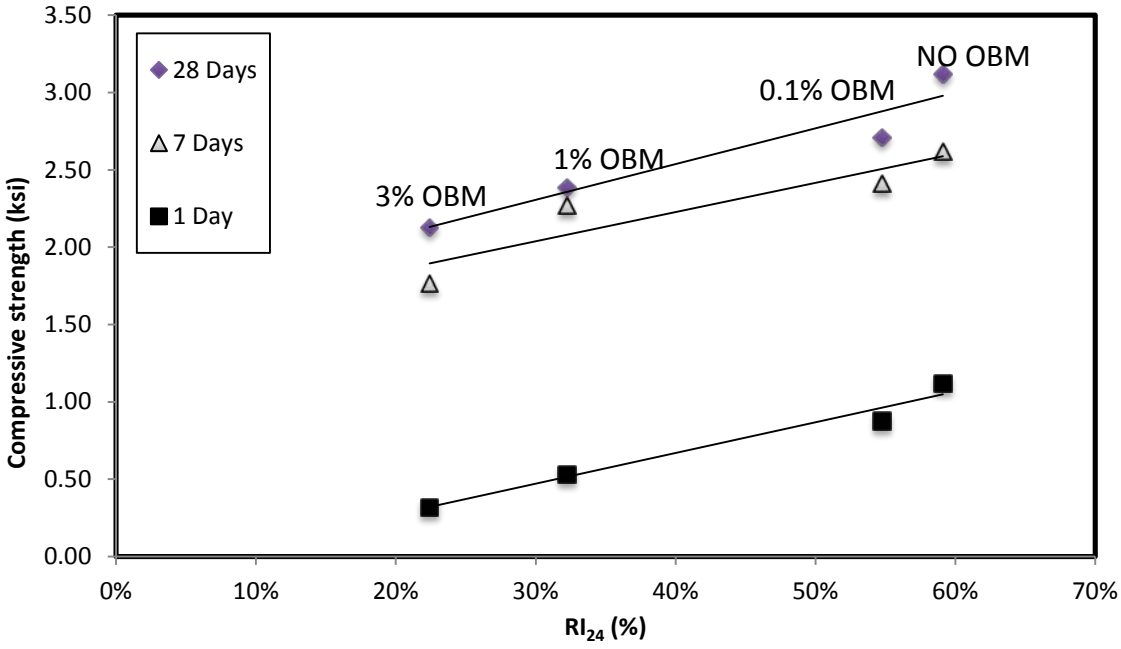

Figure 5-5. Linear relationship between 1-day electrical resistivity change and 1-day, 7-day and 28-day compressive strength for uncontaminated and OBM contaminated cement

5.5 Piezoresistivity

The piezoresistive behavior (compressive stress versus change in resistivity) of uncontaminated and contaminated cement is shown in Figs. 5-6 to 5-10. Electrical resistivity was sensitive to the compressive loading. All the figures indicate an increase in change in resistivity when mechanical compressive load is applied. Figures show that electrical resistivity change increased during compressive loading, and there was a sharp increase when minor and major cracks were formed.

OBM contamination affected the piezoresistive response of smart cement. At compressive stress of 400 psi, which is marked by the horizontal dashed line in Fig. 5-6, change in resistivity was 378% for cement without contamination. At the same stress level change in resistivity was 327%, 271% and 220% for 0.1%, 1% and 3% OBM contaminated cement, respectively. After one day of curing the uncontaminated smart cement failed at a resistivity change of 780 percent, while the 3% OBM contaminated cement failed at a resistivity change of 220 percent (Fig 5-8). The same pattern can be seen in Figs 5-9 and 5-10; hence, the piezoresistive sensitivity was abruptly reduced by the contamination of cement after 1 and 28 days of curing. For 3% OBM contaminated specimen after 28 days of curing, the change in electrical resistivity at failure was 3 times lower than that of the uncontaminated cement. The formation of the cracks can be observed by the normalized plots [Figs 5-7(b) to 5-10(b)]. There was a great increase in the $\Delta\rho/\rho$ value when cracks were formed and also when at the failure of cement. The trends clearly showed the high sensitivity of responses to OBM contaminations. Also it was revealed from the experiment that contaminating the cement with oil-based mud had reduced the piezoresistivity of cement dramatically.

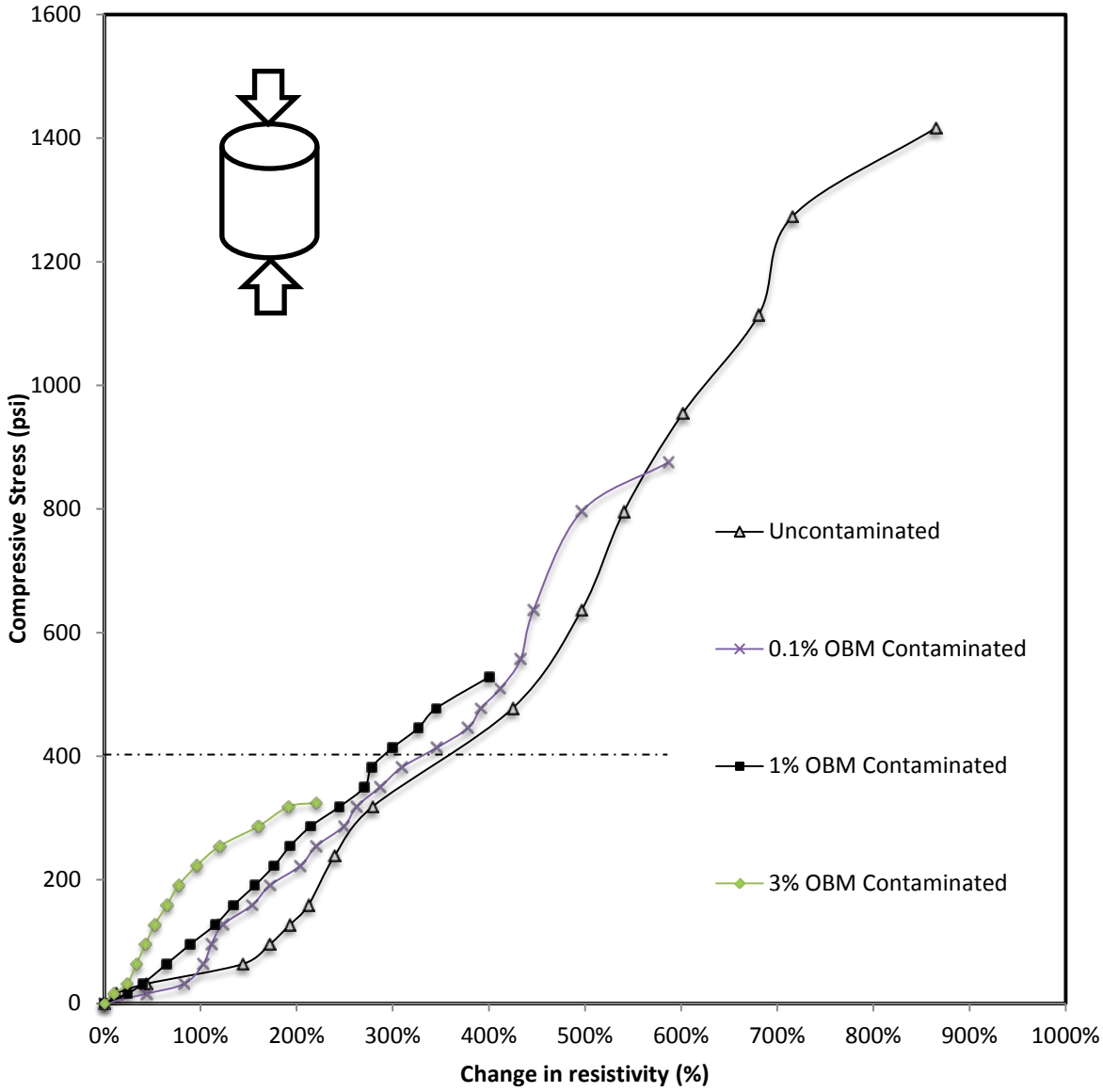

Figure 5-6. Piezoresistive behavior of cement with various OBM contaminations after 1 day of curing

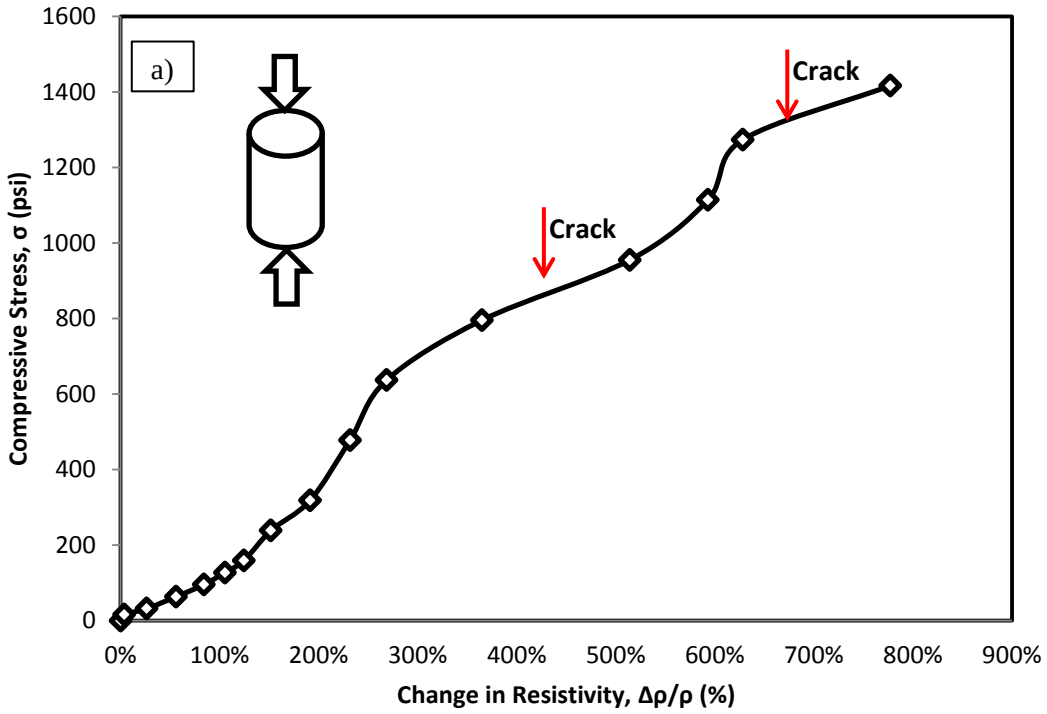

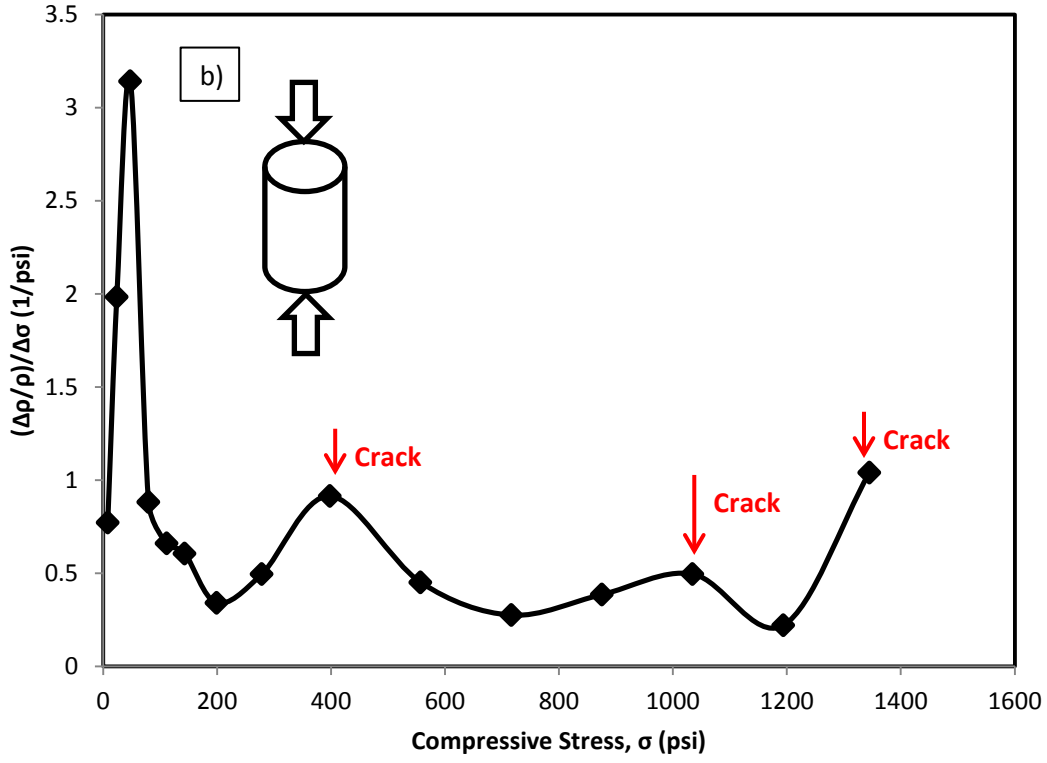

Figure 5-7. Piezoresistive behavior of cement without contamination after 1 day of curing a) Compressive stress vs. change in resistivity b) Change in resistivity normalized by change in stress vs. compressive stress

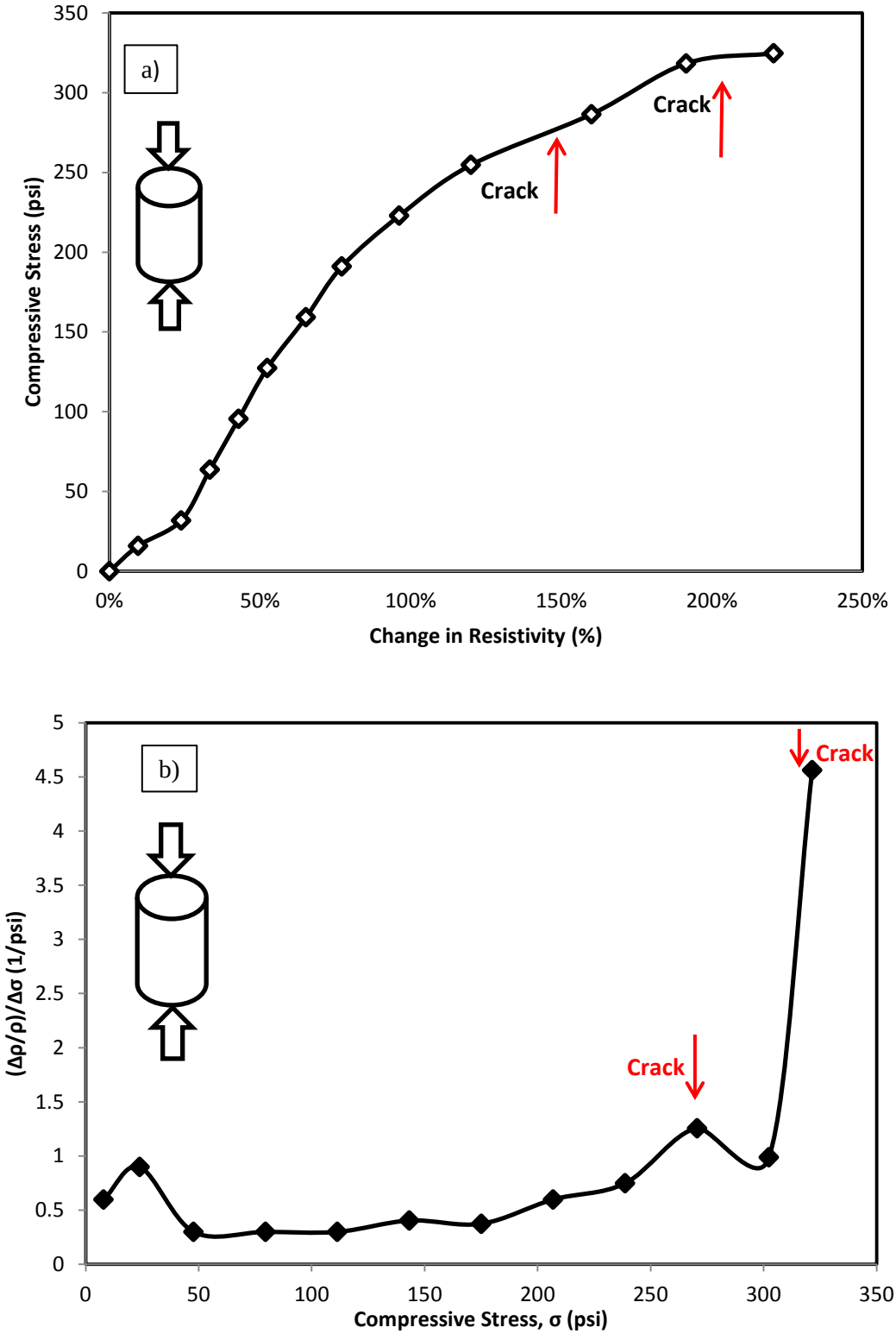

Figure 5-8. Piezoresistive behavior of cement with 3% OBM contamination after 1 day of curing a) Compressive stress vs. change in resistivity b) Change in resistivity normalized by change in stress vs. compressive stress

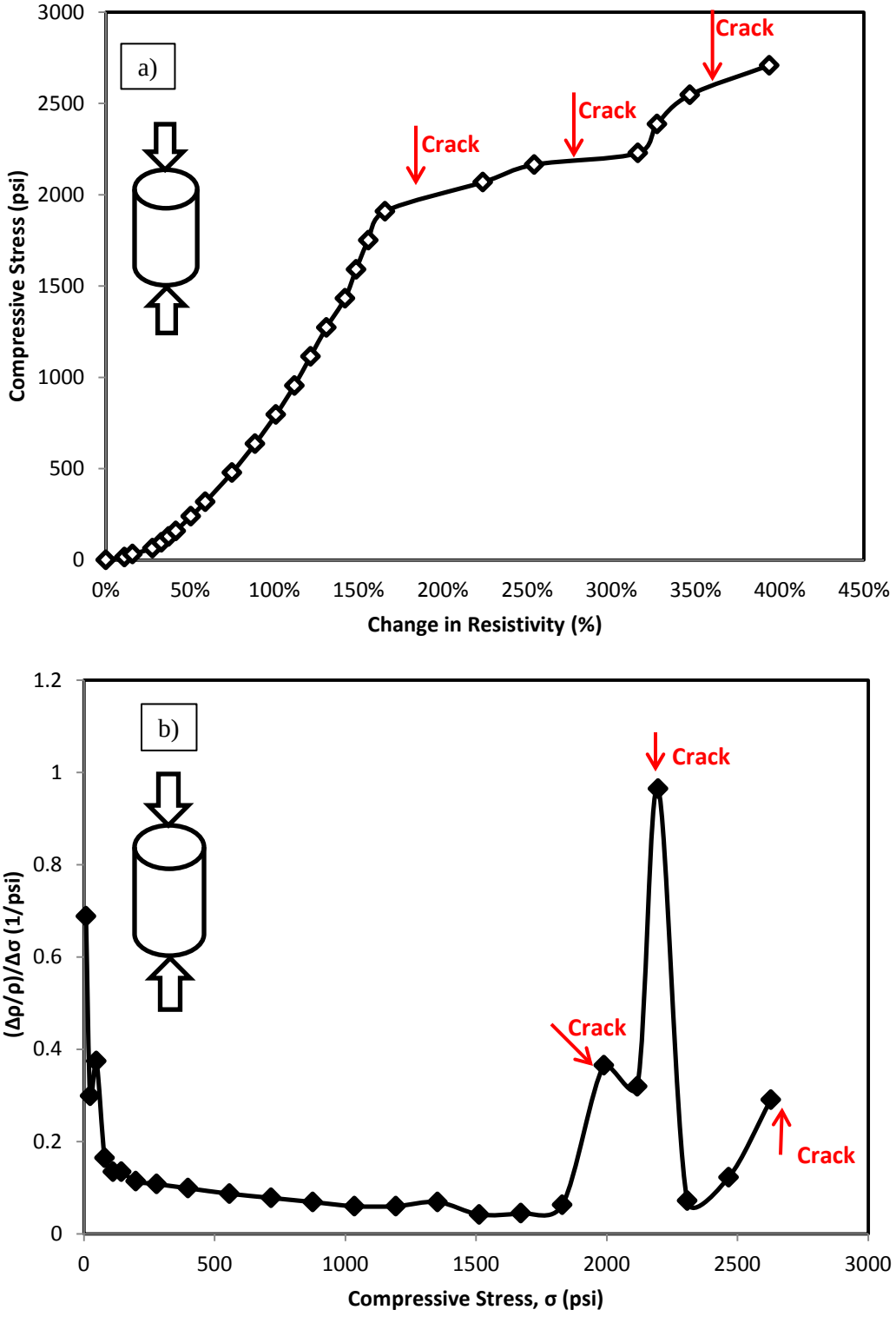

Figure 5-9. Piezoresistive behavior of cement without contamination after 28 days of curing a) Compressive stress vs. change in resistivity b) Change in resistivity normalized by change in stress vs. compressive stress

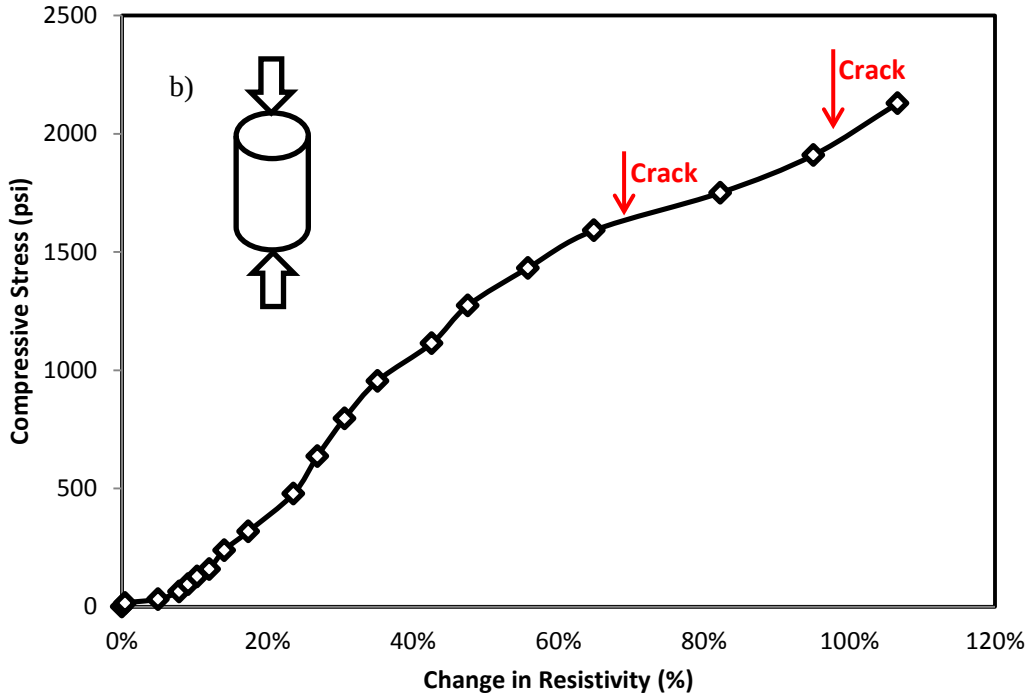

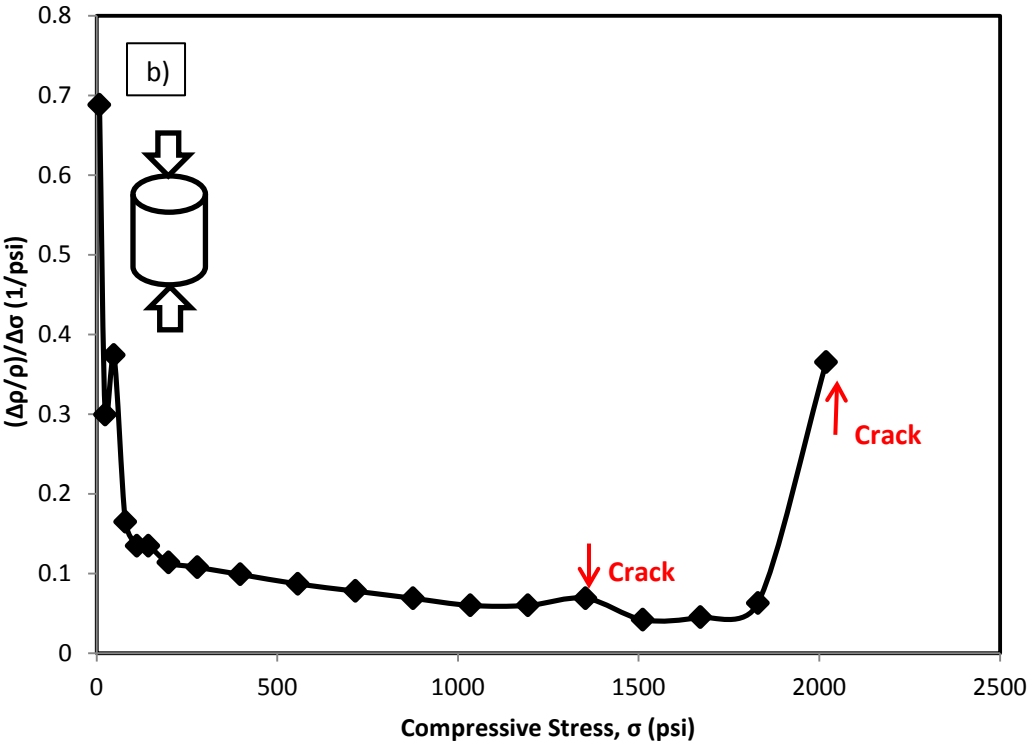

Figure 5-10. Piezoresistive behavior of cement with 3% OBM contamination after 28 day of curing a) Compressive stress vs. change in resistivity b) Change in resistivity normalized by change in stress vs. compressive stress

5.6 Summary

Based on experimental and analytical study on smart cement with up to 3% OBM contamination, following conclusions are advanced:

1. OBM contamination reduced the density of smart cement slurry. With 0.1% and 3% OBM contamination, the density reduced by 0.98% and 5.5%, respectively.

2. OBM contaminated cement had reduced viscosity and yield points, based on the level of contamination. The developed hyperbolic model predicted the shear-thinning behavior of samples with and without contamination.

3. The initial resistivity of up to 3% OBM contaminated cement was increased by more 304%. Initial electrical resistivity can be used as a good indicator the capture the OBM contamination.

4. Electrical resistivity developments with hydration time of the cement with different contamination level, follow a similar pattern, first drop to a minimum point, and then gradually increase with time. The resistivity index (RI_{24}) of the uncontaminated cement (higher strength) was higher than that of the OBM contaminated cement (lower strength). A linear correlation was found between resistivity index and compressive strength at different curing ages.

5. The smart cement showed piezoresistive behavior. The change in resistivity increased with increasing the compressive loading. OBM contamination reduced the piezoresistivity of smart cement at all curing ages investigated in this study.

Chapter 6

CONCLUSIONS AND RECOMMENDATIONS

Oil wells are drilled to depths of thousands of feet for efficient oil and gas production. The productivity of oil wells is affected by the oil well cement sheath quality. The rheology, strength, and integrity of the cement sheath are major requirements for successful oil well cementing. This study focused on development of a method to monitor the behavior of oil well cement from the time of mixing during its hardening. Cement with high sensing property, smart cement, was characterized and effect of various compositions and water-to-cement ratios were investigated through experimental and analytical studies.

6.1 Conclusions

Based on this study the following conclusions were determined:

1. With the addition of 0.1% carbon fiber, the resistivity of the cement slurry decreased from about 1.06 Ω.m to 0.98 Ω.m. Addition of carbon fibers had minimal effect on rheological and mechanical properties of oil well cement.
2. It was observed from the impedance spectroscopy tests that smart cement was a “resistance-only” material, meaning that the resistance of cement at high frequency was in the range of the its bulk resistance.
3. The modification of cement with carbon fibers made the cement a piezoresistive material. Piezoresistive sensitivity of cement (change in electrical resistivity with the

applied stress) was varied from 60% to more than 780% based on the different admixture incorporations, age of cement and curing conditions.

4. The electrical resistivity responses during the initial curing for various samples followed the same trend. Resistivity reduced to a minimum point, increased sharply and then increased gradually with a lower rate.
5. Monitoring the resistivity of the cement could provide a better understanding of the chemical (ion solution) and physical (formation of solid hydration products) changes during hydration of cement.
6. A linear correlation was found between percentage change in electrical resistivity (resistivity index) and the compressive strength of cement with different water-to-cement ratios and ages of curing.
7. The rheological test showed that class H cement had shear-thinning behavior and a hyperbolic model was proposed to predict shear stress- strain relationship. The model predicted the experimental data for cement with several compositions.
8. Comparing the Bingham-plastic, Herschel-Bulkley and the hyperbolic models proved that determination of the yield stress is highly dependent upon the selection of model.
9. The study revealed that both yield stress and apparent viscosity increased with reducing the water-to-cement ratio and increasing the temperature.
10. OBM contamination reduced the density of smart cement slurry. With 0.1% and 3% OBM contamination, the density reduced by 0.98% and 5.5%, respectively.

11. OBM contaminated cement had reduced viscosity and yield stress, based on the level of contamination. The developed hyperbolic model predicted the shear-thinning behavior of samples with and without contamination
12. The initial resistivity of up to 3% OBM contaminated cement was increased by more 304%. Initial electrical resistivity can be used as a good indicator the capture the OBM contamination.
13. The resistivity index (RI_{24}) of the uncontaminated cement (higher strength) was higher than that of the OBM contaminated cement (lower strength). A linear correlation was found between resistivity index and compressive strength at different curing ages.
14. The change in resistivity increased with increasing the compressive loading. OBM contamination reduced the piezoresistivity of the cement at failure at all curing ages.
15. Calorimetric tests showed that applying external electrical current to cement led to increase in the rate of hydration. Compared to the control sample, the peak temperature was 12% higher and the time to reach the peak temperature was 50% less for the cement with applied electrical current.

6.2 Recommendations

1. In drilling applications, the efficiency of cementing job is almost unknown to the operators. The electrical resistivity method is a simple and practical method with the advantage of monitoring the behavior of cement in real time throughout the service life of the well.

2. Due to the resistivity contrast of the materials used in well drilling, the developed method for monitoring of smart cement can be used to control the quality of the

cementing job. For instance, if resistivity of the cement in the well is significantly different from what it was initially measured, there is high chance of cement contaminations. This must be verified with the model tests.

3. The electrical resistivity index had been developed and can be used to linearly correlate the cement strength based on the curing time. This index can be used to obtain the wait on cement times in the field. More tests are needed to verify the repeatability and practicality of the method.

4. Oil based mud contamination affected the rheological, resistivity and piezoresistiviy properties of smart cement. Monitoring the change in electrical resistivity is a good indicator to detect oil based mud contamination in the cement at early stages.

5. The change of resistivity to cement failure is more than 400 times of the strain at the failure; hence, this method has appropriate sensitivity to detect damage and failures of well cement.

REFERENCES

Azhari, F., and Banthia, N. (2012). “Cement-based Sensors with Carbon Fibers and Carbon Nanotubes for Piezoresistive sensing” *Cement and Concrete Composites*, *34*(7), 866–873. doi:10.1016/j.cemconcomp.2012.04.007

Backe, K.R. Lile, and O.B. Lyomove, S.K., (1997). “Laboratory Study on Oilwell Cement and Electrical Conductivity,” *Society of Petroleum Engineers, SPE56539*, 1-9.

Baeza, F. J., Galao, O., Zornoza, E., and Garcés, P. (2013). “Effect of Aspect Ratio on Strain Sensing Capacity of Carbon Fiber Reinforced Cement Composites” *Materials and Design*, *51*, 1085–1094. doi:10.1016/j.matdes.2013.05.010

Banthia, N., and Mindess, S. (1989). “Water Permeability of Cement Paste.” *Cement and Concrete Composites*, *19*(c), 727–736.

Banthia, N., and Dubeau, S. (1994), “Carbon and Steel Micro-Fiber Reinforced Cement Based Composites for Thin Repairs”, *Journal of Materials in Civil Engineering*, Vol. 6, No. 1, pp. 88-99.

Baoguo H., and Jinping O., (2008). “Humidity sensing property of cements with added carbon," *New Carbon Materials*, Vol: 23, 382-384.

Choolaei M, Rashidi A.M, Ardjmand.M, Yadegari.A, and Soltanian H. (2012). “The Effect of Nanosilica on the Physical Properties of Oil Well Cement,” *Materials Science and Engineering*, 288-294.

Davies, D. R., Hartog, J. J., Cobbett, J. S. (1981). "Foamed Cement- A Cement with Many Applications," *SPE 9598, Middle East Oil Tech, Conf. Manama, Bahrain*, March 9-12.

Douglas J.F., Gassiorek J.M. and Swaffield J.A. (1995). “Fluid Mechanics”. Longman Scientific and Technical, Third Edition, ISBN 0582234085, pp. 287-292.

Fink, J. K. (2012). Petroleum Engineer’s Guide to Oil Field Chemicals and Fluids (First Edit.). Gulf Professional Publishing.

Gibson, S. (2011). “Novel Solution to Cement Strength Retrogression”, *Society of Petroleum Engineers, SPE/IADC 138852* (March), 35–40.

Guillot, D. (2006). “Rheology of Well Cement Slurries” In: E.B. Nelson and Guillot, D. (Eds.), *Well Cementing*, Schlumberger, Texas, pp. 93-142.

Han, B., Zhang, K., Yu, X., Kwon, E., and Ou, J. (2012). “Composites Electrical Characteristics and Pressure-Sensitive Response Measurements of Carboxyl MWNT/Cement Composites”. *Cement and Concrete Composites*, *34*(6), 794–800.

Han, B., Zhang, K., Yu, X., Kwon, E., & Ou, J. (2012). “Fabrication of Piezoresistive CNT / CNF Cementitious Composites with Superplasticizer as Dispersant”, *ASCE Journal of Material in Civil Engineering*, 658–665.

Harder, C. A., Carpenter, R. B., Freeman, E. R., Brookey, T. E., Fluids, S. D., and Gandy, R. G. (1993). “Optimization of Oil-Base Mud Chemistry for Cementing.”, *SPE 25183*

Harms, W. M., Ligenfelter, J. T. (1981). "Microspheres Cut Density of Cement Slurry" *Oil and Gas J.*, 59-66.

Joshi, R.C., and Lohtia, R.P. (Eds.), (1997). “Advances in Concrete Technology, 2, Fly Ash in Concrete: Production, Properties and Uses”, Amsterdam, Netherlands: Gordon and Breach Science Publishers, 1-269.

Ma, H., Tang, S., & Li, Z. (2014). “New Pore Structure Assessment Methods for Cement Paste”. *ASCE, Journal of Materials in Civil Engineering*, MT.1943-5533.0000982.

McCarter, W. J. (1994). “A Parametric Study of the Impedance Characteristics of Cement-Aggregate Systems during Early Hydration”, *Cement and Concrete Research*, *24*(6), 1097–1110.

McCarter, W. J., Starrs, G., & Chrisp, T. M. (2000). “Electrical conductivity, diffusion, and Permeability of Portland Cement-Based Mortars”. *Cement and Concrete Research*, *30*, 1395–1400.

McCarter, W. J., Chrisp, T. M., Starrs, G., & Blewett, J. (2003). “Characterization and Monitoring of Cement-Based Systems Using Intrinsic Electrical Property Measurements”, *Cement and Concrete Research*, Vol: *33*, 197–206.

Mueller, D. T., and Dillenbeck, R. L. (2013). “The Versatility of Silica Fume as an Oilwell Cement Admixture.” *SPE Production Operations Symposium*, 529–536. doi:10.2118/21688-MS

Nehdi, M., and Rahman, M.A. (2004). “Estimating Rheological Properties of Cement Pastes Using Various Rheological Models for Different Test Geometry, Gap and Surface Friction”, *Cement and Concrete Research*, Vol. 34, No. 11, pp. 1993-2007.

Nelson, E.B., Michaux, M., and Drocho, B. (2006). “Cement Additives And Mechanism Of Action”, In: E.B. Nelson and Guillot, D. (Eds.), *Well Cementing*, Schlumberger, Texas, pp. 49-91.

Natarajan R., (2005). “Phosphate Based Oil Well Cements,” PhD Thesis-Dept. of Materials Eng., University of Illinois, Chicago, Illinois, 1-131.

Olowolagba, K., and Brenneis, C. (2010). “Techniques for the Study of Foamed Cement Rheology”, *Society of Petroleum Engineers, SPE 133050* (June), 8–10.

Page, H. (1996). “Design and Control of Concrete Mixtures, Chapter 3: Fly Ash, Slag, Silica Fume, and Natural Pozzolans” (54048).

Pane, I., and Hansen, W. (2005). “Investigation of Blended Cement Hydration by Isothermal Calorimetry and Thermal Analysis.” *Cement and Concrete Research*, *35*(6), 1155–1164. doi:10.1016/j.cemconres.2004.10.027

Polder, R.B., (2001) “Test Methods for on Site Measurements of Resistivity of Concrete-a RILEM TC-154 Technical Recommendation,” *Construction and Building Materials*, Vol. 15

Popovics, S. (1992). “Concrete Materials: Properties, Specifications, And Testing. ” 2nd edition, Noyes Publication, 661 p.

Pourafshary, P. Azimipour, S.S. Motamedi, P. Samet, M. Taheri, S.A. Bargozin, and H.Priority, 2009. “Priority Assessment of Investment in Development of Nanotechnology in Upstream Petroleum Industry,” *Society of Petroleum engineers, SPE126101*, 1-11.

Power, D. and Zamora, M. (2003). “Drilling Fluid Yield Stress: Measurement Techniques for Improved Understanding of Critical Drilling Fluid Parameters” *AADE-03-NTCE-35*, pp.1-9.

Ravi, K., Bosma, M., and Gastebled, O. (2002). “Improve The Economics Of Oil And Gas Wells By Reducing The Risk Of Cement Failure”. *IADC/SPE Drilling Conference*, Dallas, February 26-28, Paper No. 74497, pp. 377-389.

Reddy, B.R. and Riley, W.D., (2004). “High Temperature Viscosifying and Fluid loss Controlling Additives for Well Cements, Well Cement Compositions and Methods”. *US Patent 6 770 604, Assigned to Halliburton Energy Services, Inc. (Duncan, OK)*

Roshan M, and Asef M.R., (2010). “Characteristics of Oilwell Cement Slurry Using CMC”. *SPE Drilling & Companies*, 129-132.

Sabins, F. L., Services, H., and Sutton, D. L. (1986). “The Relationship of Thickening Time, Gel Strength, and Compressive Strength of Oilwell Cements”, (March).

Shahriar, A., (2011) “Investigation on Rheology of Oil Well Cement Slurries”, PhD Thesis- Dept. of Civil and Env. Eng., University of Western Ontario, London, Ontario, Canada, 1-256

Smith, D.K. (1987). “Cementing”, Monograph Series, 4, SPE, Dallas, 264 p.

Smith, D.K., (1990). “Cementing,” Revised ed., Society of Petroleum Engineers Inc., Compliments of Halliburton Services, Richardson, TX, 1-264.

Smith, D. K., Calvert, D. G., (1990). “API Oil Well Cementing Practices” *Offshore Technology Conference* (November)

Taylor, H.F.W., (1997). “Cement Chemistry,” 2nd ed., Telford, London, 1-439.

Thiercelin, M. J., Dargaud, B., Baret, J. F., Rodriquez, W. J., and Intevep, S. A. (1998). “Cement Design Based on Cement Mechanical Response”, (December).

Vipulanandan, C., Heidari, M., Qu, Q., Farzam, H., and Pappas, J. M. (2014). “Behavior of Piezoresistive Smart Cement Contaminated with Oil Based Drilling Mud.” *Offshore Technology Conference*. doi:10.4043/25200-MS

Vipulanandan, C., and Prashanth, P. (2013). “Impedance Spectroscopy Characterization of a Piezoresistive Structural Polymer Composite Bulk Sensor”, *Journal of Testing and Evaluation*, *41*(6), 898–904. doi:10.1520/JTE20120249

Wei, X., & Li, Z. (2006). “Early Hydration Process of Portland Cement Paste”, *ASCE Journal of Material in Civil Engineering*, 99–105.

Wei, X., Xiao, L., and Li, Z. (2008). “Electrical Measurement to Assess Hydration Process and the Porosity Formation”, *Journal of Wuhan University of Technology-Mater. Sci. Ed.* 761–766.

Wei, X., Xiao, L., and Li, Z. (2012). “Prediction of Standard Compressive strength of Cement by the Electrical Resistivity Measurement.” *Construction and Building Materials*, *31*, 341–346. doi:10.1016/j.conbuildmat.2011.12.111

Liao, Y., and Wei, X. (2014). “Relationship between Chemical Shrinkage and Electrical Resistivity for Cement Pastes at Early Age”, ASCE *Journal of Materials in Civil Engineering*, 384–387.

Wen, S., and Chung, D. D. . (2000). “Uniaxial Tension in Carbon Fiber Reinforced Cement, Sensed by Electrical Resistivity Measurement in Longitudinal and Transverse Directions.” *Cement and Concrete Research*, *30*(8), 1289–1294. doi:10.1016/S0008-8846(00)00304-5

Wen S., and Chung D.D.L, (2001). “Electric Polarization in Carbon Fiber-Reinforced Cement,” *Cement and Concrete Research*, Vol. 31, 141-147.

Wen, S., and Chung, D. D. L. (2006). “Effects of Strain and Damage on Strain-Sensing Ability of Carbon Fiber Cement,” *Journal of Materials in Civil Engineering* (June), 355–360.

West, A. R., Sinclair, D. C., and Hirose, N. (1997). “Characterization of Electrical Materials, Especially Ferroelectrics, by Impedance Spectroscopy”, *Journal of Electroceramics*, 65–71.

Xiao, L., and Li, Z. (2008). “Early-Age Hydration of Fresh Concrete Monitored by Non-contact Electrical Resistivity Measurement.” *Cement and Concrete Research*, *38*(3), 312–319. doi:10.1016/j.cemconres.2007.09.027

Yahaba, N. (2010). “How Does A Decrease in Oil Production Affect The World Economy?” *ASIA Pacific Economic Papers*, No. 388, pp. 32.

Zhang, J., Weissinger, E. a., Peethamparan, S., and Scherer, G. W. (2010). “Early Hydration and Setting of Oil Well Cement”. *Cement and Concrete Research*, *40*(7), 1023–1033. doi:10.1016/j.cemconres.2010.03.014

Zuo, Y., Zi, J., and Wei, X. (2014). “Hydration of Cement with Retarder Characterized via Electrical Resistivity Measurements and Computer Simulation.” *Construction and Building Materials*, *53*, 411–418. doi:10.1016/j.conbuildmat.2013.11.01